Sudan University of Science and Technology

College of Graduate Studies

Diagnosis of Ischemic Heart Disease Using Cardiac Magnetic Resonance Imaging and Two-dimensional Echocardiography

تشخيص مرض القلب الإفقاري بإستخدام تصوير القلب بالرنين المغناطيسي وتخطيط صدى القلب ثنائي الأبعاد

A Thesis Submitted for the Fulfillment of the Requirements of the Awardance of the Philosophy Doctorate Degree (PhD) in Diagnostic Radiologic Technology

By:

Moram Abdelazim Abdalla Fagiry

Supervisor:

Dr. Ikhlas Abdelaziz Hassan

November 2020

قال تعالى:

﴿ الَّذِينَ آمَنُواْ وَتَطْمَئِنُّ قُلُوبُهُم بِذِكْرِ اللَّهِ أَلاَ بِذِكْرِ اللَّهِ تَطْمَئِنُّ الْقُلُوبُ ﴾

سورة الرعد الآية (28)

DEDICATIONS

This thesis is dedicated to my father Abdelazim, who taught me that the best kind of knowledge to have is that which is learned for its own sake.

It is also dedicated to my mother, Leila, who taught me that even the largest task could be accomplished if it is done one-step at a time.

I dedicate the benefits of this humble work to my beloved husband Mustafa, who prays always for my success and my beloved kids Abdelrahman, Jory, Zuhair and Joud.

My sincere gratitude and dedications are also extended to my brothers, sisters, colleagues and friends, for their endless support. Great motivation and encouragement during writing this thesis.

ACKNOWLEDGEMENTS

First of all, I would like to thank Allah, for giving me the strength and health to make this project work until it is done completely.

I expressed my utmost gratitude to Associate Professor Dr. Ikhlas Abdelaziz Hassan; my supervisor of this study for her steadfast support that was greatly needed and deep appreciation.

I would like to express my gratitude to Associate Professor Dr. Mustafa Zuhair Alhassen; for his sage advice, insightful criticisms, and patient encouragement aided the writing of this thesis in innumerable ways.

My thanks extended also to Associate Professor Dr. Mohamed Yousef; the former Dean of the College of Medical Radiologic Sciences (CMRS) – Sudan University of Science and Technology (SUST), for his abundantly helpful and useful advices, complete support and guidance.

ABSTRACT

Background: Ischemic heart disease (IHD) also known as coronary artery disease (CAD) is one of the major causes of morbidity and mortality in adults. **Objectives:** The aims of this research was to study the value of usage CMRI and 2D echo as a diagnostic tool to diagnose IHD. In addition, it will determine the recent advances on the prognostic and diagnostic value, drawbacks and the future directions of cardiac magnetic resonance imaging (CMRI) and two-dimensional echocardiography (2D echo) in the diagnosis of IHD. **Materials and methods:** One hundred patients who were clinically diagnosed to have IHD were enrolled prospectively in this study. The patients were examined using CMRI; Siemens Magnetom Sola 1.5T MRI scanner and 2D echo; Siemens Acuson SC2000 Prime ultrasound system. Conventional coronary angiography was used to confirm the diagnosis. The process of analyzing data was carried out using the Statistical Package for the Social Sciences (SPSS) version 20 for Windows (IBM Corporation, Armonk, NY, USA). The statistical diagnostic test was used to detect sensitivity, specificity and accuracy of CMRI and 2D echo in the diagnosis of IHD. **Results:** CMRI revealed that the left ventricular (LV) volumes and systolic function by age decile in male to female patients were 28.9±3.5%; 32±1.7%, 53.3±11.2; 58±6.6 ml, 5.4±1.4; 5.8±1.5 L/min, 189±14.3; 180±10.9 ml and 136±3.1; 123±4.4 ml for the left ventricle ejection fraction (LVEF), stroke volume (SV), cardiac output, end diastolic volume (EDV) and end systolic volume (ESV), respectively. 2D echo found that a 75% myocardial infarction involving mid anterior segment with low likelihood of viability was common in male (93.4%) and female (82.1%) patients. CMRI and 2D echo presents a sensitivity, specificity and accuracy of 97.98%; 97.87%, 25%; 11.11% and 95.15%; 90.29%, for each. **Conclusion:** CMRI is given a complete assessment of LV function, myocardial perfusion and viability and as well as the coronary anatomy. 2D echo is central to the diagnosis, management and prognosis of the entire spectrum of IHD.

الملخص

المقدمة: مرض القلب الإفقاري المعروف أيضاً بإسم مرض الشريان التاجي هو أحد الأسباب الرئيسية للمرض والوفيات لدى البالغين. **الأهداف:** كان الهدف من هذا البحث هو دراسة قيمة إستخدام التصوير بالرنين المغناطيسي للقلب وتخطيط صدى القلب ثنائي الأبعاد كأدوات تشخيصية لتشخيص مرض القلب الإفقاري. بالإضافة إلى ذلك، فان الدراسة الحالية سوف توضح التطورات الأخيرة على القيمة التكهنية والتشخيصية بجانب إيراد العيوب والتوجهات المستقبلية للتصوير بالرنين المغناطيسي للقلب وتخطيط صدى القلب ثنائي الأبعاد في تشخيص مرض القلب الإفقاري. **المواد والطريقة:** تم فحص مائة مريض بعد أن تم تشخيصهم إكلينيكيًا بأنهم مصابون بمرض القلب الإفقاري وذلك بإستخدام ماسح الرنين المغنطيسي المصنع بواسطة شركة سيمنز (Magnetom Sola 1.5T)، المتميز بإستخدام مغناطيس فائق التوصيل ولفحص وتخطيط صدى القلب ثنائي الأبعاد، تم إستخدام جهاز الموجات فوق الصوتية (Acuson SC2000 Prime) المصنع أيضا بواسطة شركة سيمنز. تم إستخدام تصوير الأوعية التاجية الإشعاعي التقليدي لتأكيد التشخيص. وقد تم إجراء عملية تحليل البيانات بإستخدام الحزمة الإحصائية (SPSS) الإصدار 20 (IBM Corporation, Armonk, NY, USA) لنظام التشغيل (Windows). تم إستخدام الإختبار التشخيصي الإحصائي للكشف عن الحساسية، النوعية والدقة لفحص التصوير بالرنين المغناطيسي للقلب وتخطيط صدى القلب ثنائي الأبعاد في تشخيص مرض القلب الإفقاري. **النتائج:** كانت أحجام البطين الأيسر والوظيفة الانقباضية حسب الفئة العمرية عند مرضى مرض القلب الإفقاري بإستخدام فحص التصوير بالرنين المغناطيسي للقلب لدى المرضى الذكور إلى الإناث 32±1.7% ;28.9±3.5%، 58±6.6 ;53.3±11.2 مل، 5.8±1.5 ;5.4±1.4 لتر / دقيقة، 180±10.9 ;189±14.3مل و 136±3.1; 123±4.4 مل لقذف البطين الأيسر للدم، حجم السكتة، النتاج القلبي، الحجم الانبساطي النهائي والحجم الانقباضي النهائي، على التوالي. أظهر فحص تخطيط صدى القلب ثنائي الأبعاد أن احتشاء عضلة القلب بنسبة 75% التي تصيب الجزء الأمامي الأوسط كان شائعاً في المرضى الذكور (93.4%) والإناث (82.1%). كشفت خصائص الإختبار التشخيصي أن فحص التصوير بالرنين المغناطيسي للقلب وفحص تخطيط صدى القلب ثنائي الأبعاد في تشخيص مرض القلب الإفقاري يقدما حساسية وخصوصية ودقة مقدارها 97.87% ;97.98%، 25% ;11.11% و 90.29% ;95.15%، على التوالي. **الخلاصة:** يعطي فحص التصوير بالرنين المغناطيسي للقلب تقييماً

كاملاً لوظيفة البطين الأيسر ونضح عضلة القلب وحيويته وكذلك تشريح الشريان التاجي. يعد تخطيط صدى القلب ثنائي الأبعاد أمرًا محوريًا لتشخيص وإدارة التكهن لكامل طيف مرض القلب الإفقاري.

TABLE OF CONTENTS

LIST OF TABLES

LIST OF FIGURES

LIST OF ABBREVIATIONS

Abbreviation	Abbreviation stands for
IHD	Ischemic heart disease
CAD	Coronary artery disease
MI	Myocardial infarction
CMRI	Cardiac magnetic resonance imaging
CMR	Cardiac magnetic resonance
ACS	Acute coronary syndrome
MRI	Magnetic resonance imaging
PET	Positron-emission tomography
ACSs	Acute coronary syndromes
ECG	Electrocardiography
2D echo	Two-dimensional echocardiography
LVEF	Left ventricular ejection fraction
CT	Computed tomography
CVDs	Cardiovascular diseases
LMP	Last menstrual period
bpm	Beats per minute
CO	Cardiac output
SV	Stroke volume
HR	Heart rate
HRs	Heart rates
DCM	Dilated cardiomyopathy
TDI	Tissue Doppler imaging

Abbreviation	Abbreviation stands for
3D	Three-dimensional
EF	Ejection fraction
LVOT	Left ventricular outflow tract
VTI	Velocity time integral
IMR	Ischemic mitral regurgitation
PISA	Proximal isovelocity surface area principle
ERO	Effective regurgitant orifice
AMI	Acute myocardial infarction
PCWP	Pulmonary capillary wedge pressure
E/Vp	Peak mitral early diastolic filling velocity/velocity of propagation
M-mode	Motion mode
PCI	Percutaneous coronary intervention
SPECT	Single photon emission computed tomography
b-SSFP	Balanced steady-state free precession
STIR	Short T_1 inversion recovery
Ce-MRI	Contrast enhanced MRI
MPR	Myocardial perfusion reserve
WMAs	Wall motion abnormalities
AHA	American heart association
MRCA	Magnetic resonance coronary angiography
Ce-MRA	Contrast-enhanced magnetic resonance angiography
SNR	Signal-to-noise ratio

Abbreviation	Abbreviation stands for
CNR	Carrier-to-noise ratio
RF	Radio frequency
CABG	Coronary artery bypass graft
SSFP	Steady-state free precession
FLASH	Fast low angle shot
LGE	Late gadolinium enhancement
MVO	Microvascular obstruction
CTCA	Computed tomography coronary angiography
MAS	Medical Advisory Secretariat
SENSE	Sensitivity encoding
TR/TE	Repetition time/echo time
FOV	Field of view
NSA	Number of signal averages
b-FFE	Balanced fast field echo
IR-b-TFE	Inversion recovery balanced turbo field echo
TI	Inversion time
ASCI	Asian Society of Cardiovascular Imaging
TSE	Turbo spin-echo
CNR	Contrast to noise ratio
EPI	Echo-planar imaging
BB	Black blood
FFE-SSFP	Fast field echo-steady state free precession
FISP	Fast imaging with steady state precession

Abbreviation	Abbreviation stands for
HASTE	Half-Fourier acquisition single-shot turbo spin-echo
PC	Phase contrast
PSIR	Phase-sensitive inversion-recovery
PWI	Perfusion weighted image
TSI	Time-signal intensity
ESV	End-systolic volume
EDV	End-diastolic volume
PFR_E	Early peak filling rate
PFR_A	Active peak filling rate
SC	Subcostal
SSN	Suprasternal notch
PLAX	Parasternal long-axis
PSAX	Parasternal short-axis
PW	Pulsed wave
HPRF	High pulse repetition frequency
CW	Continuous wave

CHAPTER ONE

INTRODUCTION

Chapter One

Introduction

1.1 Introduction

Ischemic heart disease (IHD) also known as coronary artery disease (CAD), refers to a group of diseases, which includes stable and unstable angina, myocardial infarction (MI) and sudden cardiac death (Wong, 2014; Mahmoud, 2017). A common symptom is chest pain or discomfort, which usually occurs with exercise or emotional stress, last less than a few minutes and improves with rest (Charison et al., 2013). Imaging in CAD helps physicians to diagnose patients more precisely and to treat them more effectively. Although in many cases, the diagnosis or the exclusion of stable CAD can be made on the basis of clinical evaluation. However, in numerous patients the tool, verifying the baseline clinical judgment is needed. Moreover, a physician needs information additional to clinical evaluation to make a decision about management strategy (Spiewak, 2015).

There is a constant need to improve the decision-making process in these situations. Among other imaging modalities, cardiac magnetic resonance imaging (CMRI) has provoked increasing interest in the potential clinical role in the non-invasive work-up of patients with suspected CAD and correct patient selection for these emerging imaging techniques (Jung & Yoon, 2017). In recent years, cardiac magnetic resonance (CMR) has become a routinely used modality for the diagnosis of IHD and can provide non-invasive evaluation of reperfusion therapy through a comprehensive evaluation of wall motion, global function, perfusion and viability. In fact, CMR is widely considered the clinical gold standard for viability imaging by providing high-resolution images of post-contrast gadolinium enhanced acquisitions that accurately depict the transmurality of MI, which is critical to guide re-vascularization therapy (Wieben et al., 2008). Thus, the growing number of patients undergoing CMR studies and

CMR centers and the evidence for the use of CMR both in patients with stable CAD, as well as acute coronary syndrome (ACS) justify reviewing its capabilities (Spiewak, 2015; Bruder et al., 2013).

Beside the facts mentioned, CMR has matured into a multipurpose non-invasive imaging tool for the assessment of IHD. The breadth of applications possible with CMR allows combined non-invasive assessment of myocardial perfusion, function and myocardial viability, which is a task that usually requires use of echocardiography and myocardial scintigraphy. As such, CMR currently holds a strong position in the non-invasive work-up of patients with CAD (Nikolaou et al., 2011). In addition, the distinct advantages of magnetic resonance imaging (MRI) over current conventional nuclear-based cardiac-imaging techniques, such as positron-emission tomography (PET) or myocardial scintigraphy, include its high spatial resolution and lack of exposure of the patient to ionizing radiation. Also, quantification of cardiac morphology and function by MRI is more accurate and image quality is more reproducible than in echocardiography, independent of the operator's experience and skill level or the patient's anatomy (Nikolaou et al., 2011; Zidan et al., 2018; Mohieldin et al., 2016; Elamin et al., 2016; Mahmoud et al., 2013).

A large number of patients present daily to the emergency department with the chief complaint of chest pain. The challenge for the physician is to identify patients who require intervention, particularly when acute coronary syndromes (ACSs) present with atypical symptoms or nondiagnostic electrocardiography (ECG) changes or normal cardiac enzyme levels. Since the mortality and morbidity of IHD, improve following early treatment, timely diagnosis is of vital importance not only to help the patient, but also to reduce hospital stay and economic costs (Esmaeilzadeh et al., 2013; Votavová, et al., 2015).

Imaging techniques represent the key method for disease extent and severity assessment and evaluation of hemodynamic complications. Two-dimensional echocardiography (2D echo) is

one of the most useful imaging methods due to its availability, ease of use, price, capacity to serve as bedside technique and repeatability. It is the most employed cardiovascular imaging modality for assessment of cardiovascular disease and is often performed in patients without a history of IHD. It is well established that several echocardiograpahic measurements provide powerful prognostic information for cardiovascular outcomes, such as presence of left ventricular hypertrophy, aortic sclerosis and left ventricular ejection fraction (LVEF). In addition, 2D echo is also very useful when it comes to rule out the possibility of other etiologies of acute chest pain or dyspnea, such as aortic dissection and pericardial effusion (Chaves, et al., 2004; Esmaeilzadeh et al., 2013; Votavová et al., 2015).

1.2 Problem of the study

Although IHD also known as CAD can be diagnosed accurately, using advanced radiodiagnostic applications such as cardiac catheterization and/or cardiac computed tomography (CT). However, such applications are associated with several limitations that affect patient safety and the quality of the diagnoses. In both cardiac catheterization and/or CT presents the problem of exposing the patient to high radiation dose during the procedure. Therefore, using a new technology as echocardiography and CMR to overcome such problems is of a great value to the patient.

1.3 Objectives

1.3.1 General objectives

This study was designed with an aim to study the value of usage 2D echo and CMRI as a diagnostic tool to diagnose IHD.

1.3.2. Specific Objectives

- This study will update the reader on the current status of CMRI, with a special focus on the basic CMR sequences in IHD. The recent advances on the prognostic and diagnostic value and future directions in the CMR evaluation of IHD was also discussed.
- Determine the fundamental principles and current applications of 2D echo imaging recommended in patients with known or suspected IHD. In addition, the recent advances on the prognostic and diagnostic value and the future directions of 2D echo in the evaluation of IHD will be addressed.
- Presents of the drawbacks of both CMRI and 2D echo in the evaluation of IHD in the study samples of the current research.

1.4. Thesis outlines

In chapter one a summarized introduction including prelude about echocardiography and CMRI in the diagnosis of IHD, statement of the study problem, study objectives either general or specific objectives and an overview of the study chapters contents were present. Chapter two of this study includes an overview of the literature, including anatomy, physiology and pathology of the heart and great cardiac blood vessels as a theoretical background in addition to the previous studies. Chapter three dealt with the materials and methods used in the practical portion of the current study, including the different materials used and the methodology of the practical setup were discussed in details. Chapter four dealt with the results of the study were the results, interpretations were given in this chapter. Lastly, chapter five included the discussion, conclusions of the study performed as well as future work and recommendations.

CHAPTER TWO

LITERATURE REVIEW

Chapter Two

Literature review – Theoretical background

2.1 Heart anatomy

2.1.1 Heart definition and development

The heart is a muscular organ (Figure 2.1) in most animals, which pumps blood through the blood vessels of the circulatory system. Blood provides the body with oxygen and nutrients, as well as assisting in the removal of metabolic wastes. In humans, the heart is located between the lungs, in the middle compartment of the chest (Moore et al., 2009). In humans, other mammals, and birds, the heart is divided into four chambers: upper left and right atria and lower left and right ventricles. Commonly the right atrium and ventricle are referred together as the right heart and their left counterparts as the left heart. In a healthy heart blood flows one way through the heart due to heart valves, which prevent backflow. The heart is enclosed in a protective sac, the pericardium, which also contains a small amount of fluid. The wall of the heart is made up of three layers: epicardium, myocardium, and endocardium (Starr et al., 2009; Reed et al., 2008).

The heart pumps blood with a rhythm determined by a group of pacemaking cells in the sinoatrial node. These generate a current that causes contraction of the heart, traveling through the atrioventricular node and along the conduction system of the heart. The heart receives blood low in oxygen from the systemic circulation, which enters the right atrium from the superior and inferior venae cavae and passes to the right ventricle. From here, it is pumped into the pulmonary circulation, through the lungs where it receives oxygen and gives off carbon dioxide. Oxygenated blood, then returns to the left atrium, passes through the left ventricle and is pumped out through the aorta to the systemic circulation – where the oxygen is used and metabolized to carbon dioxide. The heart beats at a resting rate close to 72 beats per minute.

Exercise temporarily increases the rate, but lowers resting heart rate (HR) in the long term, and is good for heart health (Hall, 2011).

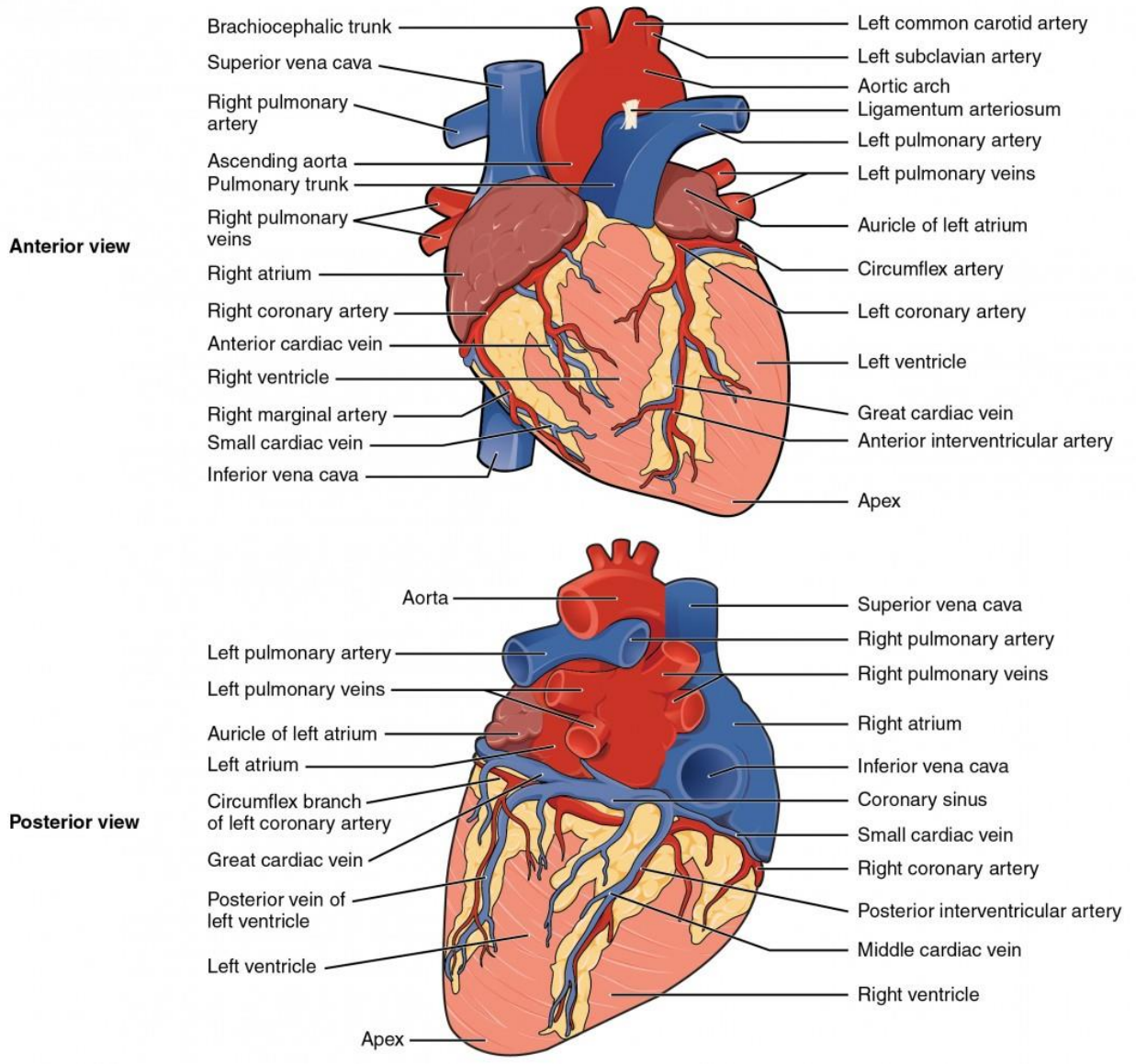

Figure 2.1: Labeled diagram of the heart from the anterior and posterior view (Moore et al., 2009).

Cardiovascular diseases (CVDs) are the most common cause of death globally as of 2008, accounting for 30% of deaths. Of these, more than three quarters are a result of coronary artery disease and stroke. Risk factors include smoking, being overweight, little exercise, high cholesterol, high blood pressure, and poorly controlled diabetes, among others. CVDs

frequently do not have symptoms or may cause chest pain or shortness of breath. Diagnosis of heart disease is often done by the taking of a medical history, listening to the heart-sounds with a stethoscope, ECG, and ultrasound. Specialists who focus on diseases of the heart are called cardiologists, although many specialties of medicine may be involved in treatment (Longo, 2011).

The heart is the first functional organ to develop and starts to beat and pump blood at about three weeks into embryogenesis (Figure 2.2). This early start is crucial for subsequent embryonic and prenatal development. The heart derives from splanchnopleuric mesenchyme in the neural plate, which forms the cardiogenic region. Two endocardial tubes form here that fuse to form a primitive heart tube known as the tubular heart. Between the third and fourth week, the heart tube lengthens, and begins to fold to form an S-shape within the pericardium. This places the chambers and major vessels into the correct alignment of the developing heart. Further development will include the septa and valves formation and remodeling of the heart chambers. By the end of the fifth week, the septa are complete and the heart valves are completed by the ninth week. Before the fifth week, there is an opening in the fetal heart known as the foramen ovale. The foramen ovale allowed blood in the fetal heart to pass directly from the right atrium to the left atrium, allowing some blood to bypass the lungs. Within seconds after birth, a flap of tissue known as the septum primum that previously acted as a valve closes the foramen ovale and establishes the typical cardiac circulation pattern. A depression in the surface of the right atrium remains where the foramen ovale was, called the fossa ovalis. The embryonic heart begins beating at around 22 days after conception (5 weeks after the last normal menstrual period, LMP). It starts to beat at a rate near to the mother's which is about 75–80 beats per minute (bpm). The embryonic HR then accelerates and reaches a peak rate of 165–185 bpm early in the early 7^{th} week (early 9^{th} week after the LMP). After 9 weeks (start

of the fetal stage), it starts to decelerate, slowing to around 145 (±25) bpm at birth. There is no difference in female and male heart rates (HRs) before birth (Betts, 2013).

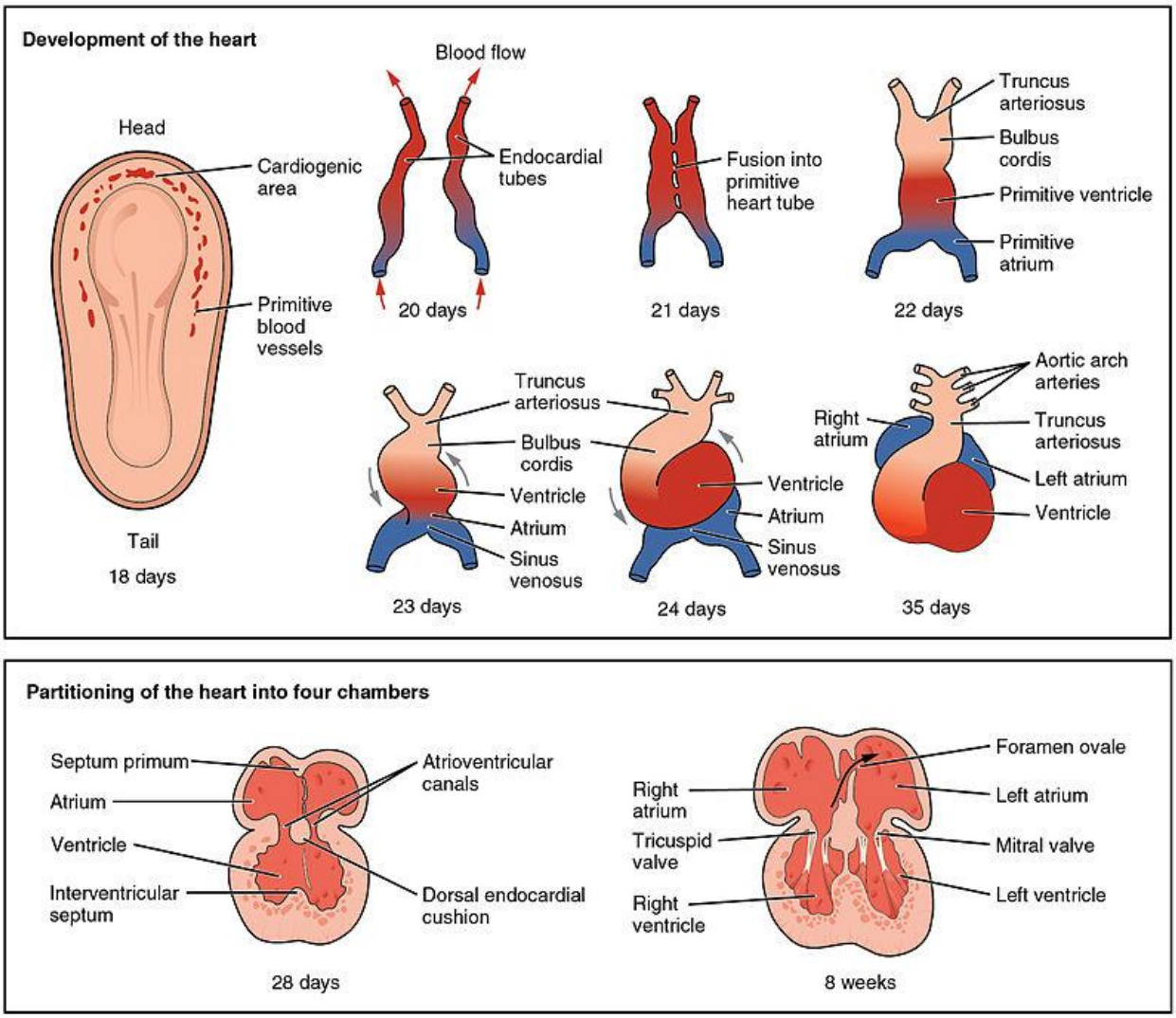

Figure 2.2: Development of the human heart during the first eight weeks (top) and the formation of the heart chambers (bottom). In this figure, the blue and red colors represent blood inflow and outflow (not venous and arterial blood). Initially, all venous blood flows from the tail/atria to the ventricles/head, a very different pattern from that of an adult (Betts, 2013).

2.1.2 Heart location and shape

The human heart is situated in the middle mediastinum (Figure 2.3), at the level of thoracic vertebrae T5-T8. A double-membraned sac called the pericardium surrounds the heart and attaches to the mediastinum. The back surface of the heart lies near the vertebral column, and

the front surface sits behind the sternum and rib cartilages. The upper part of the heart is the attachment point for several large blood vessels—the venae cavae, aorta and pulmonary trunk. The upper part of the heart is located at the level of the third costal cartilage. The lower tip of the heart, the apex, lies to the left of the sternum (8 to 9 cm from the midsternal line) between the junction of the fourth and fifth ribs near their articulation with the costal cartilages (Betts, 2013; Dorland's, 2012).

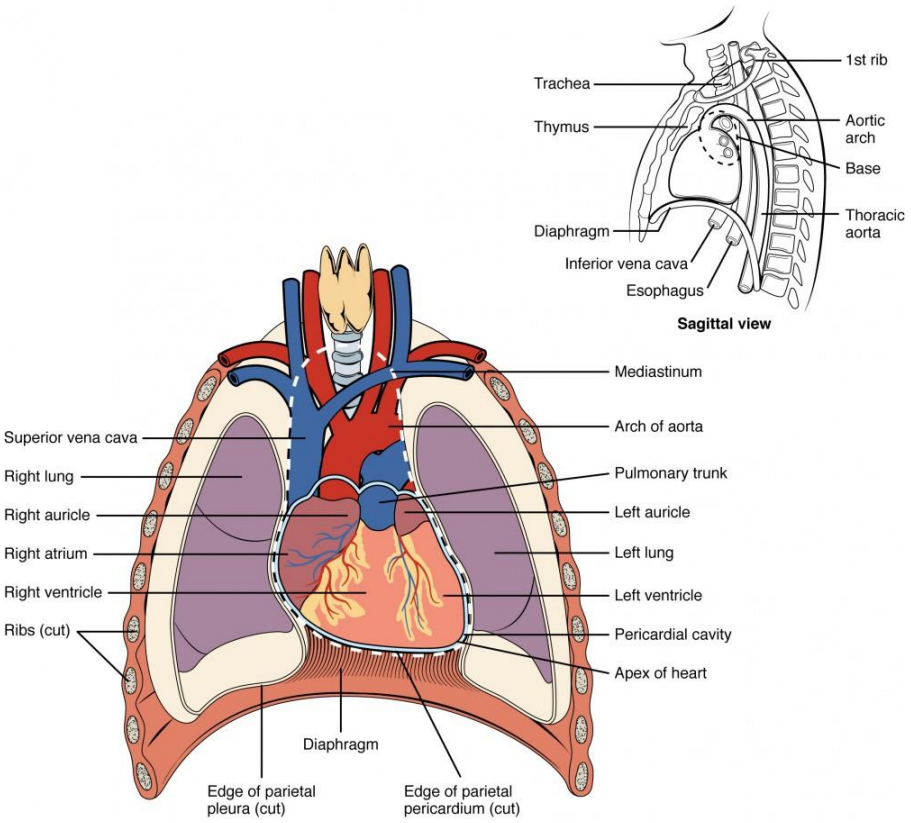

Figure 2.3: The heart is located within the thoracic cavity, medially between the lungs in the mediastinum. It is about the size of a fist, is broad at the top, and tapers toward the base (Ampanozi et al., 2018).

The largest part of the heart is usually slightly offset to the left side of the chest (though occasionally it may be offset to the right) and is felt to be on the left because the left heart is stronger and larger, since it pumps to all body parts. Because the heart is between the lungs, the left lung is smaller than the right lung and has a cardiac notch in its border to accommodate

the heart. The heart is cone-shaped, with its base positioned upwards and tapering down to the apex. An adult heart has a mass of 250–350 grams (9–12 Oz). The heart is often described as the size of a fist: 12 cm (5 in) in length, 8 cm (3.5 in) wide, and 6 cm (2.5 in) in thickness, although this description is disputed, as the heart is likely to be slightly larger. Well-trained athletes can have much larger hearts due to the effects of exercise on the heart muscle, similar to the response of skeletal muscle (Ampanozi et al., 2018).

2.1.3 Heart chambers

The heart has four chambers, two upper atria, the receiving chambers, and two lower ventricles, the discharging chambers (Figure 2.4). The atria open into the ventricles via the atrioventricular valves, present in the atrioventricular septum. This distinction is visible also on the surface of the heart as the coronary sulcus. There is an ear-shaped structure in the upper right atrium called the right atrial appendage, or auricle, and another in the upper left atrium, the left atrial appendage. The right atrium and the right ventricle together are sometimes referred to as the right heart. Similarly, the left atrium and the left ventricle together are sometimes referred to as the left heart. The ventricles are separated from each other by the interventricular septum, visible on the surface of the heart as the anterior longitudinal sulcus and the posterior interventricular sulcus (Susan, 2008).

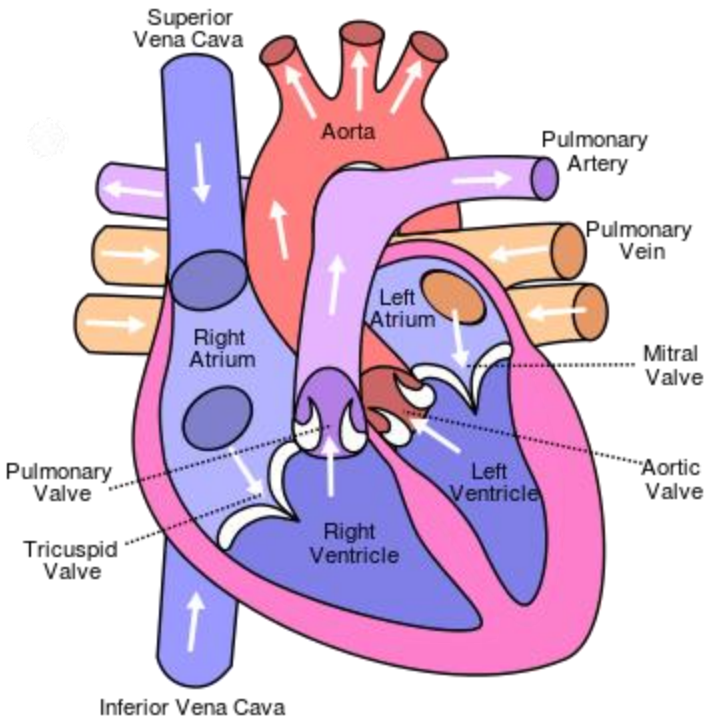

Figure 2.4: Labeled illustration of the human heart. The heart has four chambers, two upper atria, the receiving chambers, and two lower ventricles, the discharging chambers (Susan, 2008).

The cardiac skeleton is made of dense connective tissue and this gives structure to the heart. It forms the atrioventricular septum, which separates the atria from the ventricles, and the fibrous rings, which serve as bases for the four heart valves. The cardiac skeleton also provides an important boundary in the heart's electrical conduction system since collagen cannot conduct electricity. The interatrial septum separates the atria and the interventricular septum separates the ventricles. The interventricular septum is much thicker than the interatrial septum, since the ventricles need to generate greater pressure when they contract (Pocock et al., 2006).

2.1.4 Heart valves

The heart has four valves, which separate its chambers (Figure 2.5). One valve lies between each atrium and ventricle, and one valve rests at the exit of each ventricle. The valves between the atria and ventricles are called the atrioventricular valves. Between the right atrium and the

right ventricle is the tricuspid valve. The tricuspid valve has three cusps, which connect to chordae tendinae and three papillary muscles named the anterior, posterior, and septal muscles, after their relative positions. The mitral valve lies between the left atrium and left ventricle. It is also known as the bicuspid valve due to its having two cusps, an anterior and a posterior cusp. These cusps are also attached via chordae tendinae to two papillary muscles projecting from the ventricular wall (Betts, 2013).

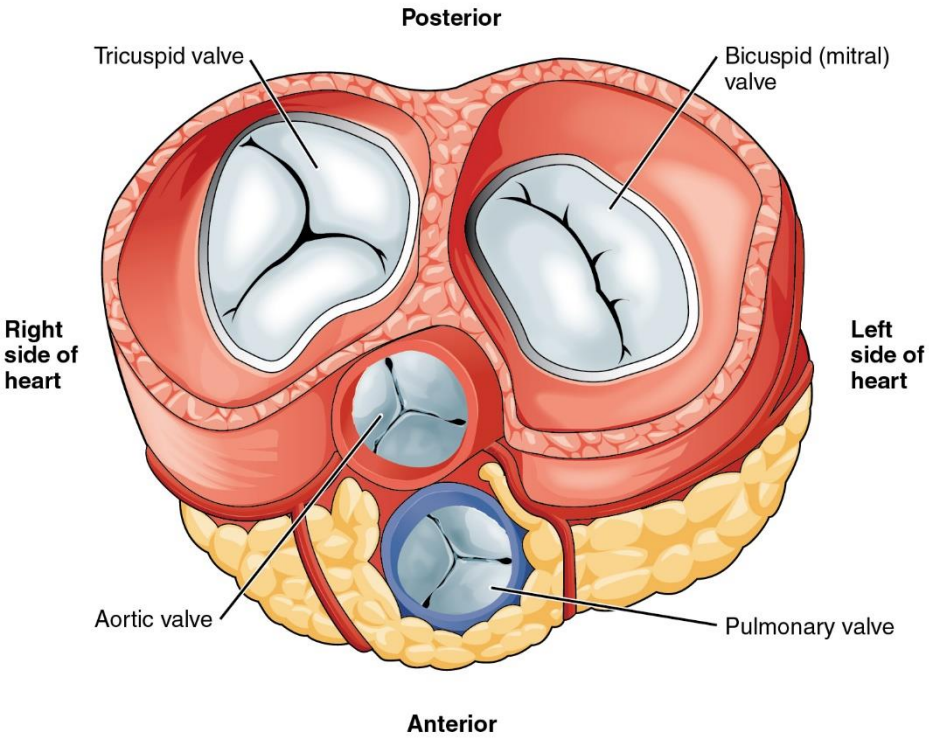

Figure 2.5: With the atria and major vessels removed, all four valves are clearly visible, although it is difficult to distinguish the three separate cusps of the tricuspid valve (Betts, 2013).

The papillary muscles (Figure 2.6) extend from the walls of the heart to the valves by cartilaginous connections called chordae tendinae. These muscles prevent the valves from falling too far back when they close. During the relaxation phase of the cardiac cycle, the papillary muscles are also relaxed and the tension on the chordae tendineae is slight. As the heart chambers contract, so do the papillary muscles. This creates tension on the chordae tendineae, helping to hold the cusps of the atrioventricular valves in place and preventing them

from being blown back into the atria. Two additional semilunar valves sit at the exit of each of the ventricles. The pulmonary valve is located at the base of the pulmonary artery. This has three cusps, which are not attached to any papillary muscles. When the ventricle relaxes blood flows back into the ventricle from the artery and this flow of blood fills the pocket-like valve, pressing against the cusps which close to seal the valve. The semilunar aortic valve is at the base of the aorta and also is not attached to papillary muscles. This too has three cusps, which close by the pressure of the blood flowing back from the aorta (Susan, 2008; Betts, 2013).

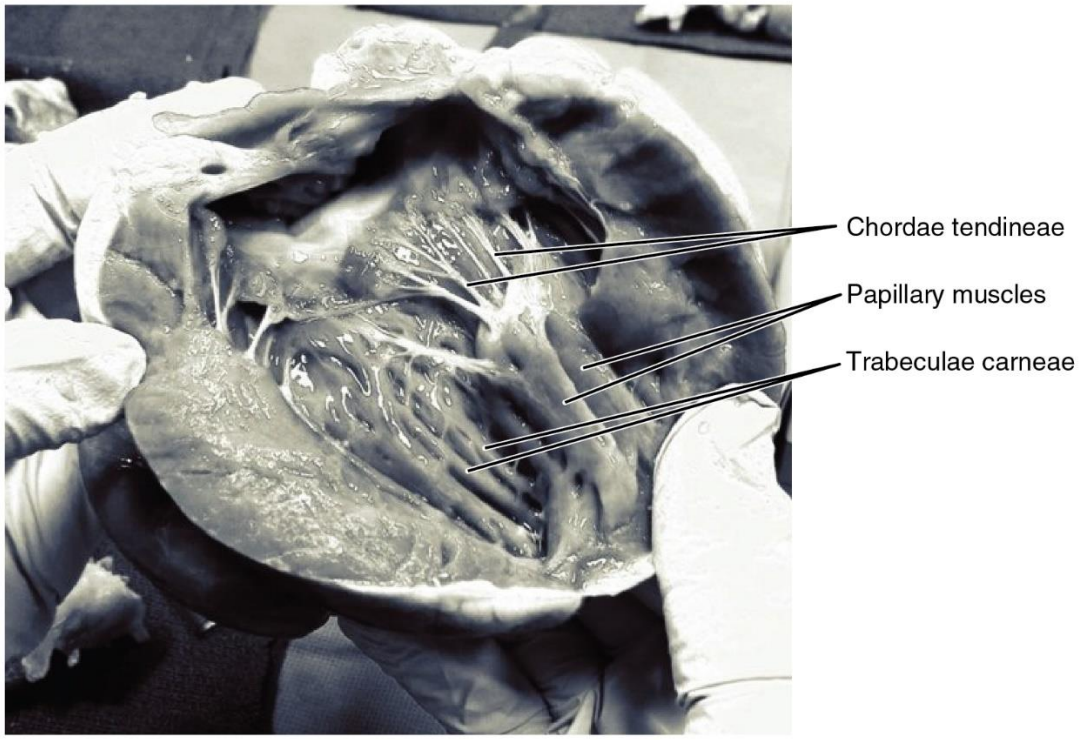

Figure 2.6: In this frontal section, you can see papillary muscles attached to the tricuspid valve on the right as well as the mitral valve on the left via chordae tendineae (Betts, 2013).

2.1.5 Heart wall

The heart wall is made up of three layers: the inner endocardium, middle myocardium and outer epicardium (Figure 2.7). These are surrounded by a double-membraned sac called the pericardium. The innermost layer of the heart is called the endocardium. It is made up of a

lining of simple squamous epithelium and covers heart chambers and valves. It is continuous with the endothelium of the veins and arteries of the heart, and is joined to the myocardium with a thin layer of connective tissue (Betts, 2013).

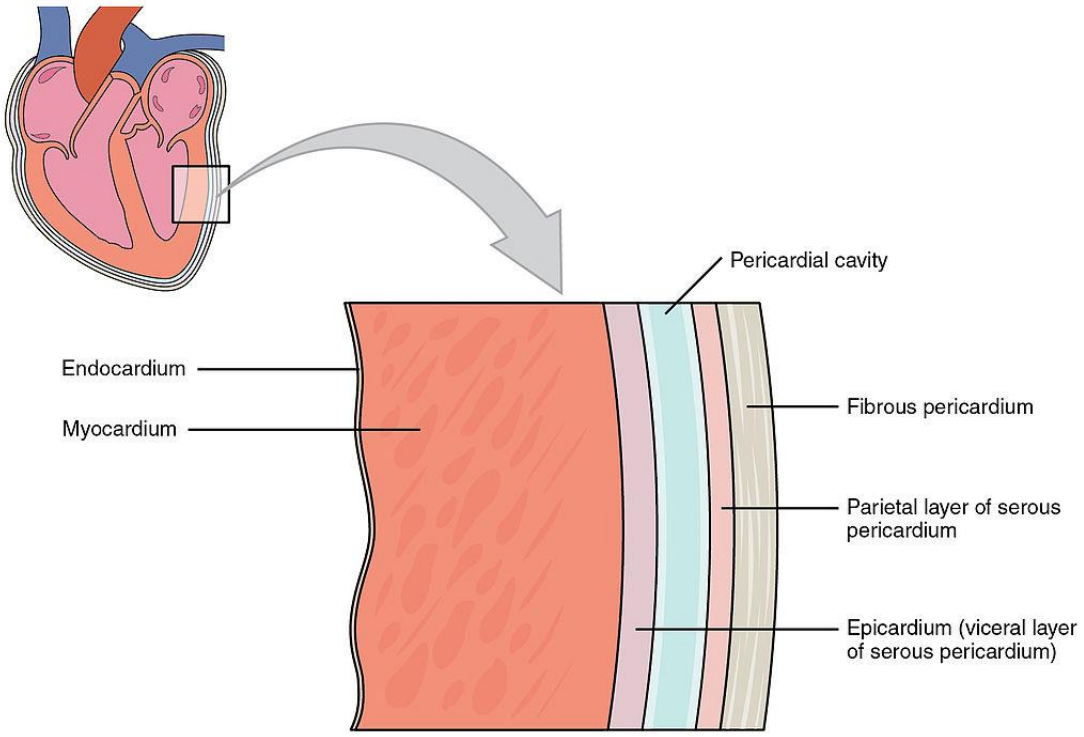

Figure 2.7: Layers of the heart wall, including visceral and parietal pericardium (Betts, 2013).

The endocardium, by secreting endothelins, may also play a role in regulating the contraction of the myocardium. The middle layer of the heart wall is the myocardium, which is the cardiac muscle – a layer of involuntary striated muscle tissue surrounded by a framework of collagen. The cardiac muscle pattern is elegant and complex, as the muscle cells swirl and spiral around the chambers of the heart, with the outer muscles, forming a figure 8 pattern around the atria and around the bases of the great vessels and the inner muscles, forming a figure 8 around the two ventricles and proceeding toward the apex. This complex swirling pattern allows the heart to pump blood more effectively (Betts, 2013).

There are two types of cells in cardiac muscle: muscle cells, which have the ability to contract easily, and pacemaker cells of the conducting system. The muscle cells make up the bulk (99%) of cells in the atria and ventricles. These contractile cells are connected by intercalated discs, which allow a rapid response to impulses of action potential from the pacemaker cells. The intercalated discs allow the cells to act as a syncytium and enable the contractions that pump blood through the heart and into the major arteries. The pacemaker cells make up 1% of cells and form the conduction system of the heart. They are generally much smaller than the contractile cells and have few myofibrils, which gives them limited contractibility (Figure 2.8). Their function is similar in many respects to neurons. Cardiac muscle tissue has autorhythmicity, the unique ability to initiate a cardiac action potential at a fixed rate – spreading the impulse rapidly from cell to cell to trigger the contraction of the entire heart. There are specific proteins expressed in cardiac muscle cells. These are mostly associated with muscle contraction, and bind with actin, myosin, tropomyosin, and troponin (Uhlén et al., 2015).

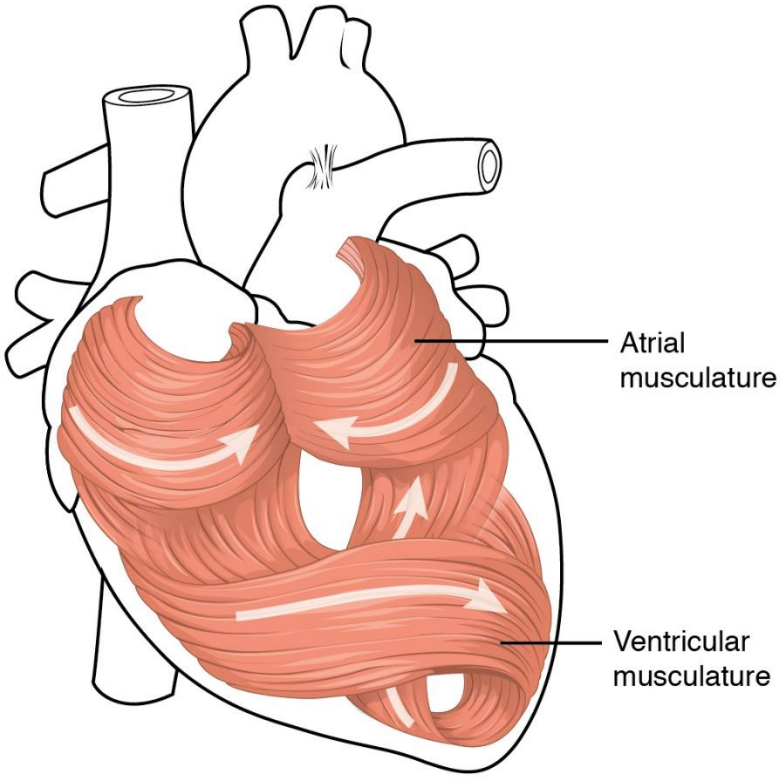

Figure 2.8: The swirling pattern of cardiac muscle tissue contributes significantly to the heart's ability to pump blood effectively (Uhlén et al., 2015).

2.1.6 Pericardium

The pericardium is the sack that surrounds the heart. The tough outer surface of the pericardium is called the fibrous membrane. This is lined with a double inner membrane called the serous membrane that produces pericardial fluid to lubricate the surface of the heart. The part of the serous membrane attached to the fibrous membrane is called the parietal pericardium, while the part of the serous membrane attached to the heart is known as the visceral pericardium (Figure 2.9). The pericardium is present in order to lubricate its movement against other structures within the chest, to keep the heart's position stabilized within the chest, and to protect the heart from infection (Tortora & Derrickson, 2009; Susan, 2008).

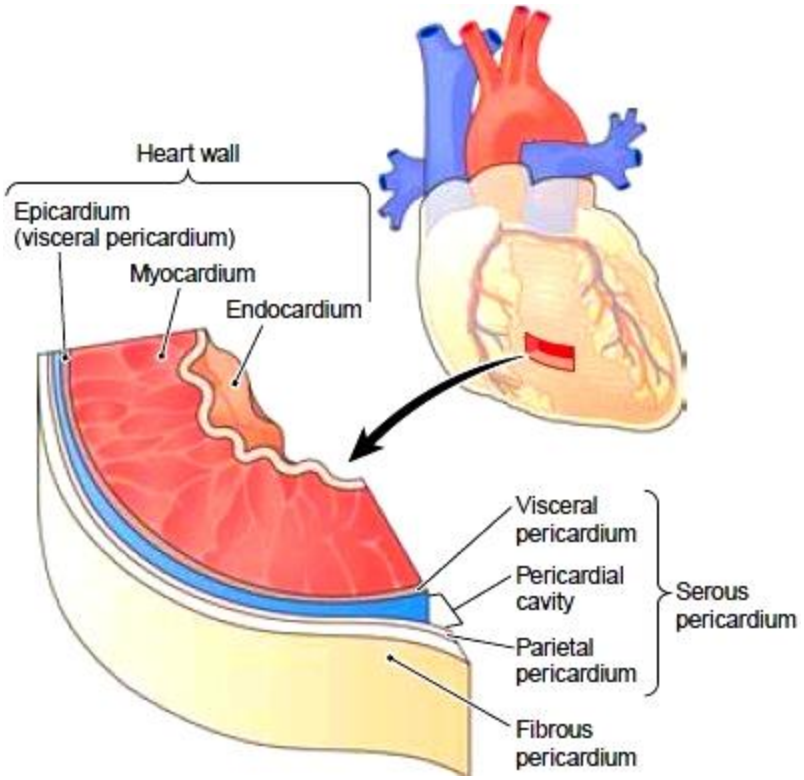

Figure 2.9: Labeled illustration of cardiac pericardium structure (Susan, 2008).

2.1.7 Coronary circulation

Heart tissue, like all cells in the body, needs to be supplied with oxygen, nutrients and a way of removing metabolic wastes. This is achieved by the coronary circulation as shown in Figure 2.10, which includes arteries, veins, and lymphatic vessels. Blood flow through the coronary vessels occurs in peaks and troughs relating to the heart muscle relaxation or contraction. Heart tissue receives blood from two arteries, which arise just above the aortic valve. These are the left main coronary artery and the right coronary artery. The left main coronary artery splits shortly after leaving the aorta into two vessels, the left anterior descending and the left circumflex artery. The left anterior descending artery supplies heart tissue and the front, outer side, and the septum of the left ventricle. It does this by branching into smaller arteries – diagonal and septal branches. The left circumflex supplies the back and underneath of the left ventricle. The right coronary artery supplies the right atrium, right ventricle, and lower posterior sections of the left ventricle. The right coronary artery also supplies blood to the

atrioventricular node (in about 90% of people) and the sinoatrial node (in about 60% of people). The right coronary artery runs in a groove at the back of the heart and the left anterior descending artery runs in a groove at the front. There is significant variation between people in the anatomy of the arteries that supply the heart. The arteries divide at their furthest reaches into smaller branches that join at the edges of each arterial distribution (Colledge et al., 2010).

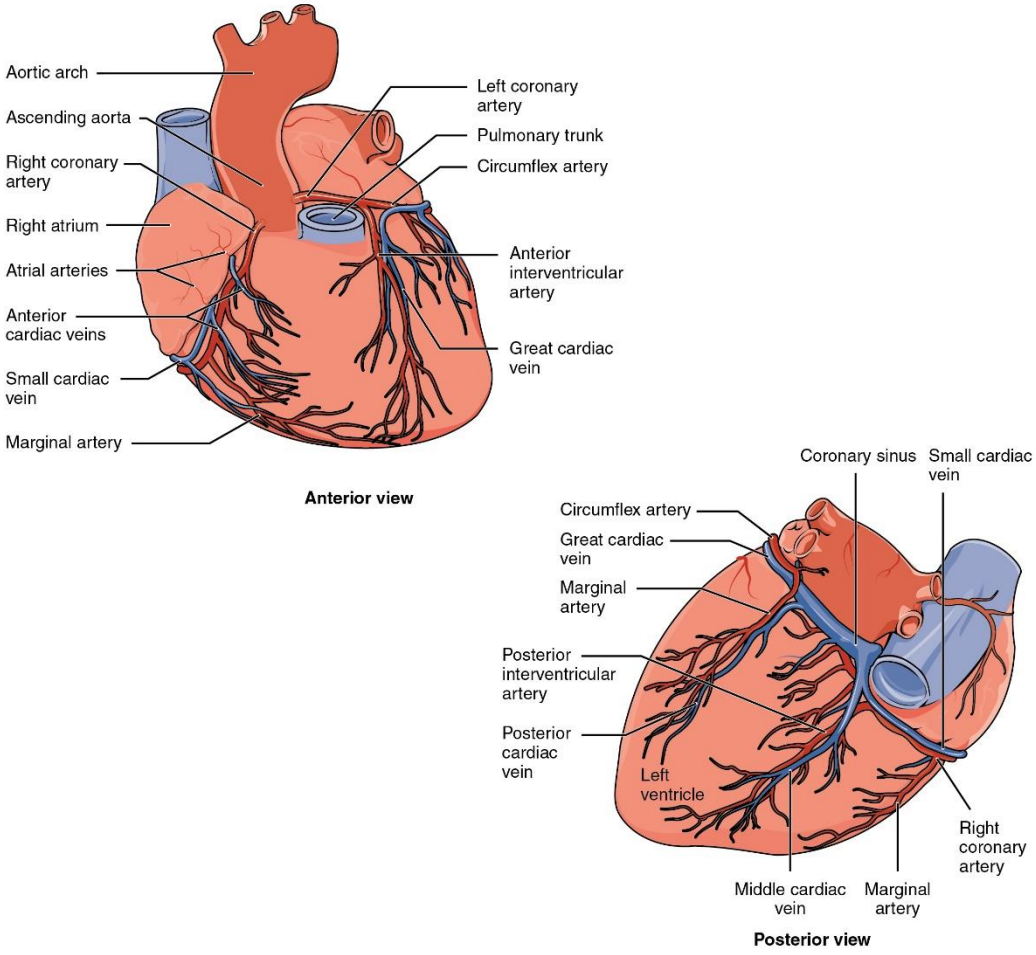

Figure 2.10: The anterior view of the heart, shows the prominent coronary surface vessels. The posterior view of the heart, shows the prominent coronary surface vessels (Colledge et al., 2010).

The coronary sinus is a large vein that drains into the right atrium, and receives most of the venous drainage of the heart. It receives blood from the great cardiac vein (receiving the left atrium and both ventricles), the posterior cardiac vein (draining the back of the left ventricle),

the middle cardiac vein (draining the bottom of the left and right ventricles), and small cardiac veins. The anterior cardiac veins drain the front of the right ventricle and drain directly into the right atrium. Small lymphatic networks, called plexuses exist beneath each of the three layers of the heart. These networks collect into a main left and a main right trunk, which travel up the groove between the ventricles that exists on the heart's surface, receiving smaller vessels as they travel up. These vessels then travel into the atrioventricular groove, and receive a third vessel, which drains the section of the left ventricle sitting on the diaphragm. The left vessel joins with this third vessel, and travels along the pulmonary artery and left atrium, ending in the inferior tracheobronchial node. The right vessel travels along the right atrium and the part of the right ventricle sitting on the diaphragm. Then it usually then travels in front of the ascending aorta and then ends with a brachiocephalic node (Susan, 2008).

2.1.8 Cardiac nerve supply

The heart receives nerve signals from the vagus nerve and from nerves arising from the sympathetic trunk (Figure 2.11). These nerves act to influence, but not control, the HR. Sympathetic nerves also influence the force of heart contraction. Signals that travel along these nerves arise from two paired cardiovascular centers in the medulla oblongata. The vagus nerve of the parasympathetic nervous system acts to decrease the HR, and nerves of the sympathetic trunk act to increase the HR. These nerves form a network of nerves that lies over the heart called the cardiac plexus. The vagus nerve is a long, wandering nerve that emerges from the brainstem and provides parasympathetic stimulation to a large number of organs in the thorax and abdomen, including the heart (Susan, 2008; Betts, 2013; Colledge et al., 2010).

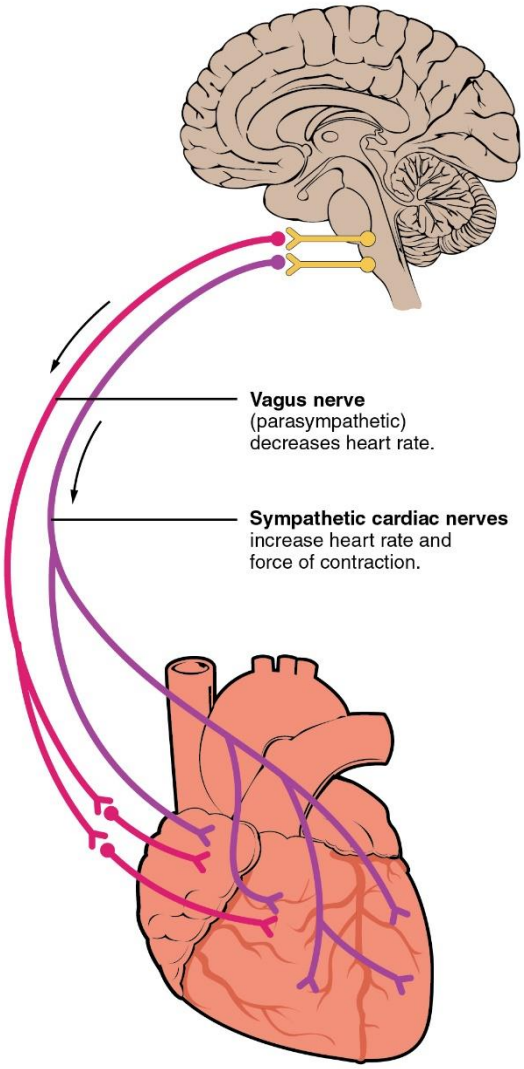

Figure 2.11: Autonomic innervation of the heart (Susan, 2008).

The nerves from the sympathetic trunk emerge through the T1-T4 thoracic ganglia and travel to both the sinoatrial and atrioventricular nodes, as well as to the atria and ventricles. The ventricles are more richly innervated by sympathetic fibers than parasympathetic fibers. Sympathetic stimulation causes the release of the neurotransmitter norepinephrine (also known as noradrenaline) at the neuromuscular junction of the cardiac nerves. This shortens the repolarization period, thus speeding the rate of depolarization and contraction, which results in an increased HR. It opens chemical or ligand-gated sodium and calcium ion channels, allowing an influx of positively charged ions. Norepinephrine binds to the beta–1 receptor (Susan, 2008; Betts, 2013; Colledge et al., 2010).

2.2 Heart physiology

2.2.1 Heart function

The heart functions as a pump in the circulatory system to provide a continuous flow of blood throughout the body. This circulation consists of the systemic circulation to and from the body and the pulmonary circulation to and from the lungs. Blood in the pulmonary circulation exchanges carbon dioxide for oxygen in the lungs through the process of respiration. The systemic circulation, then transports oxygen to the body and returns carbon dioxide and relatively deoxygenated blood to the heart for transfer to the lungs (Betts, 2013).

The right heart collects deoxygenated blood from two large veins, the superior and inferior venae cavae. Blood collects on the right and left atrium continuously. The superior vena cava drains blood from above the diaphragm and empties into the upper back part of the right atrium. The inferior vena cava drains the blood from below the diaphragm and empties into the back part of the atrium below the opening for the superior vena cava. Immediately above and in the middle of the opening of the inferior vena cava is the opening of the thin-walled coronary sinus. Additionally, the coronary sinus returns deoxygenated blood from the myocardium to the right atrium. The blood collects in the right atrium. When the right atrium contracts, the blood is pumped through the tricuspid valve into the right ventricle. As the right ventricle contracts, the tricuspid valve closes and the blood is pumped into the pulmonary trunk through the pulmonary valve. The pulmonary trunk divides into pulmonary arteries and progressively smaller arteries throughout the lungs, until it reaches capillaries. As these passes by alveoli, carbon dioxide is exchanged for oxygen. This happens through the passive process of diffusion (Betts, 2013).

In the left heart, oxygenated blood is returned to the left atrium via the pulmonary veins. It is then pumped into the left ventricle through the mitral valve and into the aorta through the aortic valve for systemic circulation. The aorta is a large artery that branches into many smaller arteries, arterioles, and ultimately capillaries. In the capillaries, oxygen and nutrients from

blood supply to body cells for metabolism, and exchanged for carbon dioxide and waste products. Capillary blood, now deoxygenated, travels into venules and veins that ultimately collect in the superior and inferior vena cavae, and into the right heart (Betts, 2013).

2.2.2 Cardiac cycle

The cardiac cycle refers to the sequence of events in which the heart contracts and relaxes with every heartbeat (Hall, 2009). The period of time during which the ventricles contract, forcing blood out into the aorta and main pulmonary artery, is known as systole, while the period during which the ventricles relax and refill with blood is known as diastole. The atria and ventricles work in concert, so in systole when the ventricles are contracting, the atria are relaxed and collecting blood. When the ventricles are relaxed in diastole, the atria contract to pump blood to the ventricles. This coordination ensures blood is pumped efficiently to the body (Betts, 2013).

At the beginning of the cardiac cycle (Figure 2.12), the ventricles are relaxing. As they do so, they are filled with blood passing through the open mitral and tricuspid valves. After the ventricles have completed most of their filling, the atria contract, forcing further blood into the ventricles and priming the pump. Next, the ventricles start to contract. As the pressure, rises within the cavities of the ventricles, the mitral and tricuspid valves are forced shut. As the pressure within the ventricles rises further, exceeding the pressure with the aorta and pulmonary arteries, the aortic and pulmonary valves open. Blood is ejected from the heart, causing the pressure within the ventricles to fall. Simultaneously, the atria refill as blood flows into the right atrium through the superior and inferior vena cavae, and into the left atrium through the pulmonary veins. Finally, when the pressure within the ventricles falls below the pressure within the aorta and pulmonary arteries, the aortic and pulmonary valves close. The

ventricles start to relax, the mitral and tricuspid valves open, and the cycle begins again (Hall, 2009).

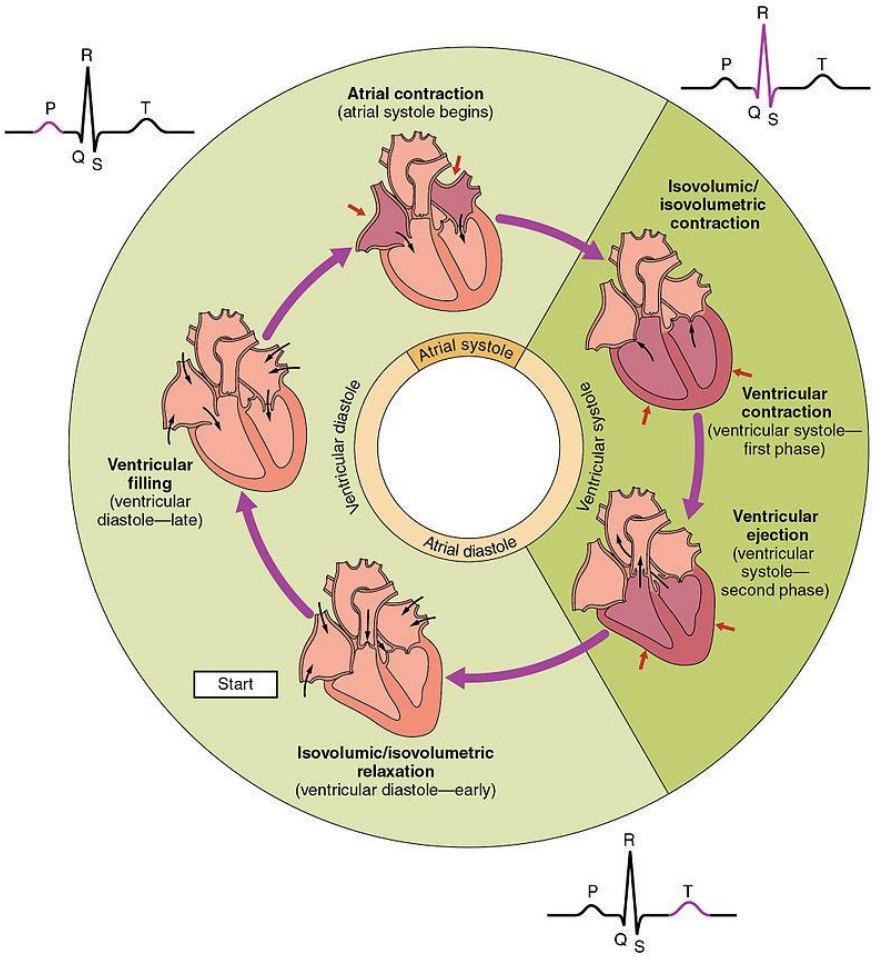

Figure 2.12: The cardiac cycle as correlated to the ECG (Hall, 2009).

2.2.3 Cardiac output (CO)

Cardiac output (CO) is a measurement of the amount of blood pumped by each ventricle (stroke volume) in one minute. This is calculated by multiplying the stroke volume (SV) by the beats per minute of the HR. So that: CO = SV x HR (Figure 2.13). The CO is normalized to body size through body surface area and is called the cardiac index. The average CO, using an average SV of about 70mL, is 5.25 L/min, with a normal range of 4.0–8.0 L/min. The SV is normally measured using an echocardiogram (Figure 2.14) and can be influenced by the size

of the heart, the physical and mental condition of the individual, sex, contractility, duration of contraction, preload and afterload (Betts, 2013).

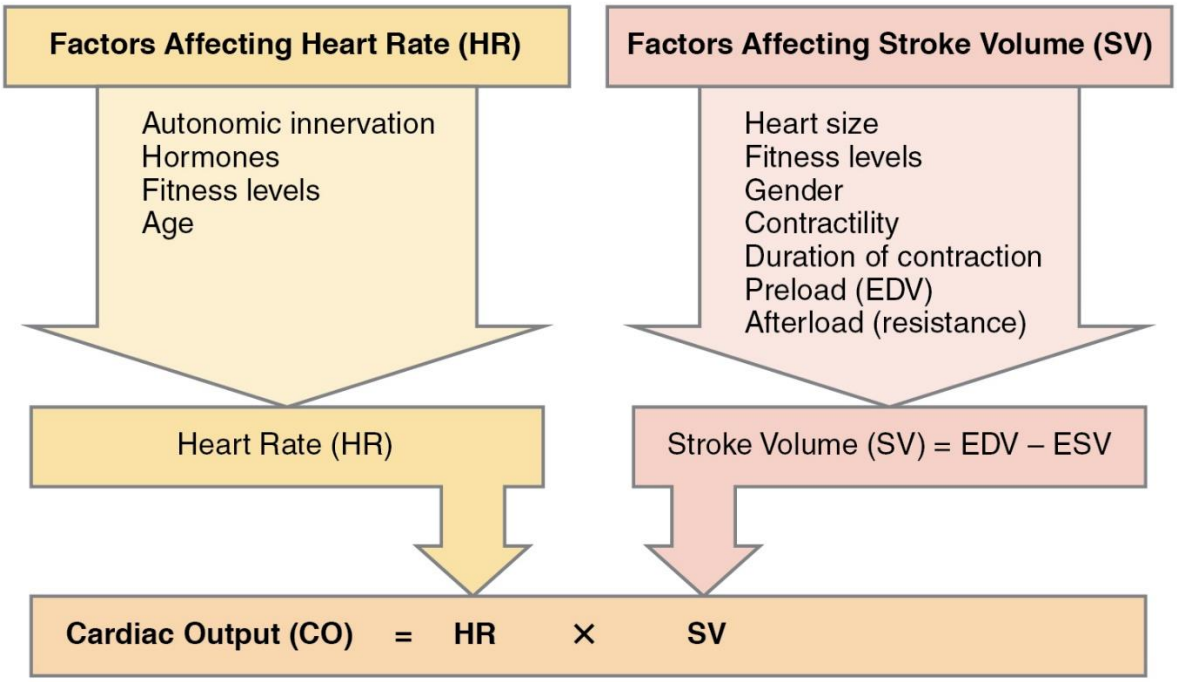

Figure 2.13: Cardiac output (CO) is influenced by heart rate (HR) and stroke volume (SV), both of which are variable (Betts, 2013).

Preload refers to the filling pressure of the atria at the end of diastole, when the ventricles are at their fullest. A main factor is how long it takes the ventricles to fill: if the ventricles contract more frequently, then there is less time to fill and the preload will be less. The preload can also be affected by a person's blood volume. The force of each contraction of the heart muscle is proportional to the preload, described as the Frank-Starling mechanism. This states that the force of contraction is directly proportional to the initial length of muscle fiber, meaning a ventricle will contract more forcefully, the more it is stretched (Betts, 2013; Hall, 2011).

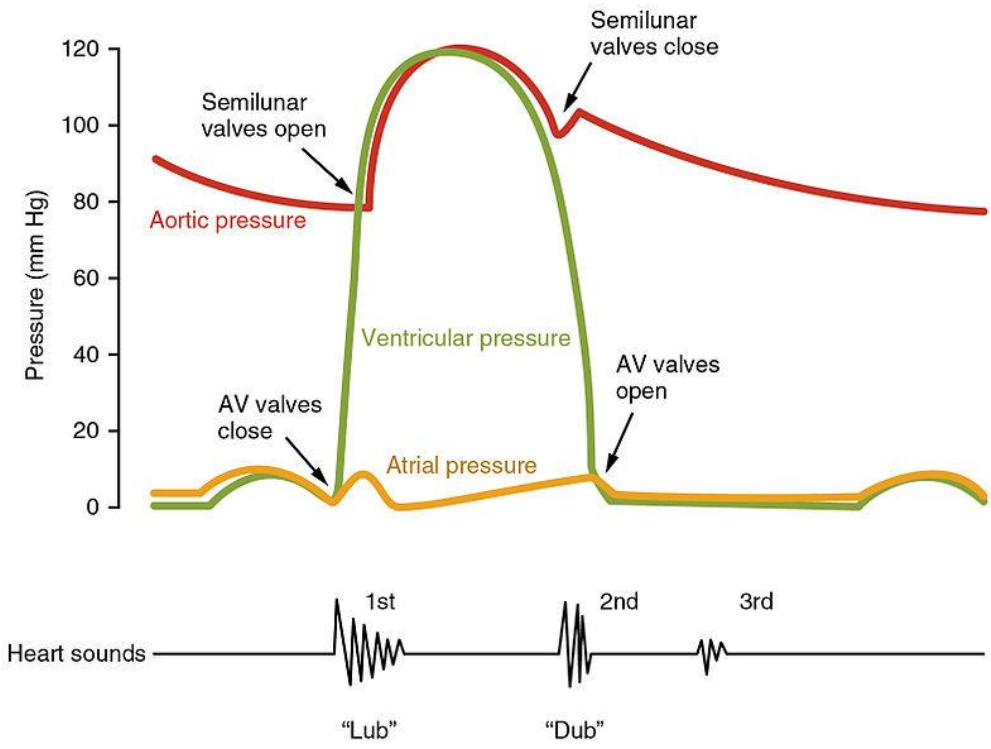

Figure 2.14: The x-axis reflects time with a recording of the heart sounds. The y-axis represents the pressure (Betts, 2013).

Afterload, or how much pressure the heart must generate to eject blood at systole, is influenced by vascular resistance. It can be influenced by narrowing of the heart valves (stenosis) or contraction or relaxation of the peripheral blood vessels (Betts, 2013). The strength of heart muscle contractions controls the SV. Agents termed inotropes can influence this positively or negatively. These agents can be a result of changes within the body, or be given as drugs as part of treatment for a medical disorder, or as a form of life support, particularly in intensive care units. Inotropes that increase the force of contraction are "positive" inotropes, and include sympathetic agents such as adrenaline, noradrenaline and dopamine. Negative inotropes decrease the force of contraction and include calcium channel blockers (Berry & Catherine, 2010; Andrew, 2013).

2.2.4 Electrical conduction

The normal rhythmical heartbeat, called sinus rhythm, is established by the sinoatrial node, the heart's pacemaker. Here an electrical signal is created that travels through the heart, causing the heart muscle to contract. The sinoatrial node is found in the upper part of the right atrium near to the junction with the superior vena cava. The electrical signal generated by the sinoatrial node travels through the right atrium in a radial way that is not completely understood. It travels to the left atrium via Bachmann's bundle, such that the muscles of the left and right atria contract together as presented in Figure 2.15 (De et al., 2002).

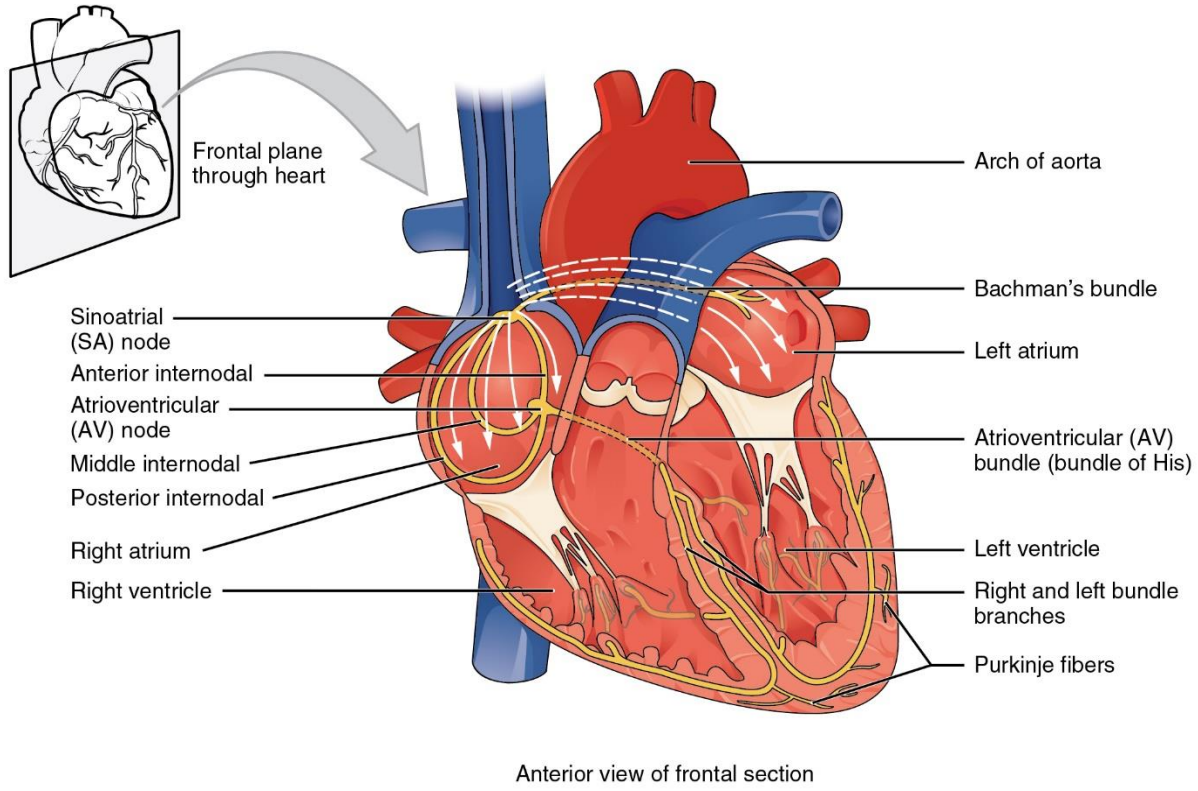

Figure 2.15: Specialized conducting components of the heart include the sinoatrial node, the internodal pathways, the atrioventricular node, the atrioventricular bundle, the right and left bundle branches, and the Purkinje fibers (De et al., 2002).

The signal then travels to the atrioventricular node. This is found at the bottom of the right atrium in the atrioventricular septum – the boundary between the right atrium and the left

ventricle. The septum is part of the cardiac skeleton, tissue within the heart that the electrical signal cannot pass through, which forces the signal to pass through the atrioventricular node only. The signal then travels along the bundle of His to left and right bundle branches through to the ventricles of the heart. In the ventricles, the signal is carried by specialized tissue called the Purkinje fibers, which then transmit the electric charge to the heart muscle as demonstrated in Figure 2.15 (De et al., 2002).

2.2.5 Heart rate (HR)

The normal resting HR is called the sinus rhythm, created and sustained by the sinoatrial node, a group of pacemaking cells found in the wall of the right atrium (Figure 2.16). Cells in the sinoatrial node do this by creating an action potential. The cardiac action potential is created by the movement of specific electrolytes into and out of the pacemaker cells. The action potential, then spreads to nearby cells. When the sinoatrial cells are resting, they have a negative charge on their membranes. However, a rapid influx of sodium ions causes the membrane's charge to become positive. This is called depolarization and occurs spontaneously. Once the cell has a sufficiently high charge, the sodium channels close and calcium ions then begin to enter the cell, shortly after which potassium begins to leave it. All the ions travel through ion channels in the membrane of the sinoatrial cells. The potassium and calcium start to move out of and into the cell only once it has a sufficiently high charge, and so are called voltage-gated. Shortly after this, the calcium channels close and potassium channels open, allowing potassium to leave the cell. This causes the cell to have a negative resting charge and is called repolarization. When the membrane potential reaches approximately – 60 mV, the potassium channels close and the process may begin again (Hall, 2011).

The ions move from areas where they are concentrated to where they are not. For this reason sodium moves into the cell from outside, and potassium moves from within the cell to outside

the cell. Calcium also plays a critical role. Their influx through slow channels means that the sinoatrial cells have a prolonged “plateau” phase when they have a positive charge. A part of this is called the absolute refractory period. Calcium ions also combine with the regulatory protein troponin C in the troponin complex to enable contraction of the cardiac muscle, and separate from the protein to allow relaxation. The adult resting HR ranges from 60 to 100 bpm. The resting HR of a newborn can be 129 bpm and this gradually decreases until maturity. An athlete's HR can be lower than 60 bpm. During exercise, the rate can be 150 bpm with maximum rates reaching from 200 to 220 bpm (Davis & Tikunova, 2008).

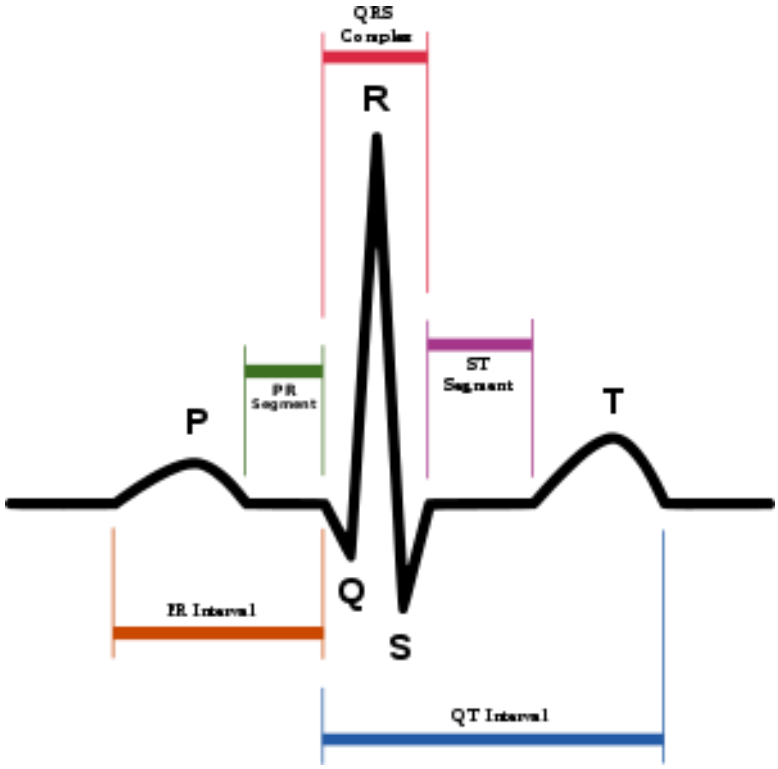

Figure 2.16: Schematic representation of normal sinus rhythm showing standard wave, segments, and intervals (Davis & Tikunova, 2008).

2.2.6 Influences on heart rate (HR)

The normal sinus rhythm of the heart, giving the resting HR, is influenced a number of factors. The cardiovascular centers in the brainstem that control the sympathetic and parasympathetic

influences to the heart through the vagus nerve and sympathetic trunk. These cardiovascular centers receive input from a series of receptors, including baroreceptors, sensing stretch the stretching of blood vessels and chemoreceptors, sensing the amount of oxygen and carbon dioxide in the blood and its pH. Through a series of reflexes, these help regulate and sustain blood flow (Hall, 2011).

Baroreceptors are stretch receptors located in the aortic sinus (Figure 2.17), carotid bodies, the venae cavae, and other locations, including pulmonary vessels and the right side of the heart itself. Baroreceptors fire at a rate determined by how much they are stretched, which is influenced by blood pressure, level of physical activity, and the relative distribution of blood. With increased pressure and stretch, the rate of baroreceptor firing increases, and the cardiac centers decrease sympathetic stimulation and increase parasympathetic stimulation. As pressure and stretch decrease, the rate of baroreceptor firing decreases, and the cardiac centers increase sympathetic stimulation and decrease parasympathetic stimulation. There is a similar reflex, called the atrial reflex or Bainbridge reflex, associated with varying rates of blood flow to the atria. Increased venous return stretches the walls of the atria where specialized baroreceptors are located. However, as the atrial baroreceptors increase their rate of firing and as they stretch due to the increased blood pressure, the cardiac center responds by increasing sympathetic stimulation and inhibiting parasympathetic stimulation to increase HR. The opposite is also true. Chemoreceptors present in the carotid body or adjacent to the aorta in an aortic body respond to the blood's oxygen, carbon dioxide levels. Low oxygen or high carbon dioxide will stimulate firing of the receptors (Betts, 2013; Hall, 2011).

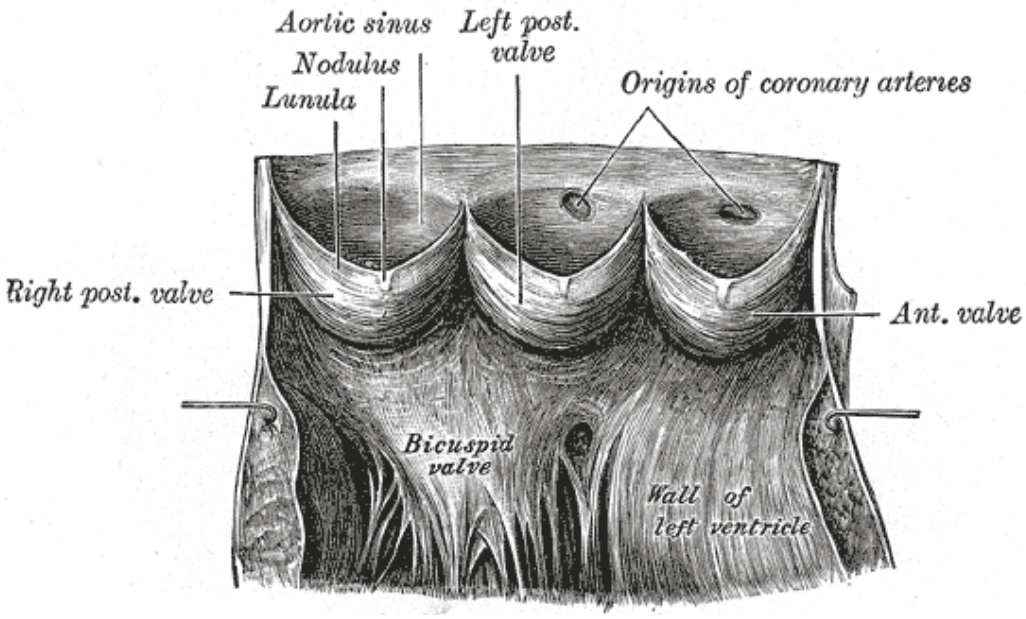

Figure 2.17: An aortic sinus is one of the anatomic dilations of the ascending aorta, which occurs just above the aortic valve. These widenings are between the wall of the aorta and each of the three cusps of the aortic valve (Hall, 2011).

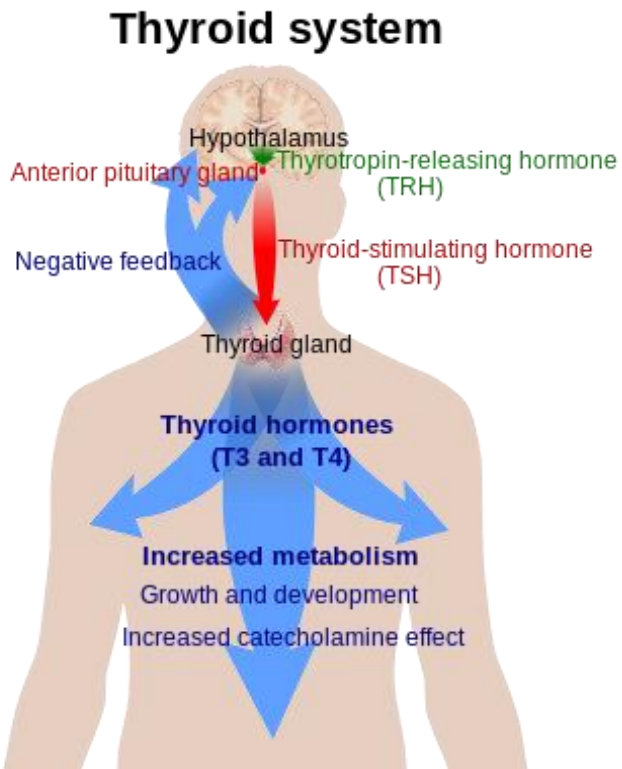

Figure 2.18: The thyroid system of the thyroid hormones T3 and T4 (Betts, 2013).

Exercise and fitness levels, age, body temperature, basal metabolic rate, and even a person's emotional state can all affect the HR. High levels of the hormones epinephrine, norepinephrine, and thyroid hormones (Figure 2.18) can increase the HR. The levels of electrolytes including calcium, potassium, and sodium can also influence the speed and regularity of the HR; low blood oxygen, low blood pressure and dehydration may increase it (Betts, 2013).

2.3 Heart pathology

CVDs, which include diseases of the heart, are the leading cause of death worldwide. The majority of CVDs are noncommunicable and related to lifestyle and other factors, becoming more prevalent with ageing. Heart disease is a major cause of death, accounting for an average of 30% of all deaths in 2008, globally. This rate varies from a low 28% to a high 40% in high-income countries. Doctors that specialize in the heart are called cardiologists. Many other medical professionals are involved in treating diseases of the heart, including doctors, such as general practitioners, cardiothoracic surgeons and intensivists, and allied health practitioners including physiotherapists and dieticians (Fauci et al., 2011).

2.3.1 Ischemic heart disease (IHD) or coronary artery disease (CAD)

CAD, also known as IHD, is caused by atherosclerosis—a build-up of fatty material along the inner walls of the arteries (Figure 2.19). These fatty deposits known as atherosclerotic plaques narrow the coronary arteries, and if severe may reduce blood flow to the heart. If a narrowing (or stenosis) is relatively minor, then the patient may not experience any symptoms. Severe narrowings may cause chest pain (angina) or breathlessness during exercise or even at rest. The thin covering of an atherosclerotic plaque can rupture, exposing the fatty center to the circulating blood. In this case a clot or thrombus can form, blocking the artery, and restricting blood flow to an area of the heart muscle, causing a MI (a heart attack) or unstable angina. In the worst case, this may cause cardiac arrest, a sudden and utter loss of output from the heart. Obesity, high blood pressure, uncontrolled diabetes, smoking and high cholesterol can all increase the risk of developing atherosclerosis and coronary artery disease (Fauci et al., 2011).

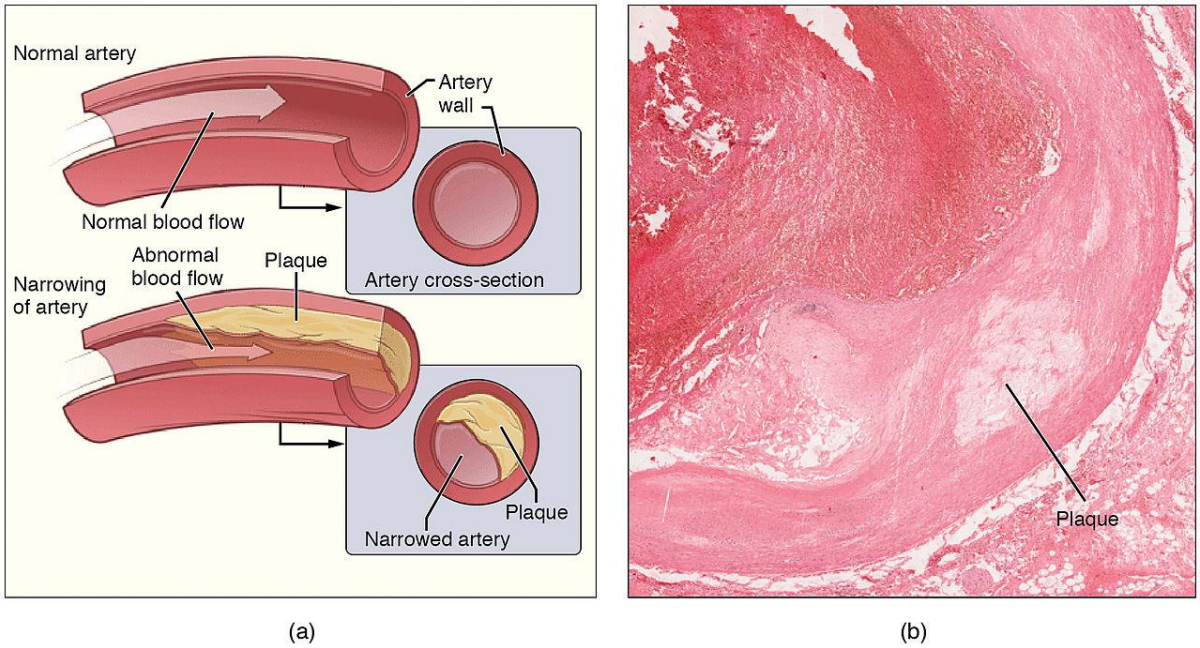

Figure 2.19: Atherosclerosis is a condition affecting the circulatory system. If the coronary arteries are affected, angina pectoris may result or at worse a heart attack. (Fauci et al., 2011).

2.3.2 Heart failure

Heart failure is defined as a condition in which the heart is unable to pump enough blood to meet the demands of the body (Figure 2.20). Patients with heart failure may experience breathlessness especially when lying flat, as well as ankle swelling, known as peripheral oedema. Heart failure is the end result of many diseases affecting the heart, but is most commonly associated with ischemic heart disease, valvular heart disease, or high blood pressure. Less common causes include various cardiomyopathies. Heart failure is frequently associated with weakness of the heart muscle in the ventricles (systolic heart failure), but can also be seen in patients with heart muscle that is strong but stiff (diastolic heart failure). The condition may affect the left ventricle (causing predominantly breathlessness), the right ventricle (causing predominantly swelling of the legs and an elevated jugular venous pressure), or both ventricles. Patients with heart failure are at higher risk of developing dangerous heart rhythm disturbances or arrhythmias (Ponikowski et al., 2016).

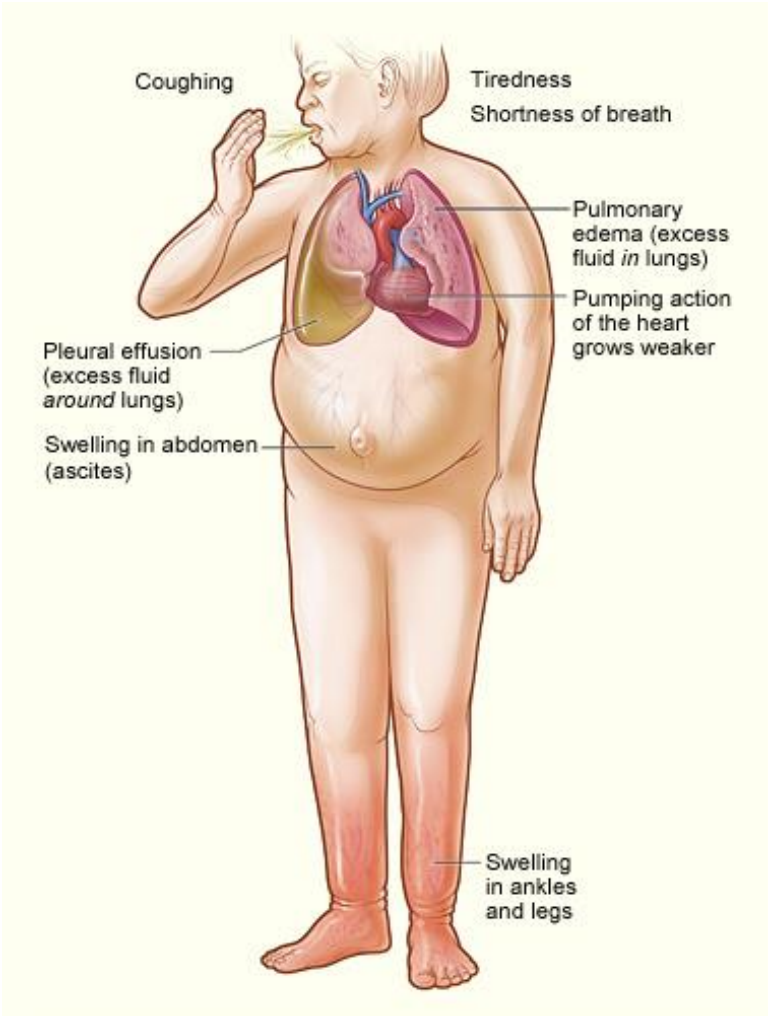

Figure 2.20: The illustration shows the major signs and symptoms of heart failure (Ponikowski et al., 2016).

2.3.3 Cardiomyopathies

Cardiomyopathies are diseases affecting the muscle of the heart. Some cause abnormal thickening of the heart muscle (hypertrophic cardiomyopathy), some cause the heart to abnormally expand and weaken (dilated cardiomyopathy; DCM) (Figure 2.21), some cause the heart muscle to become stiff and unable to fully relax between contractions (restrictive cardiomyopathy) (Figure 2.22) and some make the heart prone to abnormal heart rhythms (arrhythmogenic cardiomyopathy). These conditions are often genetic and can be inherited, but some, such as DCM may be caused by damage from toxins such as alcohol. Some cardiomyopathies such as hypertrophic cardiomyopathy are linked to a higher risk of sudden

cardiac death, particularly in athletes. Many cardiomyopathies can lead to heart failure in the later stages of the disease (Ponikowski et al., 2016).

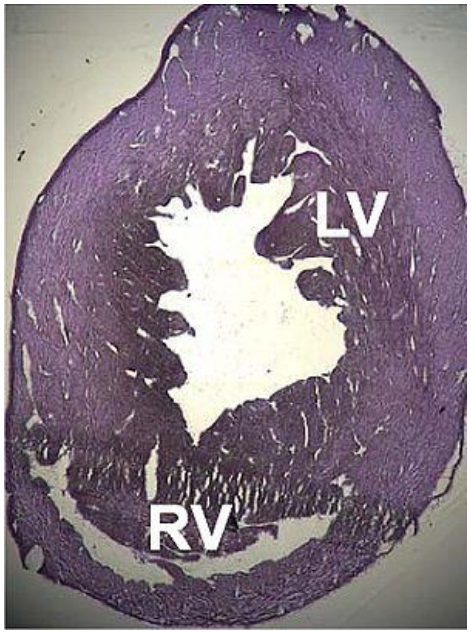

Figure 2.21: Dilated cardiomyopathy (DCM) is a condition in which the heart becomes enlarged and cannot pump blood effectively. (Ponikowski et al., 2016).

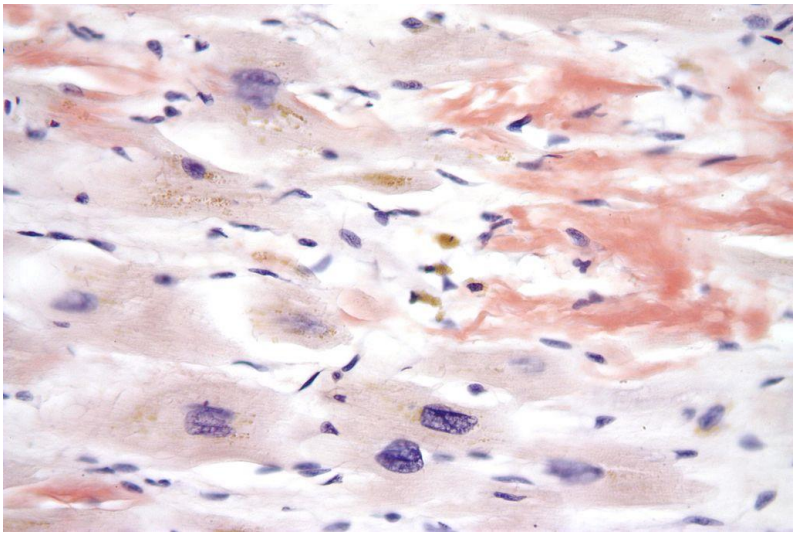

Figure 2.22: High magnification micrograph of senile cardiac amyloidosis. Congo red stain. Autopsy specimen. The micrograph shows amyloid (extracellular washed-out red material) and abundant lipofuscin (yellow granular material) (Ponikowski et al., 2016).

2.3.4 Valvular heart disease

Healthy heart valves allow blood to flow easily in one direction, but prevent it from flowing in the other direction. Diseased heart valves may have a narrow opening and therefore restrict the flow of blood in the forward direction (referred to as a stenotic valve) (Figure 2.23), or may allow blood to leak in the reverse direction (referred to as valvular regurgitation). Valvular heart disease may cause breathlessness, blackouts, or chest pain, but may be asymptomatic and only detected on a routine examination by hearing abnormal heart sounds or a heart murmur (Figure 2.24) (Vahanian et al., 2012).

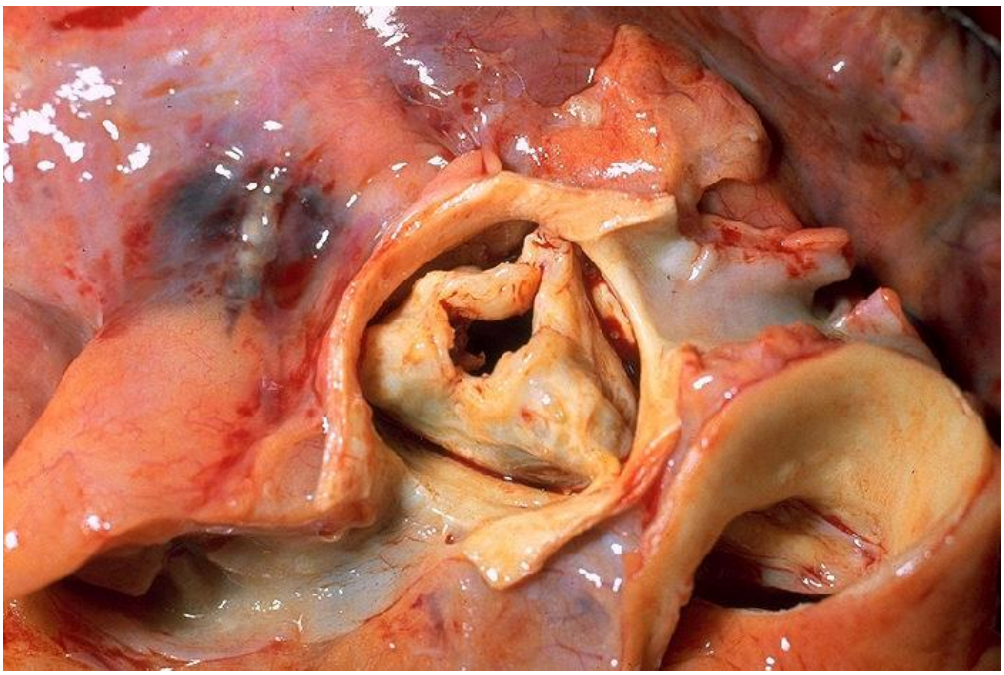

Figure 2.23: Gross pathology of rheumatic heart disease: aortic stenosis. The aorta has been removed to show thickened, fused aortic valve leaflets and opened coronary arteries from above (Vahanian et al., 2012).

In the developed world, valvular heart disease is most commonly caused by degeneration secondary to old age, but may also be caused by infection of the heart valves (endocarditis). In some parts of the world rheumatic heart disease is a major cause of valvular heart disease,

typically leading to mitral or aortic stenosis and caused by the body's immune system reacting to a streptococcal throat infection (Vahanian et al., 2012).

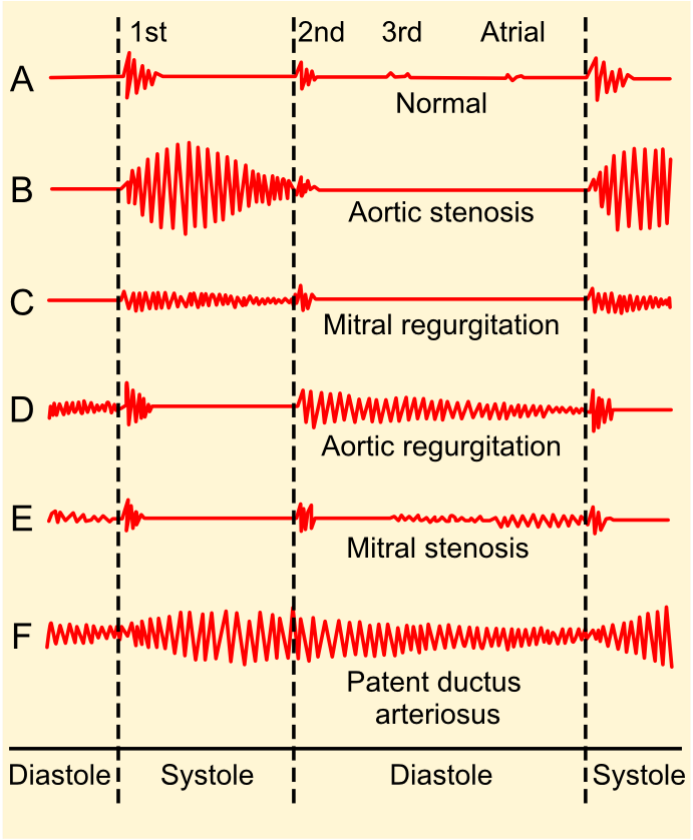

Figure 2.24: Phonocardiograms from normal and abnormal heart sounds (Vahanian et al., 2012).

2.3.5 Cardiac arrhythmias

While in the healthy heart, waves of electrical impulses originate in the sinus node before spreading to the rest of the atria, the atrioventricular node, and finally the ventricles (referred to as a normal sinus rhythm), this normal rhythm can be disrupted (Figure 2.25). Abnormal heart rhythms or arrhythmias may be asymptomatic or may cause palpitations, blackouts, or breathlessness. Some types of arrhythmia such as atrial fibrillation increase the long-term risk of stroke (Kirchhof et al., 2016).

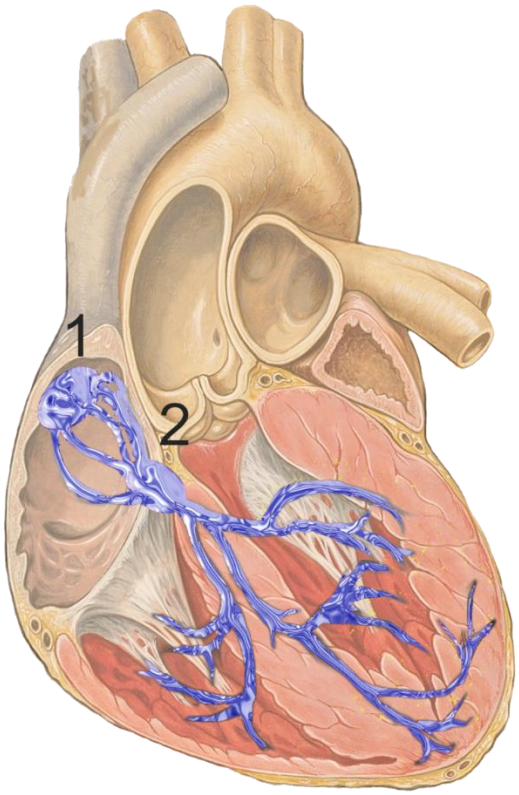

Figure 2.25: Image shows the conduction system of the heart. The sinoatrial node is labelled (1) and the artrioventricular node is labelled (2) (Kirchhof et al., 2016).

Some arrhythmias cause the heart to beat abnormally slowly, referred to as a bradycardia or bradyarrhythmia. This may be caused by an abnormally slow sinus node or damage within the cardiac conduction system (heart block). In other arrhythmias the heart may beat abnormally rapidly, referred to as a tachycardia or tachyarrhythmia. These arrhythmias can take many forms and can originate from different structures within the heart—some arise from the atria (e.g. Atrial flutter), some from the atrioventricular node (e.g. Artrioventricular nodal reentrant tachycardia) whilst others arise from the ventricles (e.g. Ventricular tachycardia). Some tachyarrhythmias are caused by scarring within the heart (e.g. Some forms of ventricular tachycardia), others with an irritable focus (e.g. Focal atrial tachycardia), while others are caused by additional abnormal conduction tissue that has been present since birth (e.g. Wolff-Parkinson-White syndrome). The most dangerous form of heart racing is ventricular

fibrillation, in which the ventricles quiver rather than contract, and which, if untreated is rapidly fatal (Kirchhof et al., 2016).

2.3.6 Pericardial disease

The sac, which surrounds the heart, called the pericardium, can become inflamed in a condition known as pericarditis. This condition typically causes chest pain that may spread to the back, and is often caused by a viral infection (glandular fever, cytomegalovirus, or coxsackievirus). Fluid can build up within the pericardial sac, referred to as a pericardial effusion. Pericardial effusions often occur secondary to pericarditis, kidney failure, or tumors, and frequently do not cause any symptoms. However, large effusions or effusions, which accumulate rapidly, can compress the heart in a condition known as cardiac tamponade (Figure 2.26), causing breathlessness and potentially fatal low blood pressure. Fluid can be removed from the pericardial space for diagnosis or to relieve tamponade using a syringe in a procedure called pericardiocentesis (Colledge et al., 2010).

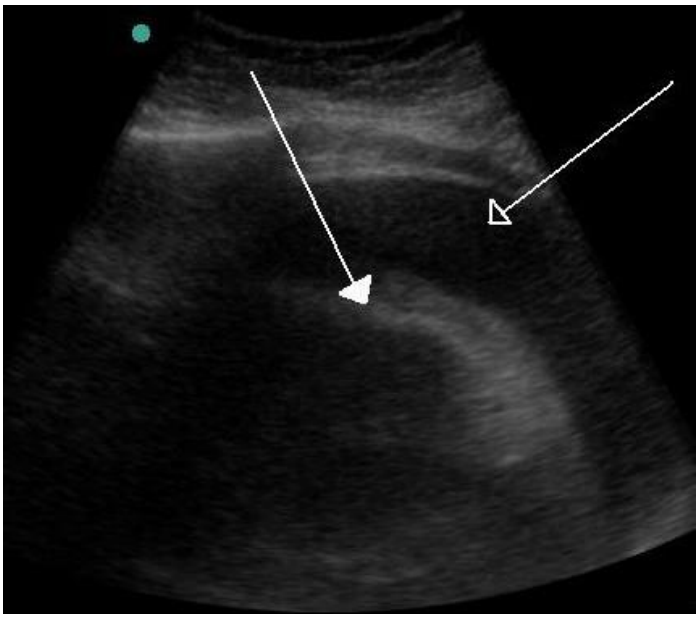

Figure 2.26: A very large pericardial effusion resulting in tamponade because of bleeding from cancer as seen on ultrasound. Closed arrow - the heart; open arrow - the effusion (Colledge et al., 2010).

2.3.6 Congenital heart disease

Some people are born with hearts that are abnormal and these abnormalities are known as congenital heart defects (Figure 2.27). They may range from the relatively minor (e.g. Patent foramen ovale, arguably a variant of normal) to serious life-threatening abnormalities, (e.g. hypoplastic left heart syndrome). Common abnormalities include those that affect the heart muscle that separates the two sides of the heart (a 'hole in the heart' e.g. ventricular septal defect). Other defects include those affecting the heart valves (e.g. Congenital aortic stenosis), or the main blood vessels that lead from the heart (e.g. Coarctation of the aorta). More complex syndromes are seen that affect more than one part of the heart (e.g. Tetralogy of Fallot) (Baumgartner et al., 2010).

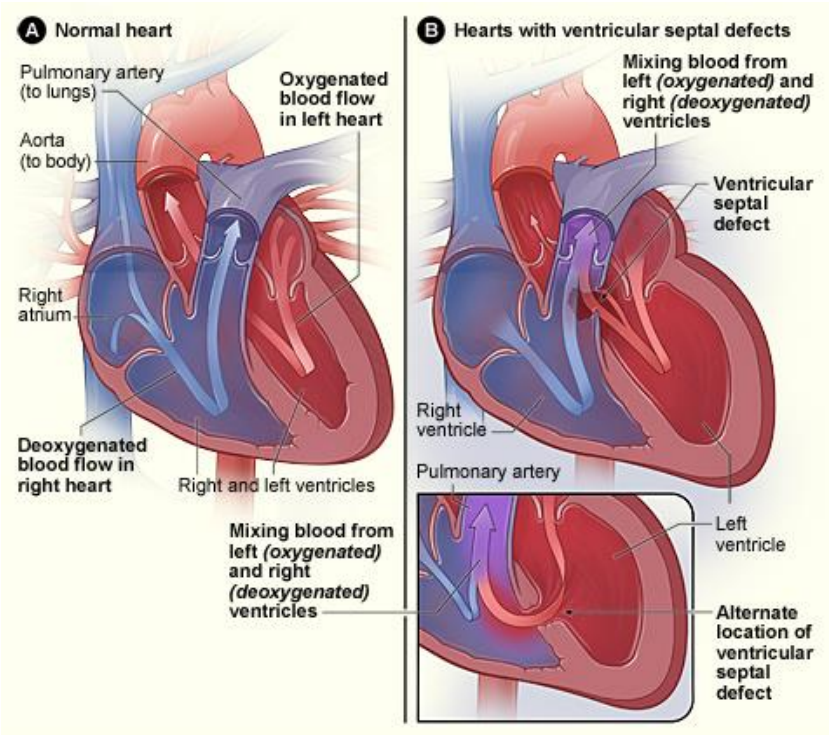

Figure 2.27: Shows the structure and blood flow in the interior of a normal heart (A). Two common locations for a ventricular septal defect (B). The defect allows oxygen-rich blood from the left ventricle to mix with oxygen-poor blood in the right ventricle (B) (Baumgartner et al., 2010).

Some congenital heart defects allow blood that is low in oxygen that would normally be returned to the lungs to instead be pumped back to the rest of the body. These are known as cyanotic congenital heart defects and are often more serious. Major congenital heart defects are often picked up in childhood, shortly after birth, or even before a child is born (e.g. transposition of the great arteries), causing breathlessness and a lower rate of growth. More minor forms of congenital heart disease may remain undetected for many years and only reveal themselves in adult life (e.g. Atrial septal defect) (Baumgartner et al., 2010).

2.4 Two-dimensional echocardiography (2D echo) in the diagnosis of ischemic heart disease (IHD)

2D echo is one of the most useful imaging methods due to its availability, ease of use, price, capacity to serve as bedside technique and repeatability. It is the most employed cardiovascular imaging modality for assessment of cardiovascular disease and is often performed in patients without a history of IHD. It is well established that several echocardiograpahic measurements provide powerful prognostic information for cardiovascular outcomes, such as presence of left ventricular hypertrophy, aortic sclerosis and LVEF. In addition, 2D echo is also very useful when it comes to rule out the possibility of other etiologies of acute chest pain or dyspnea, such as aortic dissection and pericardial effusion (Chaves et al., 2004; Esmaeilzadeh et al., 2013; Votavová et al., 2015).

2.4.1 Two-dimensional echocardiography (2D echo) in the evaluation of regional and global systolic function

2D echo is a non-invasive diagnostic technique for the provision of information on cardiac function and hemodynamics and is the most frequently utilized cardiovascular diagnostic test after ECG and chest X-ray (Esmaeilzadeh et al., 2013). Major consequences of ischemia include an impairment of regional systolic contractility. If severe ischemia persists myocardial necrosis develops, followed by scarring which affects the regional function permanently. The regional myocardial function is usually assessed only visually by evaluating wall thickening and endocardial motion of myocardial segments. It is widely recognized that myocardial movements may be caused by adjacent segment tethering or overall left ventricular displacement. It seems, therefore, preferable that regional deformation should be analyzed by using methods that are at least partially independent of tethering such as speckle tracking though keeping in mind that even the deformation may be passive (Lang et al., 2015).

In IHD cases regional wall motion should be assessed on multiple image views in the parasternal long-axis and short-axis views and the apical four-chamber, two-chamber, and three-chamber views. The subcostal (SC) views can prove extremely helpful, especially when parasternal or apical views are of poor quality, and off-axis or foreshortened views should be avoided in that they render the interpretation of regional wall motion difficult and increase the likelihood of error. Second harmonic imaging with high signal-to-noise ratio (SNR) can augment the clarity of the images (Esmaeilzadeh et al., 2013). The use of deformation imaging, nowadays mostly using the strain and strain rate derived from speckle tracking, should allow less subjective evaluation of myocardial contraction as compared to simple visual assessment. The speckle tracking echocardiography replaced techniques based on tissue Doppler imaging (TDI) originally used for myocardial motion and deformation assessment. The strain and strain rate derived from 2D echo are based on computer algorithms tracking the movement of speckles clusters of natural acoustic markers generated within the myocardium by an interaction with ultrasonic waves. These techniques are independent of the ultrasound beam propagation angle and allow evaluation of longitudinal, radial, and circumferential strains (Hoit, 2011). In the normal myocardium, strains and strain rates are nearly homogeneously distributed and even subtle changes may suggest myocardial contractile impairment. Jamal et al. (2002) proposed that particularly the longitudinal strain decrease correlates with the presence of decreased coronary perfusion in segments that appear visually normal (Figure 2.28).

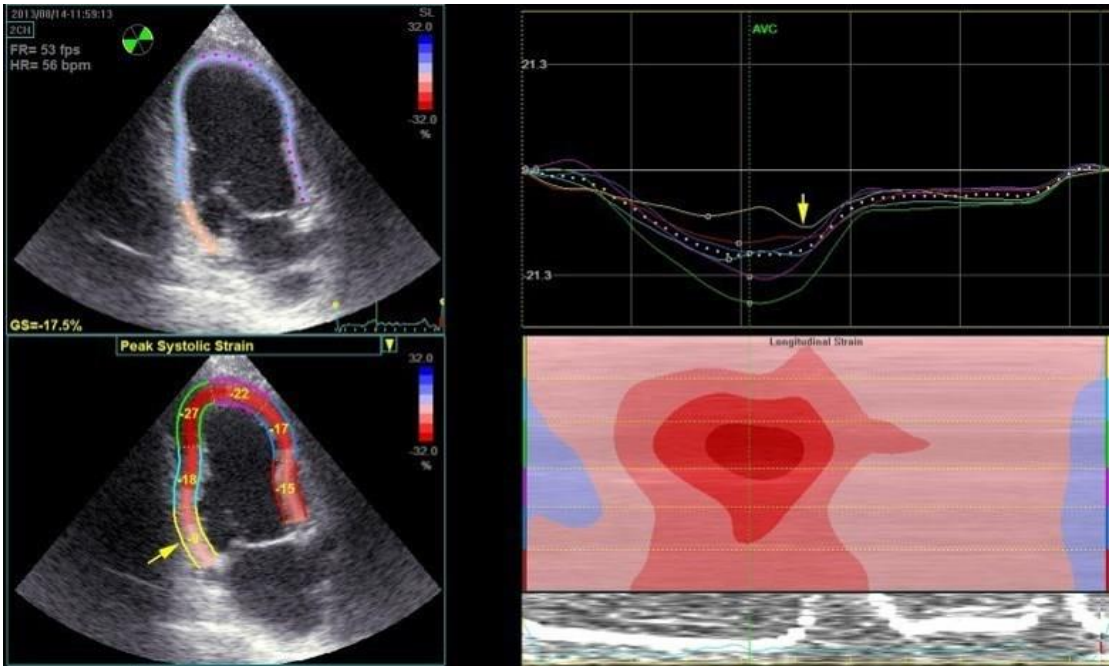

Figure 2.28: Two-dimensional (2D) apical two-chamber view with speckle tracking showing a significant decrease of longitudinal strain within the basal inferior wall (yellow segment, arrow) with a clear post-systolic deformation (arrow) on the yellow curve (Jamal et al., 2002).

Assessment of global systolic function parameters should be based on 2D or three-dimensional (3D) echocardiographic imaging. Although 3D echo begins to change the clinical practice in many ways, the 2D approach is still prevailing. left ventricular volumes should be measured from apical four and two chamber views. During scanning attention should be paid to maximize cavity areas to avoid left ventricular foreshortening. The most commonly used methods for 2D volume calculations is the Simpson's biplane method of disc summation (Figure 2.29) (Lang et al., 2015; Votavová et al., 2015).

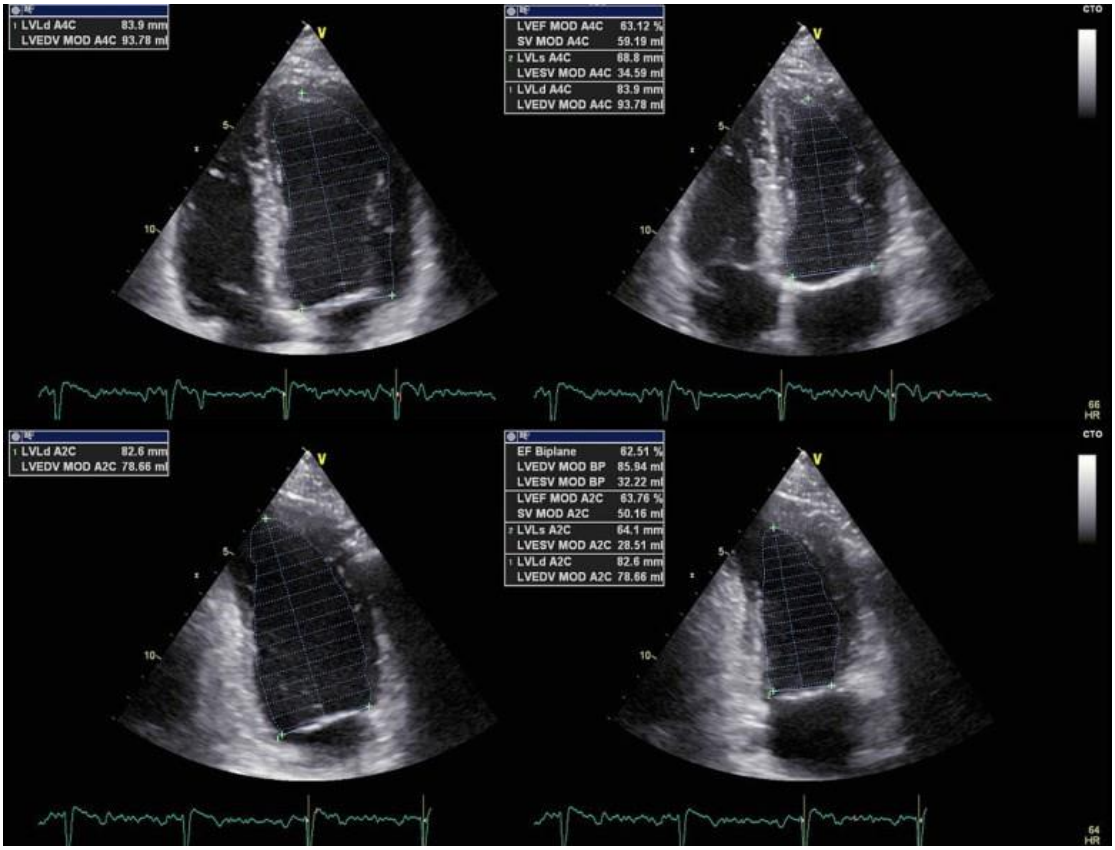

Figure 2.29: Biplane disc summation method (modified Simpson's rule) for left ventricular volumes and left ventricular ejection fraction (LVEF) calculations (Votavová et al., 2015).

Upper normal limits of 2D echo end-diastolic volumes are proposed at 74 mL/m^2 for men and 61 mL/m^2 for women. In contrast to previous recommendations proposing a uniform lower limit for ejection fraction (EF) at 55%, current guidelines suggest that EF of <52% in a man and <54% of women are suggestive of abnormal left ventricular systolic function (Lang et al., 2015; Lang et al., 2005). In addition to measurements of left and right regional and global ventricular function, 2D echo allows a reasonably precise evaluation of CO. The most clinically accepted technique is combining the measurement of left ventricular outflow tract (LVOT) dimension and velocity time integral (VTI_{LVOT}) of the flow through the LVOT measured from apical views (Figure 2.30). The CO is then calculated as: $\pi \times (\frac{LVOT^2}{4}) \times VTI_{LVOT}) \times heart\ rate$. This approach is very useful, particularly in acute settings for evaluation of the overall hemodynamic situation (Votavová et al., 2015).

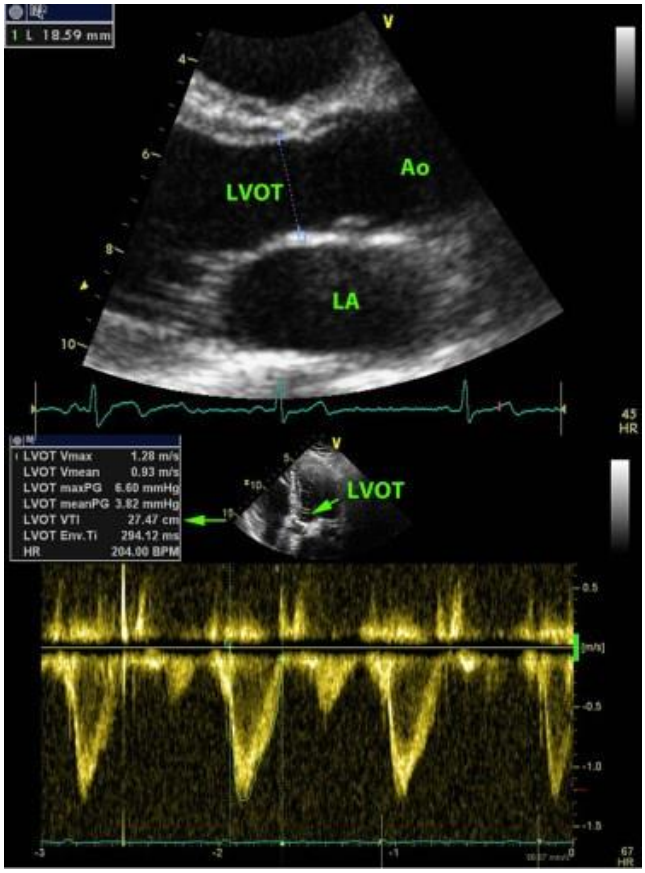

Figure 2.30: Two-dimensional echocardiography (2D echo) measurements needed for calculations of cardiac output (CO) (Votavová et al., 2015).

2.4.2 Two-dimensional echocardiography (2D echo) in the evaluation of left ventricular filling

2D echo provides crucial information for predicting ventricular remodeling and functional recovery, left ventricular size and volume, regional wall motion abnormality, myocardial viability, left ventricular filling pressures, severity of mitral regurgitation, and systolic pulmonary artery pressure (Esmaeilzadeh et al., 2013). The recognition of diastolic dysfunction or worsening of diastolic function can be indicative of the IHD presence at rest even without the systolic dysfunction or obvious wall motion abnormalities (WMAs) (McMurray et al., 2012). 2D echo allows evaluation of left ventricular filling using Doppler measurements of transmittal flow and pulsed wave TDI recordings of mitral annular movements (Figure 2.31) (Votavová, et al., 2015). The evaluation should be completed by analyzing the pulmonary

venous inflow pattern, using Valsalva maneuvers and considering the left atrial size and volume. The prognosis of the patients depends also on left atrium volumes which should be preferred over linear atrial measurements and performed by using two perpendicular apical views, applying either disc summation methods or area-length (Gillebert et al., 2013; Tsang et al., 2006). The tracing of left atrium is closed at the level of mitral annulus and left atrium appendage or pulmonary vein inflows are not included (Lang et al., 2015).

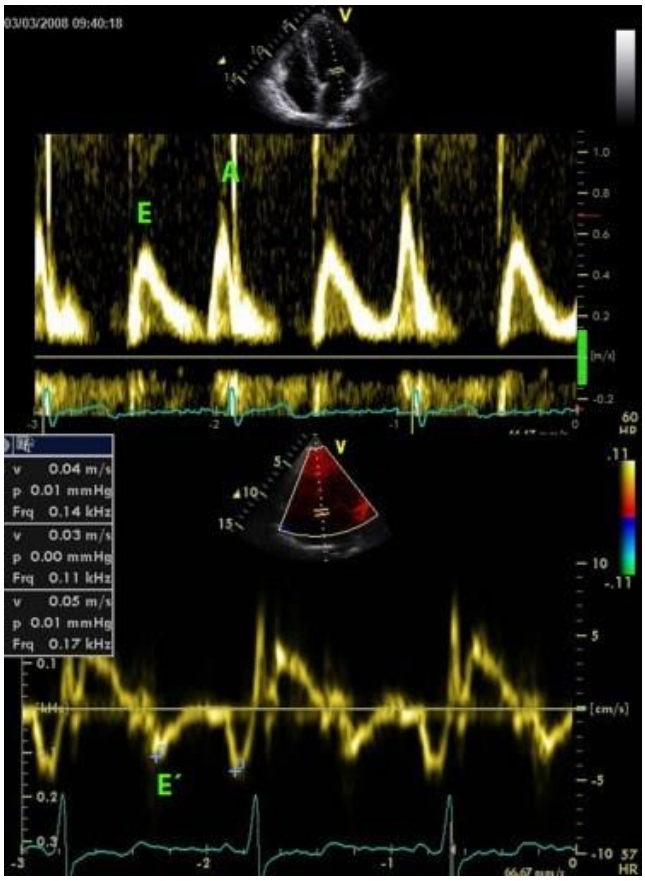

Figure 2.31: An impaired relaxation pattern showing an inverse relationship between waves € and (A) on transmitral flow and a decrease of E′ wave velocity recorded by pulsed wave tissue Doppler imaging (TDI) (Votavová et al., 2015).

2.4.3 Two-dimensional echocardiography (2D echo) in the evaluation of ischemic mitral valve regurgitation

The pathophysiology of ischemic mitral valve regurgitation or ischemic mitral regurgitation (IMR) is complex (Votavová et al., 2015). Functional mitral regurgitation occurs when the leaflets and chordae are relatively normal, but systolic co-aptation and apposition of the leaflets are lessened (Figure 2.32) (Sutton and Scott, 2002). In most cases, the IMR develops as a consequence of MI inducing left ventricular cavity dilatation and systolic dysfunction. This leads to mitral leaflet tethering and to an inappropriate co-aptation of the mitral valve leaflets. The cavity dilatation contributes by secondary mitral annular dilatation and loss of annular contraction (Votavová et al., 2015).

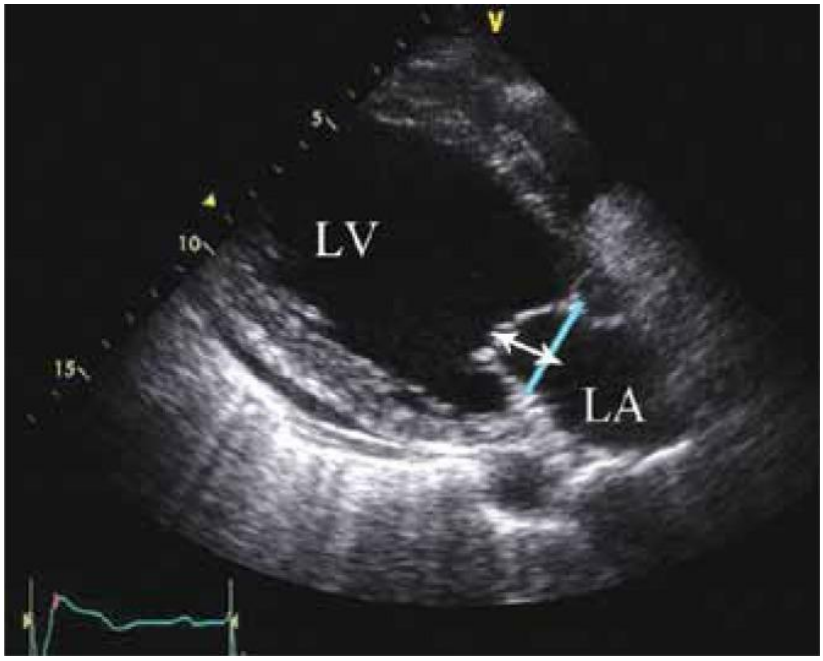

Figure 2.32: Demonstration of the mechanism of functional mitral regurgitation. Two-dimensional echocardiography (2D echo) image in the parasternal long-axis view at end-systole in a patient with dilated cardiomyopathy (DCM) and severe mitral regurgitation. The mitral annulus plane is indicated by the line. Notice that the leaflets are "tented" at end-systole in the patient with dilated cardiomyopathy, with a greater distance between the annulus plane and leaflet closure line (arrow) (Esmaeilzadeh et al., 2013).

In addition, global left ventricular dysfunction is associated with a decrease in closing forces necessary for the appropriate mitral valve closure. In patients with IHD, the posterior leaflet motion in systole is restricted or tethered secondary to the inadequate contraction of the posterolateral wall. The resulting malcoaptation and malapposition is allied to a posteriorly directed mitral regurgitation jet. The dilation of the mitral annulus also may contribute to the development of mitral regurgitation. Mitral regurgitation, in turn, leads to left ventricular volume overload resulting in further cavity dilatation, which exacerbates the vicious circle by aggravating the mitral regurgitation. In patients with IHD, functional mitral regurgitation is associated principally with an inferior MI and the lateral displacement of the posterior papillary muscle. It is also worthy of note that significant IMR is correlated with a poor outcome (Badiwala et al., 2009; Esmaeilzadeh et al., 2013; Grigioni et al., 2005; Levine & Schwammenthal, 2005; Otsuji et al., 2001).

2D echo allows quantitation of IMR and detailed assessment of underlying mechanisms. The quantitation should not be based solely on semi-quantitative evaluation of the regurgitant jet area. A mean value of >8 mm obtained from several views seems to identify a severe mitral insufficiency regardless of the etiology (Piérard & Carabello, 2010). Either a quantitative analysis based on the Doppler volumetric method or proximal isovelocity surface area principle (PISA) is preferable (Figure 2.33) (Votavová et al., 2015). Unfortunately, the estimation of LVOT area is often inaccurate and mitral valve orifice has an elliptic shape dynamically changing throughout the diastole. Also, the PISA method may lead to underestimation or overestimation of the regurgitant volume and orifice as well as PISA radius is changing during systole. Therefore a simple comparison of mitral to aortic velocity time integral (VTI) may be helpful, severe mitral regurgitation should be suspected whenever their ratio exceeds 1.4 and detailed assessment of mitral anatomy is recommended (Lancellotti et al., 2010; Piérard & Carabello, 2010).

Severity grading of IMR differs from organic mitral regurgitation. Severe IMR is defined by regurgitant volume >30 mL and effective regurgitant orifice (ERO) >20 mm^2. Currently, there is an expert consensus that mitral valve surgery should be offered to patients with severe IMR undergoing surgical and may be considered as an isolated surgical procedure. The indication of surgery in patients with moderate IMR (ERO >10 mm^2 but <20 mm^2) is controversial (Smith et al., 2014). Several other parameters have been suggested for evaluation of IMR mechanisms, including leaflet angle measurements and posterior displacement of papillary muscles assessments. Before any indication of surgery, it is important to determine the origin of the jet and its direction (Lancellotti et al., 2010).

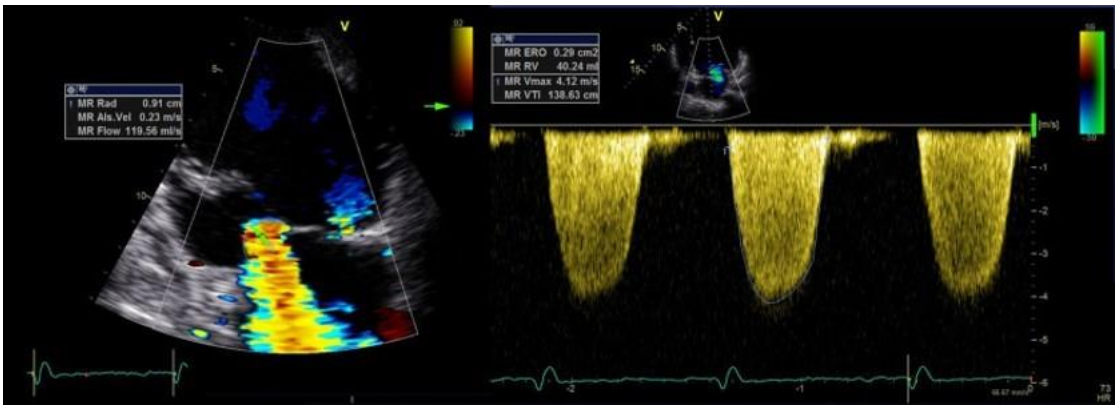

Figure 2.33: Measurement of regurgitant mitral flow volume and effective regurgitant orifice (ERO) by using the proximal isovelocity surface area principle (PISA) method. The variance signal of the color Doppler is switched off and zero shift method applied for the correct PISA radius measurement (Votavová et al., 2015).

2.4.3 Two-dimensional echocardiography (2D echo) in the localization of acute myocardial infarction (AMI)

The potential value of 2D echo as a diagnostic tool in acute or subacute complications of MI was discovered very early, and a large number of studies reported its high sensitivity, both qualitatively and quantitatively. Generally, for the differentiation of normal from infarcted myocardium, wall thickening is preferred to wall motion. Moreover, 2D echo is extremely

accurate for the localization of the infarction. Exceptions are multi-vessel disease, previous infarction, and overlap between the perfusion territories on the right and circumflex coronary arteries. There is a significant relationship between infarction and contractile dysfunction; consequently, the absence of wall motion abnormality or wall thinning rules out a clinically significant infarction (Esmaeilzadeh et al., 2013).

In addition, a meticulously performed Doppler echocardiographic examination can provide sufficient information to determine the hemodynamic category after an infarction without increased mortality. This noninvasive measurement of the CO and pulmonary capillary wedge pressure (PCWP) in patients with acute myocardial infarction (AMI) and cardiac failure can guide therapy and predict prognosis. In post-infarction patients with a LVEF smaller than 35%, a mitral deceleration time less than 120 msec is deemed highly predictive of a PCWP greater than 20 mmHg. In addition, in patients with AMI, a systolic fraction of the pulmonary venous flow smaller than 45% was highly correlated with a PCWP greater than 18 mmHg. TDI measurement of mitral annular velocities is a well-validated method for PCWP estimation. The measurement of peak mitral early diastolic filling velocity/velocity of propagation (E/Vp) by color motion mode (M-mode) Doppler in patients with AMI is strongly allied with PCWP. An E/Vp equal to or greater than 2 is believed to predict a PCWP equal to or greater than 18 mmHg with a respective sensitivity and specificity of 95% and 98% (Gerber & Foster, 2007).

Elevated pulmonary artery pressure is allied to increased mortality in AMI patients. Doppler echocardiography can estimate systolic pulmonary artery pressure by using tricuspid regurgitation and the Bernoulli equation. Pulmonary artery pressure can also be measured based on the size and the respiratory variation of the inferior vena cava using 2D echo imaging. Needless to say, hemodynamic information obtained from an echocardiographic examination only at a single point in time should be complemented by continued invasive monitoring in patients with ongoing instability (Gerber & Foster, 2007; Goldstein, 2002). Moreover, 2D echo

is a vital, non-invasive, and readily available tool in the diagnosis and evaluation the mechanical complications of AMI. The major mechanical complications of AMI are papillary muscle rupture with severe mitral regurgitation (Figure 2.34), ventricular free wall rupture with tamponade or pseudoaneurysm formation (Figure 2.35), and ventricular septal rupture (Figure 2.36) (Esmaeilzadeh et al., 2013; Figueras et al., 2010; Imazio et al., 2009; Votavová et al., 2015).

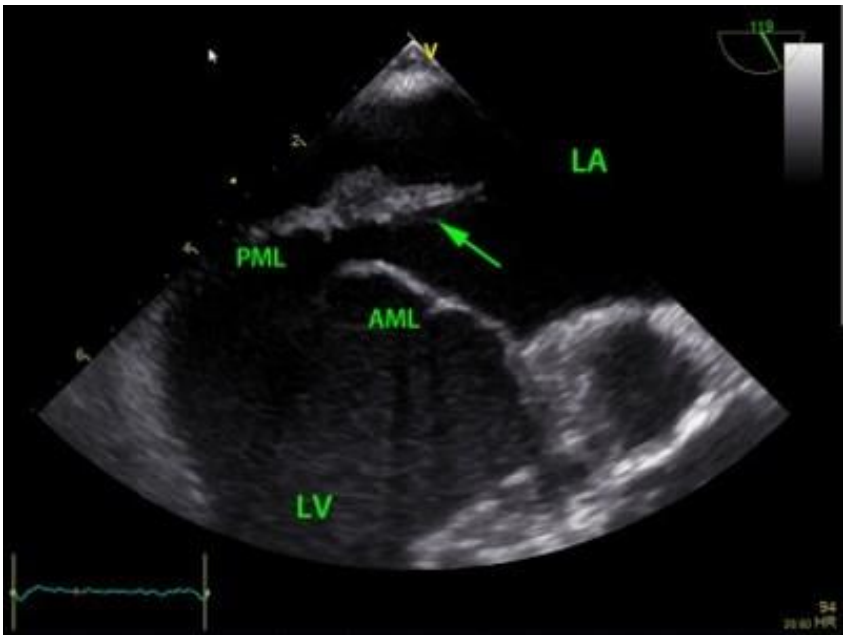

Figure 2.34: A two-dimensional echocardiography (2D echo) showing a ruptured papillary muscle prolapsing together with the posterior leaflet to the left atrium (Votavová, et al., 2015).

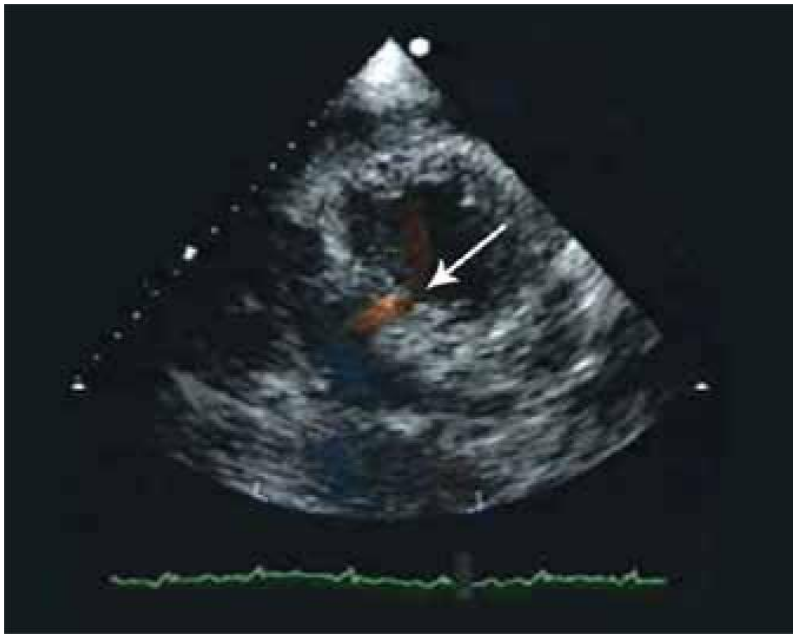

Figure 2.35: A Doppler echocardiography in the SC view shows a direct visualization of a free wall rupture (arrow) (Esmaeilzadeh et al., 2013).

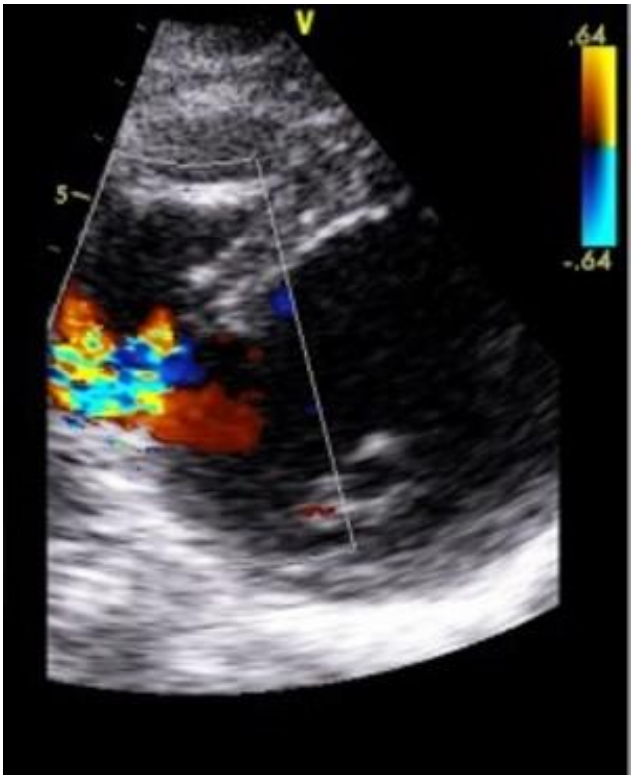

Figure 2.36: A two-dimensional echocardiography (2D echo) with color flow Doppler presents an intraventricular septal rupture due to inferoseptal myocardial infarction (MI) generating a significant left-to-right shunting (Votavová et al., 2015).

Finally, the 2D echo is very helpful in identifying the post-infarction pericarditis developing during the subacute phase of MI, which occurs between three and ten days from admission. Before the era of reperfusion, the presence of some pericardial effusion was reported to be as high as 25% to 28%. Currently only about 4% patients with AMI treated by emergency percutaneous coronary intervention (PCI) have some degree of pericardial effusion. However, an effusion exceeding 10 mm in the parasternal long axis was reported to be associated with some risk of free wall myocardial rupture (Figueras et al., 2010; Imazio et al., 2009). Thus, 2D echo is a sensitive technique for the diagnosis of pericardial effusion along with pericarditis; the absence of fluid, however, does not exclude pericarditis (Greaves, 2002).

2.4.4 The recent advances on the prognostic and diagnostic value of Two-dimensional echocardiography (2D) echo evaluation of ischemic heart disease (IHD)

2.4.4.1 Three-dimensional (3D) echocardiography

The 3D echo recent advances have enabled real-time volumetric acquisitions. Initial methods required manual rotation of the transducer to sequentially collect images in multiple planes, which were then, reconstructed offline. Advances in material science, parallel processing electronics, and software have enabled the development of phased array transducers that can image large pyramidal volumes in real time. Corresponding improvements in software have enabled both online and offline visualization of volumetric datasets. As a result, 3D imaging is now a routine part of both transthoracic and transesophageal echocardiography protocols in many laboratories. For the evaluation of IHD, there are several important advantages of 3D volumetric imaging over 2D echo. Volumetric data sets also allow more reliable and accurate quantification of chamber volume and mass. The ability to rapidly and simultaneously acquire multiple views may simplify stress echocardiography and may improve diagnostic accuracy (Abusaid & Ahmad, 2012; Hung et al., 2007; Kleijn et al., 2011).

2.4.4.2 Tissue Doppler imaging (TDI) and speckle tracking methods

Two methods hold promise in this area are TDI and speckle tracking. As in traditional pulse Doppler imaging, the TDI measures the velocities in a region of interest. However, in contrast to traditional pulse Doppler imaging, a low-pass filter is applied to exclude high-velocity signals from moving blood, enabling measurement of myocardial tissue velocities. Speckle tracking methods use computer algorithms to evaluate changes in distance between 'speckles' observed in normal myocardium to compute the strain and the strain rate. Both TDI and speckle tracking methods have been used for assessment of systolic and diastolic dysfunction in the setting of IHD. Currently, most echocardiography systems include capabilities for acquiring and analyzing TDI images. Software for speckle tracking is available from multiple vendors both for offline and for real-time analysis. However, because speckle-tracking analysis is time consuming, few laboratories have integrated it into routine workflows (Asanuma et al., 2012; Shah & Solomon, 2012).

2.4.4.3 Future directions of Two-dimensional echocardiography (2D echo) evaluation of ischemic hear disease (IHD)

Within the last two decades, the standard laboratory echocardiography machine has shrunk from the size of a household refrigerator to potentially the size of a laptop computer. The most recent advance has been the development of a truly handheld device, which may be carried within a coat pocket. Such devices, offer diagnostic quality 2D images with simplified color Doppler and will become an adjunct to the physical examination. These devices will have most to offer in the setting of IHD and heart diseases. In IHD, 2D echo has been shown to be of value at all stages of the progression of the disease, ranging from acute chest pain presentations, confirmation of acute infarction, acute infarct complications, and the evaluation and management of chronic IHD. The integration of echocardiography and clinical decision-

making is well illustrated by the use of the test in patients presenting with chest pain. 2D imaging obtained during pain or shortly thereafter has a negative predictive value of 95% for the identification of infarction, with similar sensitivity for patients presenting with documented infarction (Cheitlin et al., 2003; Marwick, 2009).

As the epidemics of hypertension and obesity extend to the developing world, the ability to identify and characterize left ventricular dysfunction will permit the better selection of patients for preventive and therapeutic strategies. Thus, the availability of relatively inexpensive, portable echocardiography machines may have a major impact on the identification and management of IHD in the developing world. The ability of high-technology echocardiography to operate in a low-infrastructure environment is unique among the imaging techniques. Also, It seems likely that there will be increasing requirements for formal training in echocardiography for potential users of the technique among emergency room and intensive care physicians, analogous to that provided during cardiology training for evaluation of IHD (Marwick, 2009).

2.5 Cardiac magnetic resonance imaging (CMRI) in the diagnosis of ischemic heart disease (IHD)

CMRI has provoked increasing interest in the potential clinical role in the noninvasive work-up of patients with suspected CAD and correct patient selection for these emerging imaging techniques (Jung & Yoon, 2017). In recent years, CMR has become a routinely used modality for the diagnosis of IHD and can provide noninvasive evaluation of reperfusion therapy through a comprehensive evaluation of wall motion, global function, perfusion and viability. In fact, CMR is widely considered the clinical gold standard for viability imaging by providing high-resolution images of post-contrast gadolinium enhanced acquisitions that accurately depict the transmurality of MI, which is critical to guide revascularization therapy (Wieben et al., 2008). Thus, the growing number of patients undergoing CMR studies and CMR centers, and the evidence for the use of CMR both in patients with stable CAD, as well as ACS justify reviewing its capabilities (Śpiewak, 2015; Bruder et al., 2013).

Beside the facts mentioned, CMR has matured into a multipurpose noninvasive imaging tool for the assessment of IHD. The breadth of applications possible with CMR allows combined noninvasive assessment of myocardial perfusion, function and myocardial viability, which is a task that usually requires use of echocardiography and myocardial scintigraphy. As such, CMR currently holds a strong position in the non-invasive work-up of patients with CAD (Nikolaou et al., 2011). In addition, the distinct advantages of MRI over current conventional nuclear-based cardiac-imaging techniques, such as PET or myocardial scintigraphy, include its high spatial resolution and lack of exposure of the patient to ionizing radiation. In addition, quantification of cardiac morphology and function by MRI is more accurate and image quality is more reproducible than in echocardiography, independent of the operator's experience and skill level or the patient's anatomy (Elamin et al., 2016; Nikolaou et al., 2011; Mahmoud et al., 2013; Mohieldin et al., 2016; Zidan et al., 2018).

2.5.1 Current status of cardiac magnetic resonance imaging (CMRI) and the basic cardiac magnetic resonance (CMR) sequences in ischemic heart disease (IHD)

CMR has emerged as a valuable tool in the assessment of patients with suspected CAD. The growing evidence supporting the use of CMR to diagnose the presence of CAD has led to the recognition of stress CMR as a method equal to well established methods of functional testing in the case of suspected CAD, namely stress echocardiography, nuclear imaging single photon emission computed tomography (SPECT) and PET perfusion (Nikolaou et al., 2011; Montalescot et al., 2013; Windecker et al., 2014). However, the very first imaging modality in patients with suspected CAD should be transthoracic echocardiography and determining LVEF (Montalescot et al., 2013). The overall and final imaging strategy for the assessment of CAD and its sequel, however, has to be chosen based on the clinical background information and the intended question for further therapeutic decisions (Nikolaou et al., 2011).

2.5.2 Basic cardiac magnetic resonance (CMR) pulse sequences in ischemic heart disease (IHD)

Currently available CMRI techniques are able to fulfill the aims of imaging in IHD patients: i) on one hand, anatomic imaging with visualization of CAD and ii) on the other hand, ischemia imaging with evaluation of the consequences of CAD of the heart, particularly myocardial perfusion and function and depiction of irreversible myocardial damage (Dall'Armellina et al., 2010; Morton et al., 2010; Sawlani & Collins, 2016). The viability protocol is the backbone of any CMR study, such that the sequences necessary for viability assessment are present in most protocols. These sequences include: i) cine imaging in long-axis (two-chamber, three-chamber, and four-chamber) and short-axis orientations and ii) delayed enhancement imaging in the same planes to assess myocardial scar and determine viability (Sawlani & Collins, 2016).

2.5.2.1 Cardiac magnetic resonance (CMR) functional imaging

ECG gated is acquired during breath holds, i) dynamic cine MRI balanced steady-state free precession (b-SSFP) sequences provide a noninvasive, accurate, and reproducible alternative to conventional echocardiography for calculating ventricular volumes and function and visualizing regional wall motion and contraction patterns. Thus, cine MRI should be considered as a fast and robust imaging modality for both daily clinical routine and research purposes. With techniques as real-time non-gated cine sequences (Figure 2.37), problems like the presence of atrial fibrillation or the incapacity for breath holding are now mostly overcome (Florian et al., 2011; Ganame et al., 2011).

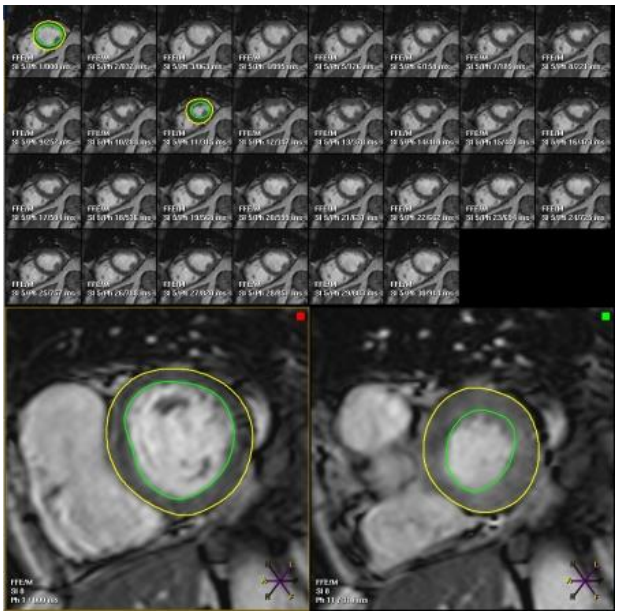

Figure 2.37: Functional analysis of short axis cine magnetic resonance imaging (MRI). End diastolic and endsystolic time frames are defined and then the endo– and epicardial borders are manually drawn for each slice (Florian et al., 2011).

The ii) myocardial tagging MRI techniques noninvasively creates tag or grid lines on the myocardium, allowing to analyze regional myocardial deformation 2 or 3 dimensionally throughout the cardiac cycle, and to calculate myocardial strains (Figure 2.38). A better characterization of the mechanisms of normal or impaired myocardial contraction is thus

achieved, but due to the elaborative post-processing, the clinical use of myocardial tagging MRI is currently limited (Bogaert et al., 2001; Florian et al., 2011).

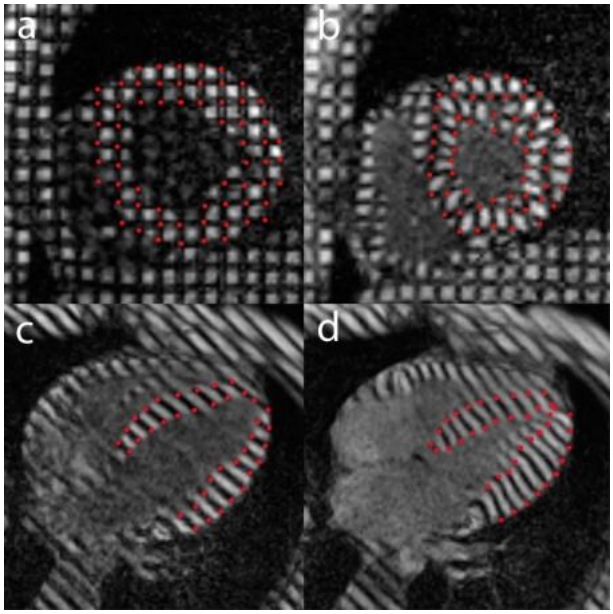

Figure 2.38: Magnetic resonance imaging (MRI) study with two-dimensional (2D) tagging analysis. Tagging in cardiac short axis (a & b) and horizontal long axis (c & d), end diastolic (left) and end diastolic time frame (right). Tracking of the grid intersections (indicated in red) on the short axis views, and the intersections of the tags with the endo- and epicardial border (indicated in red) on the long-axis views, allow analyzing the local myocardial deformation (Florian et al., 2011).

2.5.2.2 Cardiac magnetic resonance (CMR) myocardial perfusion imaging

The most frequently used approach to assess myocardial perfusion with MRI is monitoring of the first pass of contrast medium through the heart, using a bolus injection of gadolinium in combination with ultra-fast cine MRI sequences. As presented in Figure 2.39 normally perfused myocardium enhances homogeneously, becoming bright, hypo-or non-perfused regions appear darker for a variable amount of time during/after first-pass, are most intense in the sub-endocardium and typically respect coronary artery perfusion territories (Florian et al., 2011).

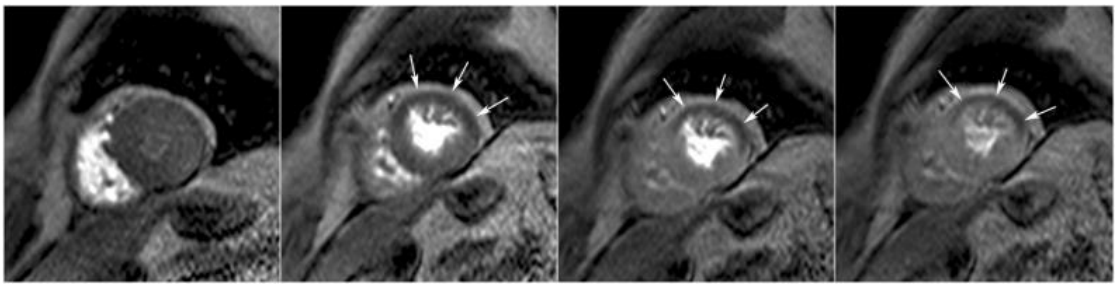

Figure 2.39: Magnetic resonance imaging (MRI) stress perfusion with suspected mid left anterior descending coronary artery in-stent stenosis. Midventricular short-axis serial time frames of first pass perfusion during Dipyridamole vasodilatory stress show contrast successively enhancing the right, left chambers and myocardium (images from left to right). A transmural perfusion defect in the anterior and lateral walls is seen (arrows) (Florian et al., 2011).

2.5.2.3 Cardiac magnetic resonance (CMR) edema imaging

Edema is visible on T_2-weighted MRI sequences in infarcted myocardium as hyper-intense areas due to increased free water in the infarcted myocardium that changes tissue magnetization properties. Abnormalities are most evident in the acute and sub-acute phase of MI and slowly fade away due to processes of infarct healing with scar formation and resorption of infarct-related myocardial edema and inflammation. T_2-weighted MRI sequences, equipped with inversion techniques to null the signal of fat and blood (will appear dark) (T_2-weighted short inversion time inversion recovery, T_2-weighted short T_1 inversion recovery (STIR) MRI, triple inversion recovery sequences), are now most commonly used for edema imaging (Figure 2.40) (Bogaert et al., 2001; Carlsson et al., 2009; Francone et al., 2011; Yelgec et al., 2007).

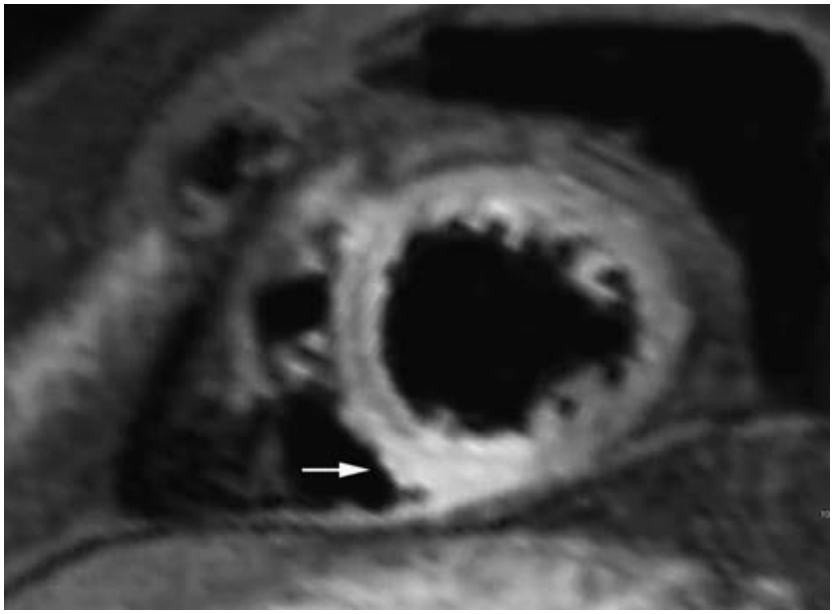

Figure 2.40: Infero-septal myocardial infarction (MI) in a 47-year-old man imaged in the acute phase. On T_2-weihted short T_1 inversion recovery (STIR) magnetic resonance imaging (MRI), tissue edema is depicted as a homogeneous transmural area of hyper-intense signal located in the inferior and infero-septal left-ventricular wall (arrow) (Francone et al., 2011).

2.5.2.4 Cardiac magnetic resonance (CMR) contrast enhanced imaging

Currently, in the routine clinical setting, contrast enhanced MRI (Ce-MRI) for MI imaging after gadolinium administration is done by an inversion recovery T_1-weighted sequence, which achieves an increased contrast between normal and pathological tissue. Also, Ce-MRI is a robust, well-validated and accurate tool to depict myocardial necrosis in the acute setting of MI. This technique (Figure 2.41) is nowadays routinely used to depict infarct-related myocardial scarring and is helpful to differentiate DCM from left ventricular dysfunction related to CAD, and to predict functional recovery post-coronary revascularization (Florian et al., 2011; Kühl et al., 2003; Larose, 2006; McCrohon et al., 2003).

2.5.2.5 Cardiac magnetic resonance (CMR) stress perfusion imaging

The first pass of an intravenously injected gadolinium contrast agent during administration of a vasodilator is used by MRI perfusion studies to depict hemodynamically significant coronary artery stenosis as demonstrated in Figure 2.42. This technique has been well validated, showing

similar or better accuracies (a sensitivity of 91% and a specificity of 81%) when compared to routinely invasive techniques used such as SPECT imaging (Florian et al., 2011; Nandalur et al., 2007). A relatively simple semi-quantitative method that has been validated against coronary flow reserve measurements is the assessment of the myocardial perfusion reserve (MPR) or MPR index. This index is defined as the ratio of regional myocardial blood flow after induced vasodilatation for that under resting conditions. As an MPR index cutoff value of 1.5 was able to distinguish between hemodynamically relevant and non-relevant coronary lesions with a sensitivity of 88% and specificity of 90% (Rieber et al., 2006).

Figure 2.41: A case recently diagnosed with dilated cardiomyopathy (DCM). Still mid ventricular short-axis (a) and vertical long-axis (b) images of cine magnetic resonance imaging (MRI) show a remodeled, dilated left ventricular and inferior wall thinning (arrows). Late contrast enhanced magnetic resonance imaging (Ce-MRI) in the same imaging planes show transmural enhancement of the base and mid inferior wall (c and d) and of the mid infero-medial right ventricular suggests an old inferior MI with right ventricular involvement (arrow head) (Florian et al., 2011).

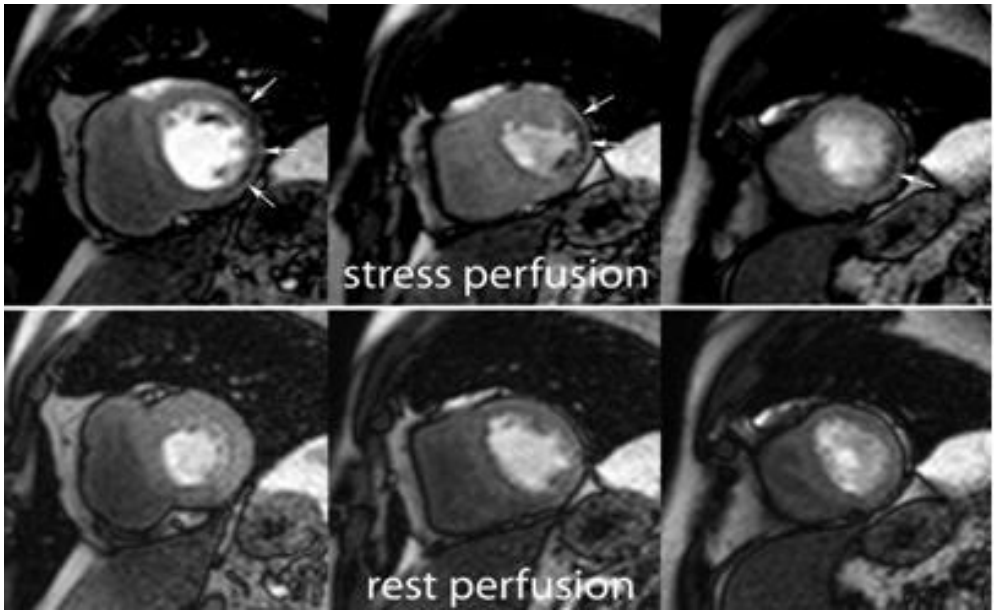

Figure 2.42: Cardiac magnetic resonance (CMR) rest and stress perfusion imaging in a case with stable angina. Midventricular short-axis cardiac magnetic resonance imaging (CMRI) images of first pass perfusion during rest (bottom) show no perfusion defects while during Dipyridamole vasodilatory stress (top) show a sub-endocardial perfusion defect in the lateral wall (arrows) (Florian et al., 2011).

2.5.2.6 Cardiac magnetic resonance (CMR) stress functional imaging

CMR stress functional imaging is usually performed during Dobutamine administration. The protocol acquisition (Figure 2.43) is started in resting conditions with cine MRI with a set of standardized imaging planes through the ventricles. This approach allows the evaluation of regional contractility in all segments of the left ventricular. In addition, the calculation of left ventricular volumes and EF is done with a single breath-hold 3D cine MRI sequence encompassing the entire left ventricle (Tops et al., 2005).

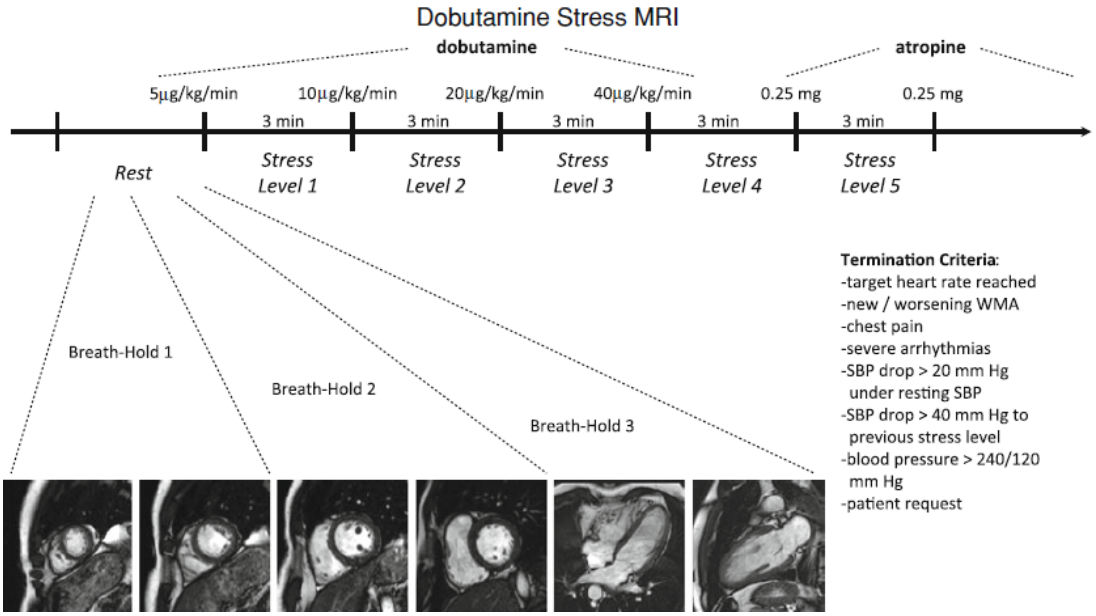

Figure 2.43: Practical schematic for Dobutamine stress magnetic resonace imaging (MRI). For each stress level, 4 short-axis and two long axis cine studies are obtained in 3 consecutive breaths-hold periods. If termination criteria are not met at the highest Dobutamine dose, Atropine can be additionally administered (Tops et al., 2005).

With respect to adverse effects, studies have shown that high-dose functional stress imaging in an MRI environment can be considered as safe and feasible in patients with suspected or known CAD. Also a higher accuracy (86.0% versus 72.7%) of high-dose stress Dobutamine MRI compared to high-dose Dobutamine stress echocardiography in detecting patients with significant CAD. Currently, the most commonly used approach for evaluating functional stress studies is a visual analysis of new or worsening WMAs using a high-dose Dobutamine/Atropine regimen using a 16 or 17 segment classification system by the American heart association (AHA), yielding a good sensitivity (82-96%) and specificity (80-100%) for detection of significant CAD (Strach et al., 2006).

2.5.3 The recent advances on the prognostic and diagnostic value and the future directions of Cardiac magnetic resonance (CMR) evaluation of ischemic heart disease (IHD)

The quest for successful magnetic resonance coronary angiography (MRCA) started in the early 1990s. These techniques relied upon a combination of segmental acquisition of data in k-

space (is the 2D or 3D Fourier transform of the MRI measured) to minimize cardiac motion, and the use of a single breath-hold to minimize respiratory motion artifacts. Only portions of the coronary arteries can be visualized within each breath-hold and the inconsistency of breath-hold position makes coronary artery imaging, even for experienced investigators in the field, a difficult task. Because of the severe limitations of the 2D breath hold approach, investigators have explored several alternatives to overcome these problems and improve image quality. They can be summarized as: i) 3D imaging approaches, ii) techniques to suppress respiratory motion either by using navigators or acquisition during breath-hold, and iii) use of intravascular contrast agents (Atkinson & Edelman, 1991).

More recent improvements in MRI technology with stronger gradient systems, shorter rise times and more sophisticated ECG triggering devices have further contributed to current high-quality sub millimeter 3D visualization of the coronary arteries. In addition, dynamic contrast-enhanced MR angiography (Ce-MRA), can now be used within very short breath-hold periods (7-23 sec) to study the aorta or the pulmonary arteries. Initial experience with extravascular MR contrast agents indicated that very high doses of gadolinium would be needed for 2D-breath-hold coronary MRA. With bolus arrival timing to catch the first pass of the gadolinium contrast agent, image quality improvements have been obtained from the 3D coronary MR angiography techniques by improving both the SNR and carrier-to-noise ratio (CNR) (Atkinson & Edelman, 1991).

2.5.3.1 High field-strength 3 Tesla (3.0T) coronary MRA

The recent approval of 3.0T systems for clinical use has opened new perspectives for overcoming some of the limitations encountered in 1.5T systems, in particular, suboptimal SNR, which limits spatial resolution and the ability to visualize the distal and branch vessel coronary segments (Figure 2.44). However, a number of potential adverse effects have been

reported at higher field strengths, such as: i) susceptibility artifacts, reduced T_2* decay and increased T_1 radio frequency (RF) field distortions, ii) at high field-strength, reliable ECG triggering becomes more challenging due to the amplified magneto-hydrodynamic effects, and iii) the flexibility of sequence design is less because of increased RF deposition30. However, these preliminary studies demonstrate that 3.0T coronary MR angiography is feasible, and with further fine-tuning of the sequence 3.0T might become the preferred field-strength to study the coronary artery lumen and wall (Stuber et a., 2002; Wieben et al., 2008).

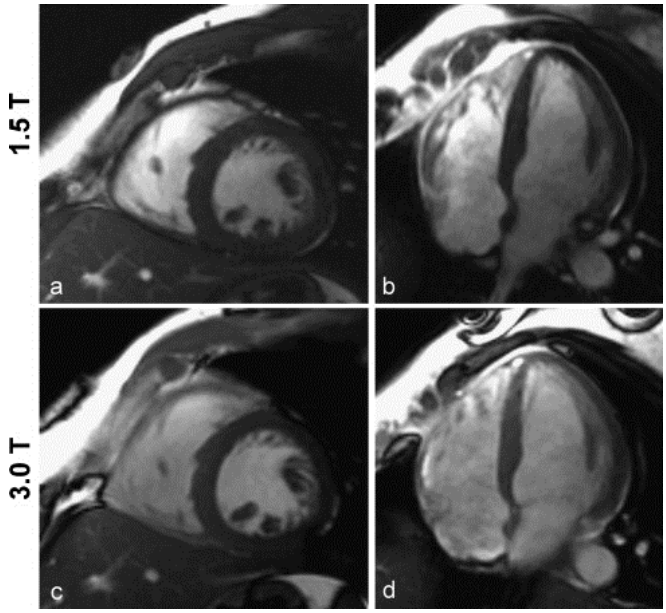

Figure 2.44: Cardiac balanced steady-state free precession (b-SSFP) acquired at 1.5T and 3.0T with identical imaging parameters except of the flip angle of 60° (1.5T) and 45° (3.0T). The images were acquired in a short axis view (left column) and four chamber view (right column) (Wieben et al., 2008).

2.5.3.2 Cardiac magnetic resonance (CMR) in coronary blood flow assessment and bypass graft imaging

Although highly challenging, magnetic resonance flow measurements can be performed in the small cardiac vessels (coronary arteries, coronary sinus) and coronary artery bypass graft (CABG) vessels (Figure 2.45), during rest and during hyperemia using fast velocity encoded cine MRI techniques. Another way to assess coronary perfusion and myocardial blood flow is

assessment of blood flow in the coronary sinus, which represents approximately 96% of the total myocardial blood flow. By measuring myocardial mass with cine MRI, the average coronary blood flow per gram of myocardial mass can be quantified by using non-invasive MRI. To assure accurate coronary flow measurements with MRI, at least four important sources of error should be taken into consideration, such as: i) partial volume effects, ii) misalignment of flow axis and flow encoding gradients, iii) intra-voxel dispersion, and iv) through- and in-plane motion (Thielmann et al., 2007).

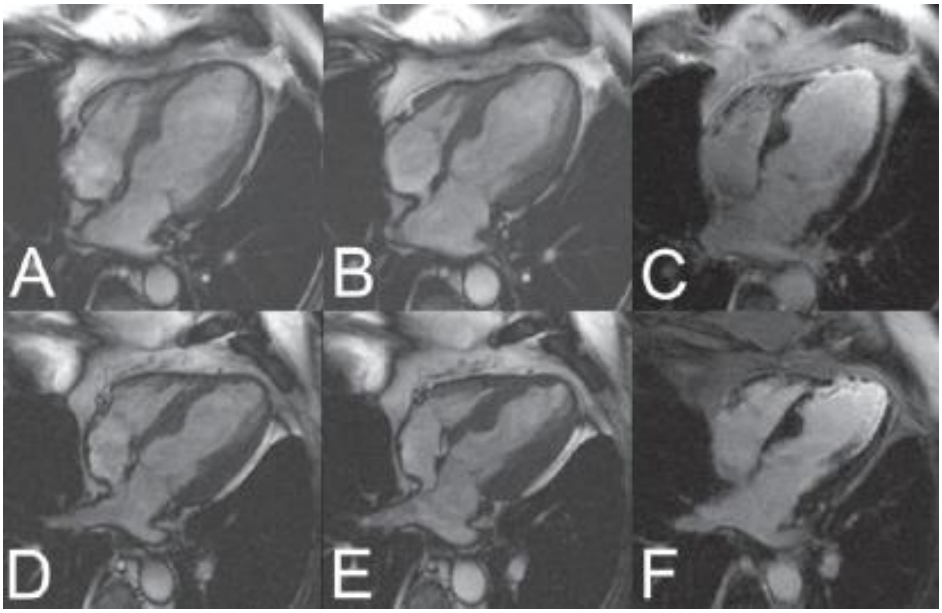

Figure 2.45: MRI of a case before (top line) and after (bottom line) 3-fold coronary artery bypass graft (CABG). Steady-state free precession (SSFP) cine images in end diastole (A) and end systole (B) reveal the severely impaired global left ventricular function before surgery (EF 30%). The Ce-turbo fast low angle shot (FLASH) image (C) shows broad sub-endocardial late enhancement (bright signal) in the apical septum, thin late gadolinium enhancement (LGE) in the lateral wall and transmural LGE in the apex meaning chronic scar. Left ventricular function after surgery (D and E) shows no improvement in the apical septum and the apex, whereas the complete lateral wall improved and became normo-kinetic. No changes in scar extent (F) (Thielmann et al., 2007).

2.5.3.3 Future directions in the Cardiac magnetic resonance (CMR) evaluation of ischemic heart disease (IHD)

The future of cardiac imaging is dynamic. With ever increasing advances in both hardware and software, CMRI will continue to evolve and improve. Increasing magnetic field strength, coupled with multi-phased array coils promise to improve CMR spatial resolution at present. With these continued advancements, CMR will continue to play an ever increasing role in the noninvasive hemodynamic evaluation of our patients (Zurick & Desai, 2013).

Chapter Two

Literature review – Previous studies

2.6 Previous studies

CAD is a leading cause of death and disability worldwide. CMR is established in clinical practice guidelines with a growing evidence base supporting its use to aid the diagnosis and management of patients with suspected or established CAD. CMR is a multi-parametric imaging modality that yields high spatial resolution images that can be acquired in any plane for the assessment of global and regional cardiac function, myocardial perfusion and viability, tissue characterization and coronary artery anatomy, all within a single study protocol and without exposure to ionizing radiation. Advances in technology and acquisition techniques continue to progress the utility of CMR across a wide spectrum of cardiovascular disease, and the publication of large scale clinical trials continues to strengthen the role of CMR in daily cardiology practice (Foley et al., 2017).

CMR is a useful diagnostic imaging modality in patients with known or suspected CAD. It provides unique information not available from other modalities, however, it is complex. CMR is not a single technique. Instead, it consists of multiple distinct techniques and a lack of understanding of which techniques to perform and how to interpret the findings in combination limits its efficacy and widespread use. Conversely, its multiparametric nature can provide a comprehensive assessment with the potential for higher accuracy than is achievable by other modalities. Moreover, its ability to directly assess myopathic processes often contributes insights that change patient management. In their article they provide a brief technical overview and focus on specific clinical scenarios in patients with known or suspected CAD (Chang & Kim, 2016).

Over the last decade the evidence base for the diagnostic accuracy of CMR for the investigation of stable coronary artery disease has been confirmed through the publication of large-scale clinical trials and meta-analyses, and CMR is now firmly established in clinical practice guidelines. CMR enables assessment of cardiac dimensions, function, ischaemia, scar burden and tissue viability in a single study without exposure to ionizing radiation. CMR also offers prognostic information with a normal stress CMR associated with a < 1% risk of death or MI at 2 years, whilst the presence of late gadolinium enhancement (LGE) confers added prognostication above and beyond the simple LVEF. New technical developments continue apace and ongoing large clinical trials will further clarify the role of CMR in routine clinical practice and guide the future development of international guidelines (Foley et al., 2017).

In patients with suspected/stable CAD, functional and perfusion imaging both at rest and during vasodilatatory stress (adenosine, dypiridamole)/dobutamine stress can accurately depict ischemic myocardium secondary to significant coronary artery stenosis. In patients with acute MI, MRI is a robust tool for differentiating and sizing the jeopardized and the infarcted myocardium by using a combination of functional, edema, perfusion and gadolinium contrast imaging. Moreover, important prognostic factors like myocardial salvage, the presence of microvascular obstruction (MVO), post reperfusion myocardial hemorrhage, right ventricular involvement and infarct related complications can be assessed in the same examination. In patients with chronic ischemic cardiomyopathy, the role of the MRI extends from diagnosis by means of gadolinium contrast scar imaging to therapy and prognosis by functional assessment and viability testing with rest and dobutamine stress imaging. In all the circumstances mentioned, MRI derived information has been proven valuable in every day clinical decision making and prognosis assessment. Thus, MRI is becoming more and more an accepted alternative to other imaging modalities both in the acute and chronic setting (Florian et al., 2011). In patients with known or suspected IHD, a comprehensive CMR protocol provides an

assessment of left ventricular function, myocardial perfusion, edema, and viability in a single sitting. There are applications for this technology in both the acute and chronic IHD settings. CMR is also a valuable tool in the assessment of patients presenting with chest pain, raised troponin levels, and unobstructed coronaries (Thompson & Maredia, 2017). CMR is a valuable tool in the evaluation of patients with CAD. A combination of functional, viability and perfusion assessment provides a comprehensive and detailed assessment of disease presence and burden. Challenges remain to improve coronary imaging, increase access and maintain a balance between the information provided and costs (La et al., 2007).

Buckert et al. (2018) compared the cardiac magnetic resonance–guided versus angiography-guided treatment of patients with stable coronary artery disease, were two hundred patients were enrolled. In group 1, 45 revascularizations (45.9%) were performed. In group 2, 27 patients (28.1%) were referred to revascularization because of ischemia on CMR. At 12-month follow-up, 7 primary events occurred: 3 in group 1 (event rate 3.1%) and 4 in group 2 (event rate 4.2%), with no statistically significant difference ($p = 0.72$). Within the next 2 years, 6 additional events could be observed, giving 4 events in group 1 and 9 events in group 2 (event rate 4.1% versus 9.4%; $p = 0.25$). Group 2 showed significant quality-of-life improvement after 1 year in comparison to group 1. They conclude that CMR-based management strategy for patients with stable coronary artery disease was safe, reduced revascularization procedures, and resulted in better quality of life at 12-month follow-up, though noninferiority could not be proved. Optimal timing for reassessment remains to be investigated. In addition, Konstantin et al. (2011) studied the MRI and CT in the diagnosis of CAD: indications and applications. They determined that in recent years, technical advances and improvements in cardiac CT and CMRI have provoked increasing interest in the potential clinical role of these techniques in the non-invasive work-up of patients with suspected CAD and correct patient selection for these emerging imaging techniques. In the primary detection or exclusion of significant CAD, e.g.

In the patient with unspecific thoracic complaints, and also in patients with known CAD or advanced stages of CAD, both CT and MRI yield specific advantages. In their study they focus on the major aspects of non-invasive MRI and CT imaging in the diagnosis of CAD. The first part of their study describes the clinical value of contrast-enhanced non-invasive computed tomography coronary angiography (CTCA), including the diagnostic accuracy of CTCA for the exclusion or detection of significant CAD with coronary artery stenoses that may require angioplastic intervention, as well as potentially valuable information on the coronary artery vessel wall. While in the second part, the potential of CT for the imaging of myocardial viability and perfusion was highlighted. The final part, the range of applications of CMRI in CAD patients was outlined.

In July 2009, the Medical Advisory Secretariat (MAS), Ontario – Canada began work on non-invasive cardiac imaging technologies for the diagnosis of CAD, an evidence-based review of the literature surrounding different cardiac imaging modalities to ensure that appropriate technologies are accessed by patients suspected of having CAD. The objective of this analysis was to determine the diagnostic accuracy of CMRI for the diagnosis of patients with known/suspected CAD compared to coronary angiography. This research came about when the Health Services Branch at the Ministry of Health and Long-Term Care asked MAS to provide an evidentiary platform on effectiveness and cost-effectiveness of non-invasive cardiac imaging modalities. After an initial review of the strategy and consultation with experts, MAS identified five key non-invasive cardiac imaging technologies for the diagnosis of CAD. Evidence-based analyses have been prepared for each of these five imaging modalities: CMRI, SPECT, 64-slice computed tomographic angiography, stress echocardiography, and stress echocardiography with contrast. For each technology, an economic analysis was also completed. A summary decision analytic model was then developed to encapsulate the data from each of these reports (Medical Advisory Secretariat [MAS], 2010).

De Carvalho et al. (2017) aimed to discuss how cardiac MRI achieves both with a single study without exposure to ionizing radiation in a research about cardiac MRI: A preferred method for assessing myocardial ischemia and infarct burden. Their findings concluded that CMR is a safe and proven modality for detecting IHD. Within a single study, CMR is able to assess rest and stress regional contraction, and localize and evaluate regions of myocardial ischemia and viability, of importance given the prognostic impact for the patient. With performance that is comparable to PET/SPECT and at times favorable compared to stress echocardiography, it is now an essential tool for diagnosing ischemia and for determining the likelihood of success following myocardial revascularization.

The clinical use of stress echocardiography in IHD proved that stress echocardiography is an established technique for the assessment of extent and severity of coronary artery disease. The combination of echocardiography with a physical, pharmacological or electrical stress allows to detect myocardial ischemia with an excellent accuracy. A transient worsening of regional function during stress is the hallmark of inducible ischemia. Stress echocardiography provides similar diagnostic and prognostic accuracy as radionuclide stress perfusion imaging or magnetic resonance, but at a substantially lower cost, without environmental impact, and with no biohazards for the patient and the physician. The evidence on its clinical impact has been collected over 35 years, based on solid experimental, pathophysiological, technological and clinical foundations. There is the need to implement the combination of wall motion and coronary flow reserve, assessed in the left anterior descending artery, into a single test. The improvement of technology and in imaging quality will make this approach more and more feasible. The future issues in stress echo will be the possibility of obtaining quantitative information translating the current qualitative assessment of regional wall motion into a number. The next challenge for stress echocardiography is to overcome its main weaknesses:

dependance on operator expertise, the lack of outcome data (a widesperad problem in clinical imaging) to document the improvement of patient outcomes (Sicari & Cortigiani, 2017).

Esmaeilzadeh et al. (2013) studied the role of echocardiography in CAD and AMI and found that echocardiography is a non-invasive diagnostic technique which provides information regarding cardiac function and hemodynamics. It is the most frequently used cardiovascular diagnostic test after electrocardiography and chest X-ray. However, in a patient with acute chest pain, transthoracic echocardiography is essential both for diagnosing acute coronary syndrome, zeroing on the evaluation of ventricular function and the presence of regional WMAs, and for ruling out other etiologies of acute chest pain or dyspnea, including aortic dissection and pericardial effusion. Echocardiography is a versatile imaging modality for the management of patients with chest pain and assessment of left ventricular systolic function, diastolic function, and even myocardial and coronary perfusion and is, therefore, useful in the diagnosis and triage of patients with acute chest pain or dyspnea.

Furthermore, echocardiography is an excellent tool for a complex and comprehensive evaluation of structural and hemodynamic changes induced by chronic or acute CAD. In skilled hands the method provides useful information for clinical management and prognosis assessment. The main drawback of echocardiography remains in the limited echogenicity of many patients and its undeniable operator-dependence. However, the possibility of bringing the echocardiographic imaging to the bedside of our patients makes the method essential and its knowledge indispensable for all cardiologists (Votavová et al., 2015). Although the availability and utilization of other noninvasive imaging modalities for the evaluation of CAD have expanded over the last decade, echocardiography remains the most accessible, cost-effective, and lowest risk imaging choice for many indications. The clinical utility of mature echocardiographic methods (i.e. 2D echo, stress echocardiography, contrast echocardiography) across the spectrum of CAD has been well established by numerous clinical studies. With

continuing advancements in ultrasound technology, emerging ultrasound technologies such as 3D echocardiography, TDI, and speckle tracking methods hold significant promise to further widen the scope of clinical applications and improve the diagnostic accuracy (Chatzizisis et al., 2013).

Daly and Kwong (2013) assessed the CMRI for myocardial ischemia and stated that the proper assessment of the physiologic impact of coronary artery stenosis on the LV myocardium can affect patient prognosis and treatment decisions. CMRI assesses myocardial perfusion by imaging the myocardium during a first-pass transit of an intravenous gadolinium bolus, with spatial and temporal resolution substantially higher than nuclear myocardial perfusion imaging. Coupled with LGE imaging for infarction during the same imaging session, CMR with vasodilating stress perfusion imaging can qualitatively and quantitatively assess the myocardial extent of hypoperfusion from coronary stenosis independent of infarcted myocardium. This approach has been validated experimentally, and multiple clinical trials have established its diagnostic robustness when compared to stress single-photon emission computed tomography. In specialized centers, dobutamine stress CMR has been shown to have incremental diagnostic value above stress echocardiography due to its high imaging quality and ability to image the heart with no restriction of imaging window.

Reeder et al. (2001) studied the advanced CMRI of IHD were the important advances in rapid MRI imaging technology and its application to cardiovascular imaging have been made during the past decade. High-field-strength clinical magnets, high-performance gradient hardware, and ultrafast pulse sequence technology are rapidly making the vision of a comprehensive “one-stop shop” cardiac MR imaging examination a reality. This examination is poised to have a significant effect on the management of CAD by means of assessment of wall motion with tagging and pharmacologic stress testing, evaluation of the coronary microvasculature with perfusion imaging, and direct visualization of the coronary arteries with MRCA. Their article

reviews current state-of-the-art pulse sequence technology and its application to the evaluation of IHD by means of MRI tagging with dobutamine stress testing, MRI perfusion imaging, and MRCA. Cutting edge areas of research in coil design and exciting new areas of metabolic and oxygen level–dependent imaging are also explored.

MRI and CT have made enormous strides over the past decades, becoming established imaging techniques in patients with suspected IHD. The impact of these imaging techniques cannot be overestimated in the diagnosis and prognostication of patients with IHD. As IHD is highly prevalent, any contribution to improving the diagnosis and work-up of these patients by noninvasive imaging techniques has direct implications for more cost-effective diagnosis and therapy (de Roos & Nikolaou, 2019). Another study investigated the role of imaging in women with IHD and found that substantial advances and insights in medical technology and treatment strategies, and the focus on sex-specific research has contributed to a reduction in cardiovascular mortality in women. Despite these advances, IHD remains the leading cause of cardiovascular morbidity and mortality of women in the Western world. Advances in cardiovascular imaging, over the past 4 decades, have significantly improved the evaluation and management of the full spectrum of coronary atherosclerosis, which contributes to IHD. The development of contemporary and novel diagnostic imaging techniques and tools have assumed an expanded role in the evaluation of symptomatic women to detect not only flow-limiting epicardial coronary stenosis and nonobstructive atherosclerosis, but also ischemia resulting from microvascular dysfunction. IHD is now diagnosed early and with greater accuracy, leading to improved risk assessment and timely therapies in women (Aggarwal et al., 2018).

Early diagnosis of CVDs in workers: role of standard and advanced echocardiography studied by Capotosto et al. (2018). Echocardiography using both conventional and more recent modalities is the primary diagnostic tool for the assessment of early cardiac dysfunction. It is

a cost-effective technique and offers real-time imaging with high spatial and temporal resolution. 3D echo and 2D and 3D speckle tracking echocardiography may provide additional diagnostic information. It is plausible that echocardiography will further evolve in the future with improvements in technology providing better clinical help. A strong professional liaison between echocardiologists and occupational physicians aids the process of offering effective support and management for the cardiovascular patients in the workplace (Capotosto et al.; 2018).

Leischik et al. (2016) investigated the used of echocardiographic in the assessment of myocardial ischemia and conclude that when using echocardiography to assess ischemia, the results obtained at rest versus those obtained during exercise need to be differentiated. They suggest that, regarding resting assessments, echocardiography combined with all of the new developments (e.g., 3D echo, harmonic imaging, TDI, strain, and contrast echocardiography) offers at least as many advantages (and can be nearly as reliable) as CMR when conducted by experienced operators, given that it is possible to obtain individual acoustic windows and a regional evaluation of the myocardium. For exercise assessments, there is a resolution limitation that is caused by non-sufficient scanning conditions in nearly 5% of patients, and for these patients, additional imaging techniques should be recommended.

Sechtem et al. (2014) focused on some of the most important studies, published in the year 2013 in cardiac imaging related to IHD. Many of the studies across the various imaging techniques addressed the prognostic impact of imaging data on outcome in patients with this disease. They concluded that imaging studies in the year 2013 underscored the value of imaging for making the diagnosis and predicting the prognosis in patients with suspected and established CAD. However, appropriately sized prospective randomized trials to prove the impact of cardiac imaging on patient management and clinical outcomes are still eagerly awaited. In addition, a study about IHD: A new insights from imaging diagnostic techniques

was done by Guaricci et al. (2018). Their results revealed that modern and thrilling technology such as CCTA and CMR has been emerging and offering the possibility to characterize both the coronary arteries and the myocardium at a very high level of detail.

CHAPTER THREE

MATERIALS AND METHODS

Chapter Three

Materials and Methods

3.1 Materials

3.1.1 Study design and patients selection

One hundred patients who were clinically diagnosed to have CAD were enrolled prospectively in this study after having provided written and verbal consent as local ethics committee at the Radiology and Medical Imaging Department, King Fahad Medical City (KFMC), Riyadh-Saudi Arabia was gained prior to the commencement of the study. Statement on informed consent from the parents/legally authorized representative was provided as minors (age <16 years) were involved in the study. The ethics procedures followed were in accordance with the Helsinki Declaration of 1975 that was revised in 2013. Patients who had been clinically examined by a referring cardiologist and were scheduled for CMRI, 2D echo and conventional coronary angiography, on gaining their consent, were included in the study. Patients were examined using CMRI and 2D echo to localize the affected coronary artery and to predict the affected myocardial segments. Conventional coronary angiography was the gold standard tool that used in all patients to confirm the diagnosis for each case. Other criteria were sinus heart rhythm, ability to hold breath for 10–20 Sec and normal serum creatinine. Exclusion criteria were hemodynamic instability, atrial fibrillation, contraindications for MRI, claustrophobia, applied pacemaker or metal implants, contraindication for contrast material, including known allergy and renal insufficiency (serum creatinine more than 1.4 mg/dl).

3.1.2 Equipment

A Siemens Magnetom Sola 1.5T MRI scanner (Siemens Healthineers AG, Erlangen, Germany), superconducting magnet was used. All patients were examined in the supine

position, head first using respiratory sensor and ECG gating. Additionally, a sensitivity encoding (SENSE) cardiac coil was used. All patients were cannulated with a wide bore intravenous line for the contrast agent.

The patients underwent a standard magnetic resonance examination that included the following steps: i) Scout images were acquired in orthogonal orientations for planning of the final long-axis and short-axis views. ii) First pass rest perfusion imaging by setting the scan angle geometry that is identical to that of the short axis cine views to carefully exclude any wraparound or trigger artifacts before starting the actual index test. This included an intravenous bolus injection of 0.025 mmol/kg of gadopentetate dimeglumine (Magnevist) at an injection rate of 5 mL/s followed by a flush of 20 mL of saline solution at the same rate. Scanning was started approximately 10 seconds after the start of contrast injection and continues for approximately 1 minute. Breath-hold first-pass perfusion MRI was performed by using a hybrid gradient echo-planar imaging pulse sequence. This pulse sequence yields three sections (at basal, mid-cavitary and apical levels) in the short-axis view covering the entire left ventricle every other heart beat with the following parameters: Repetition time/echo time (TR/TE): 2.9/1.46, field of view (FOV): 350 × 350 mm^2, phases: 25, number of signal averages (NSA): 1, matrix: 128 × 128, bandwidth: 125 kHz, flip angle: 200, scan time: 1 Sec, slice thickness: 8 mm, slice number: 3. iii) An additional bolus of 0.2 mmol/kg gadopentetate dimeglumine immediately after ending of the rest perfusion scan. iv) Functional cine images: These images were acquired using electrocardiographic gated, breath hold balanced fast field echo (b-FFE) sequence in short axis view. Stack of eight to eleven sections in short-axis views, were obtained during repeated breath-holds, starting from the mitral valve insertion and covering the entire left ventricle with the following parameters: TR/TE: 4.4/2.5, FOV: 300 × 300 mm^2, phases: 25, NSA: 1, matrix: 128 × 128, slice thickness: 8 mm, slice number:

8–11. This sequence was performed during the interval period between the aforementioned injection of an additional bolus of contrast and the delayed gadolinium enhancement sequences. v) Standard delayed gadolinium enhancement imaging, using segmental inversion recovery balanced turbo field echo (IR-b-TFE) was acquired in 10–15 min interval delay after the last injected intravenous bolus. Contrast-enhanced images were acquired in short axis plane and at least one of the long axis planes with the following parameters: TR/TE: 3.8/1.86, FOV: 300×300 mm^2, inversion time (TI): 260–350, NSA: 1, matrix: 128×128, bandwidth: 125 kHz, flip angle: 15°, scan time: 9–15 Sec, slice thickness: 8 mm, slice number: 8–11. The mean time of the CMRI imaging examination was about 30–35 min.

Results of CMRI were subdivided into two groups: i) Viable myocardial segment was defined as no myocardial scarring or ≤50% myocardial scarring. Subendocardial scarring was defined as 25% myocardial scarring and partial thickness scarring was defined as 50% myocardial scarring. ii) Nonviable myocardial segment was defined as >50% thickness myocardial scarring. A no-reflow zone (microvascular obstruction) was evident on delayed-enhancement imaging as a dark region surrounded by hyperenhancing myocardium and/or first pass resting perfusion defect corresponding to delayed myocardial enhancement.

For 2D echo examination, a Siemens Acuson SC2000 Prime ultrasound system (Siemens Healthineers AG, Erlangen, Germany) equipped with a high frequency Siemens PH4-1 cardiac sector probe and an appropriate Sony UP-X898MD black and white digital ultrasound printer was used. This system provides high image quality with a focus and real-time true volume image and increases productivity powered with one-click measurements, automated protocols and navigational tools were used. The role of 2D echo in the diagnosis of IHD in the current study was based on the evaluation of myocardial WMAs, localization of infarction, assessment of infarct size and detection of complications of MI. The findings of the CMRI and 2D echo in this research were compared to those of the corresponding conventional coronary angiograms.

3.2 Methods

3.2.1 Cardiac magnetic resonance imaging (CMRI) technique in ischemic heart disease (IHD)

Adequate patient preparation before a CMRI examination is a mandatory part of good CMRI practice. General tips for patient preparation were as follows: i) In cases of difficulty with breath holding, arrhythmia, or motion artifacts, considered a single-shot module or free breathing with real-time image acquisition. ii) In cases of difficulties due to profound respiratory motion, considered an abdominal band to reduce artifacts. iii) In cases of difficulties due to pericardial effusion and a weak ECG signal, considered a peripheral pulse gating. iv) In cases of difficulties due to ghost artifacts caused by pleural effusion and respiratory difficulties, considered postponing the CMRI imaging until after pleural effusion drainage. These guidelines on IHD patient preparation for CMRI were compatible with that of the Asian Society of Cardiovascular Imaging (ASCI) standardized practice protocol for cardiac magnetic resonance imaging (Asian Society of Cardiovascular Imaging [ASCI] et al., 2010). CMRI sequences implemented in IHD patients examined in the current study (Table 3.1) were in line with the practical and standard CMRI protocol and guideline for CMRI from the Korean Society of Cardiovascular Imaging (KOSCI) (Jo et al., 2019).

CMRI was performed based on the exact planes that meet the purpose of imaging. Even though recent MRI units provide a support system for the CMRI plane, MRI technologists in this study were familiar with various image axes for accurate imaging interpretation. The imaging plane of CMRI in IHD patients used in this study were in line with the practical and standard CMRI protocol and guideline for CMRI from the KOSCI (Jo et al., 2019).

Table 3.1: Cardiac magnetic resonance imaging (CMRI) sequences in ischemic heart disease (IHD) patients using Siemens (1.5 Tesla) scanner

Module	Sequence	Siemens (1.5 Tesla) scanner
Morphology imaging	Black or dark blood imaging	HASTE
	T_1, T_2 IR or Triple IR	TSE BB
Cine imaging	Bright blood cine and cine tagging	Cine True FISP
	SSFP or FFE gradient echo	
Perfusion imaging	PWI, TSI, EPI	EPI
LGE imaging	IR GRE or SSFP, PSIR	IR TurboFLASH
Flow imaging	Velocity-encoded cine imaging	PC

BB = black blood, EPI = echo planar imaging, FFE-SSFP = fast field echo-steady state free precession, FISP = fast imaging with steady state precession, FLASH = fast low angle shot, GRE = gradient echo, HASTE = half-Fourier acquisition single-shot turbo spin-echo, IR = inversion recovery, LGE = late gadolinium enhancement, PC = phase contrast, PSIR = phase-sensitive inversion-recovery, PWI = perfusion weighted image, TSE = turbo spin echo, TSI = time-signal intensity.

CMRI analysis was performed with a personal computer and semiautomated software (CMRStools, Cardiovascular Imaging Solutions, London, UK). The analysis included 3 principal steps: first, LV endocardial and epicardial borders were delineated in all planes in all cardiac phases; second, the systolic descent and twist of the mitral valve was calculated by tracking of the valve motion on the long axis cines and used to correct for loss of systolic LV volume due to atrioventricular ring descent; and third, blood pool thresholding was used to

delineate the papillary muscles. LV mass was calculated from the end-systolic frames. End-systolic (ESV) and end-diastolic (EDV) volumes were calculated from the LV volume/time curve generated from all frames of all cines, and there was no requirement to choose the largest and smallest ventricular frames. Stroke volume (SV) was calculated as the difference between EDV and ESV, and EF was calculated as SV/EDV. Papillary muscles were included when measuring mass (equivalent to weighing the LV) and excluded when measuring volumes (equivalent to blood pool techniques). The longitudinal atrioventricular plane descent was measured in the septum and lateral wall and expressed as a ration of the ventricular length. Finally, end-diastolic and end-systolic sphericity index was measured. Diastolic function was calculated from the derivative of the time/volume curve and expressed as a peak filling rate (PFR). The early and active peak filling rates (PFR_E and PFR_A) and the ratio were calculated (Maceira et al., 2006).

CMRI at 1.5T requires protocol optimization, careful shimming, and adjustment of the RF pulses to prevent artifacts. In addition, shortening the relaxation times of nuclei within the body is essential while using Gadolinium-based MRI contrast agents. These considerations and patient safety applied in this current study were the same to the considerations and patient safety of CMRI in IHD patients stated in the guideline for CMRI from the KOSCI (Jo et al., 2019).

In this study, the CMRI exam modules in IHD patients include cine imaging, perfusion imaging, LGE imaging, flow imaging, morphological imaging, tissue characterization T_1, T_2 and T_2 star (T_2*) mapping and coronary angiography. The purpose of each exam module was summarized in Table 3.2. These modules of scanning were compatible with the exam modules followed in the guideline for CMRI from the KOSCI (Jo et al., 2019).

3.2.2 Guidelines for performing a comprehensive transthoracic echocardiographic examination in ischemic heart disease (IHD) patients

The following guidelines for performing a comprehensive transthoracic echocardiographic examination in IHD patients were in line with recommendations from the American Society of Echocardiography (ASE) in their guidelines for performing a comprehensive transthoracic echocardiographic examination in adults (Mitchell et al., 2019).

In this study, each patient was positioned in the left lateral decubitus position (as long as the patient was able to move) for image acquisition in the left parasternal and apical windows. The parasternal long-axis (PLAX) view is located on the left side of the sternum and will provide imaging planes of the long axis of the heart with the index marker pointed toward the patient's right shoulder. The initial parasternal short-axis (PSAX) view is located in the same location as the PLAX view, but the index marker is pointed toward the patient's left shoulder. This view provides images of the heart in an axial plane. The apical window is located below the left breast tissue, where operator felt the apical impulse. In the apical window, the index marker was initially placed in the 4 to 5 o'clock position to demonstrate the apical four-chamber view. The (SC) window is located on the anterior surface of the body, just below the sternum. Image acquisition for this window was performed with the patient in the supine position. The initial view from this window was the SC four-chamber view, which was obtained with the index marker directed toward the patient's left side at the 3 o'clock position.

Table 3.2: Demonstrates purpose of cardiac magnetic resonance imaging (CMRI) exam modules in ischemic heart disease (IHD) patients

No.	CMRI exam modules in IHD patients	Purpose
1.	Cine imaging	Assess cardiac wall motion
2.	Perfusion imaging	Evaluate myocardial perfusion (ischemia)
3.	Late gadolinium enhancement (LGE) imaging	Evaluate myocardial viability
4.	Flow imaging	Measure flow velocity and volume
5.	Morphology imaging	Delineate anatomic structures
6.	Tissue characterization T_1 mapping	Evaluate the absolute T_1 value of the myocardium
7.	Tissue characterization T_2 mapping	Evaluate the absolute T_2 value of the myocardium
8.	Tissue characterization T_2* mapping	Evaluate the absolute T_2* value of the myocardium and assess cardiac iron deposition in diseases such as thalassemia major
9.	Coronary angiography	Evaluate coronary artery disease

The suprasternal notch (SSN) window is located just superior to the manubrium of the sternum. Images were obtained from this window with the patient in the supine position. The initial view demonstrated is the long axis of the aortic arch. The transducer orientation index marker was

initially directed toward the left shoulder, and the face of the transducer was directed inferior, so that the transducer was almost parallel with the neck. Small movements of rocking and angling may be used to demonstrate the best view of the aortic arch.

Scanning maneuvers followed in the current study were as follows: The terms tilt, sweep, rotate, slide, rock, and angle were used to define transducer movements. Throughout this study the term optimize refers to making the appropriate transducer movements to produce the best possible image. Signal manipulation is presented to the operator as a series of grayscale maps that allows the operator to select a setting that best displays images for a specific type of patient. Cardiac grayscale maps are designed to optimize the blood-tissue border (specular echoes) and demonstrate subtle differences in scattered echoes from weak reflectors, such as myocardium. Once laboratory protocols are selected, it is important to maintain consistent settings, as this may facilitate longitudinal comparisons with previous studies. Spectral Doppler parameters that were adjusted by the operator at the time of image acquisition include velocity scale, baseline position, sweep speed, velocity filters, sample volume size and Doppler gain.

3.3 Statistical analysis

The process of analyzing data was carried out using the Statistical Package for the Social Sciences version 20 for Windows (IBM Corporation, Armonk, NY, USA), while the layout of the results was initially summarized in a comparison tables and graphs. All study variable were presented as mean±SD. The statistical diagnostic test was used to detect sensitivity, specificity, accuracy, positive and negative likelihood ratio, disease prevalence and positive a negative predictive value of CMRI and 2D echo in the diagnosis of IHD in the study samples.

CHAPTER FOUR

RESULTS

Chapter Four

Results

4.1 Results

One hundred (61% males and 39% females; mean age of 50±20.1 and 35±18.4 for males and females, respectively) patients that were clinically diagnosed to have IHD were enrolled prospectively in this study after having their written and verbal consent as well as an agreement of the local ethics committee at the Radiology and Medical Imaging Department, King Fahad Medical City, Riyadh- Saudi Arabia (Table 4.1 and Figure 4.1). They all were examined using CMRI and 2D echo to localize the affected coronary artery and to predict the affected myocardial segments. Conventional coronary angiography was the gold standard tool that used in all patients to confirm the diagnosis for each case. The major inclusion criterion was scheduled for CMRI, 2D echo and conventional coronary angiography. Other criteria were, sinus heart rhythm, ability to hold breath for 10–20 sec and normal serum creatinine. Exclusion criteria were hemodynamic instability, atrial fibrillation, contraindications for MRI, claustrophobia, applied pacemaker or metal implants, contraindication for contrast material, including known allergy and renal insufficiency (serum creatinine more than 1.4 mg/dl).

Table 4.1: Age range (years), age distribution (n; %) and mean age (mean±SD) in the ischemic heart disease (IHD) patients

Age ranges (years)	**Male distribution (n; %)**	**Female distribution (n; %)**	**Total (n; %)**	**Male mean age (mean±SD)**	**Female mean age (mean±SD)**
13-23	(11; 18%)	(4; 10.3%)	(15; 15%)	(21±3.4)	(19.5±2.4)
24-34	(7; 11.5%)	(3; 7.7%)	(10; 10%)	(27±3.0)	(29±2.9)
35-45	(8; 13.1%)	(10; 25.6%)	(18; 18%)	(38±1.3)	(38.5±4.2)
46-56	(16; 26.2%)	(4; 10.3%)	(20; 20%)	(53±3.1)	(51±3.4)
57-67	(11; 18%)	(14; 35.9%)	(25; 25%)	(63±3.1)	(60.5±2.1)
68-78	(4; 6.6%)	(4; 10.3%)	(8; 8%)	(75±2.1)	(71±2.2)
79-89	(3; 4.9%)	(0; 0%)	(3; 3%)	(85±0.6)	(0±0.0)
90-100	(1; 1.6%)	(0; 0%)	(1; 1%)	(91±0.0)	(0±0.0)
Total	(61; 100%)	(39; 100%)	(100; 100%)	(50±20.1)	(35±18.4)

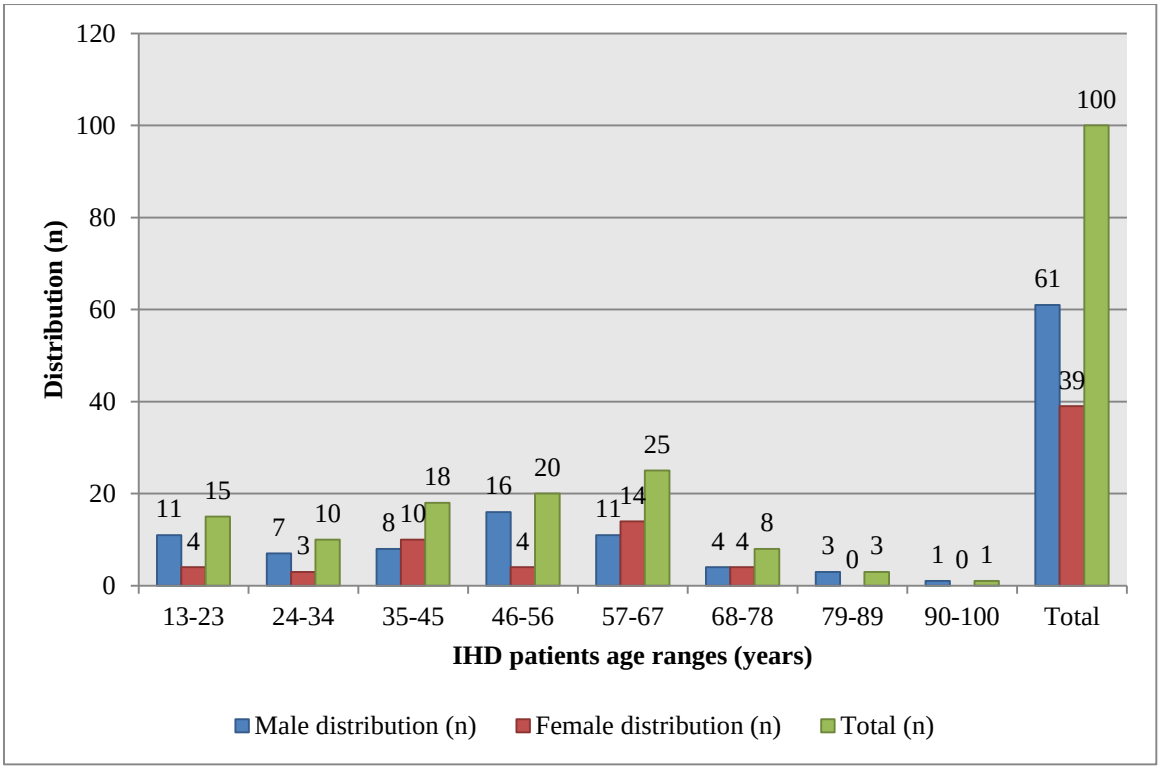

Figure 4.1: Age range (years), age distribution (n; %) and mean age (mean±SD) in the ischemic heart disease (IHD) patients.

Results revealed that the majority of IHD male patients were from the Center of Saudi Arabia (44.3%) and the least location of IHD male patients was the East of Saudi Arabia (8.2%), while for IHD, female patients, the majority were located in the Center of Saudi Arabia (48.7%) and the least location was the West of Saudi Arabia (5.1%) as demonstrated in Table 4.2 and Figure 4.2. Regarding IHD male patients occupation (Table 4.3 and Figure 4.3), they were soldiers (50.8%), manager (32.8%), teacher (6.6%), driver (4.9%), employee (3.3%) and worker (1.6%). The distribution of percentage of IHD, female patients (Table 4.3 and Figure 4.3) were housewife (35.9%), teacher (25.6%), manager (23.1%) and employee (15.4%).

Table 4.2: Location (n; %) of the ischemic heart disease (IHD) patients in Saudi Arabia

Patients location	Male location (n; %)	Female location (n; %)	Total (n; %)
Center	(27; 44.3%)	(19; 48.7%)	(46; 46%)
North	(11; 18%)	(6; 15.4%)	(17; 17%0
South	(12; 19.7%)	(8; 20.5%)	(20; 20%)
East	(5; 8.2%)	(4; 10.3%)	(9; 9%)
West	(6; 9.8%)	(2; 5.1%)	(8; 8%)
Total	(61; 100%)	(39; 100%)	(100; 100%)

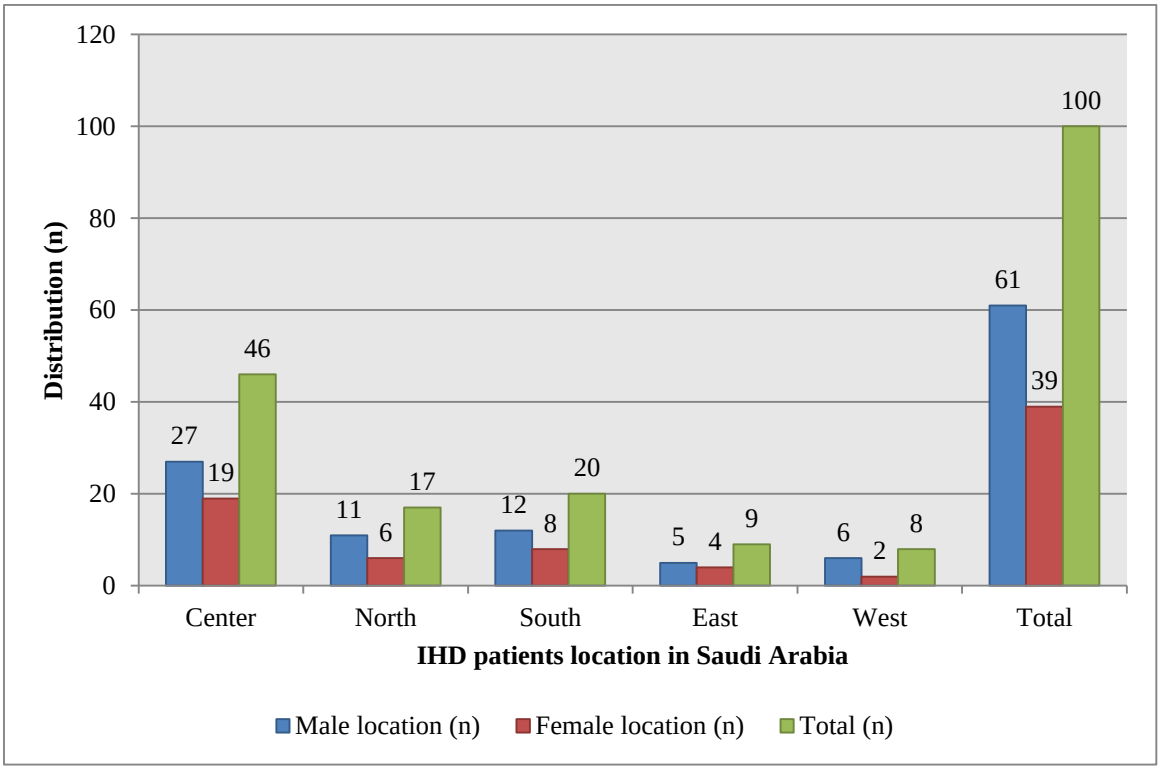

Figure 4.2: Location (n; %) of ischemic heart disease (IHD) patients in Saudi Arabia.

Table 4.3: Distribution (n; %) of occupation among ischemic heart disease (IHD) patients

Patients' occupation	Male patients (n; %)	Female patients (n; %)	Total (n; %)
Employee	(2; 3.3%)	(6; 15.4%)	(8; 8%)
Manager	(20; 32.8%)	(9; 23.1%)	(29; 29%)
Teacher	(4; 6.6%)	(10; 25.6%)	(14; 14%)
Housewife	(0; 0%)	(14; 35.9%)	(14; 14%)
Worker	(1; 1.6%)	(0; 0%)	(1; 1%)
Soldier	(31; 50.8%)	(0; 0%)	(31; 31%)
Driver	(3; 4.9%)	(0; 0%)	(3; 3%)
Total	(61; 100%)	(39; 100%)	(100; 100%)

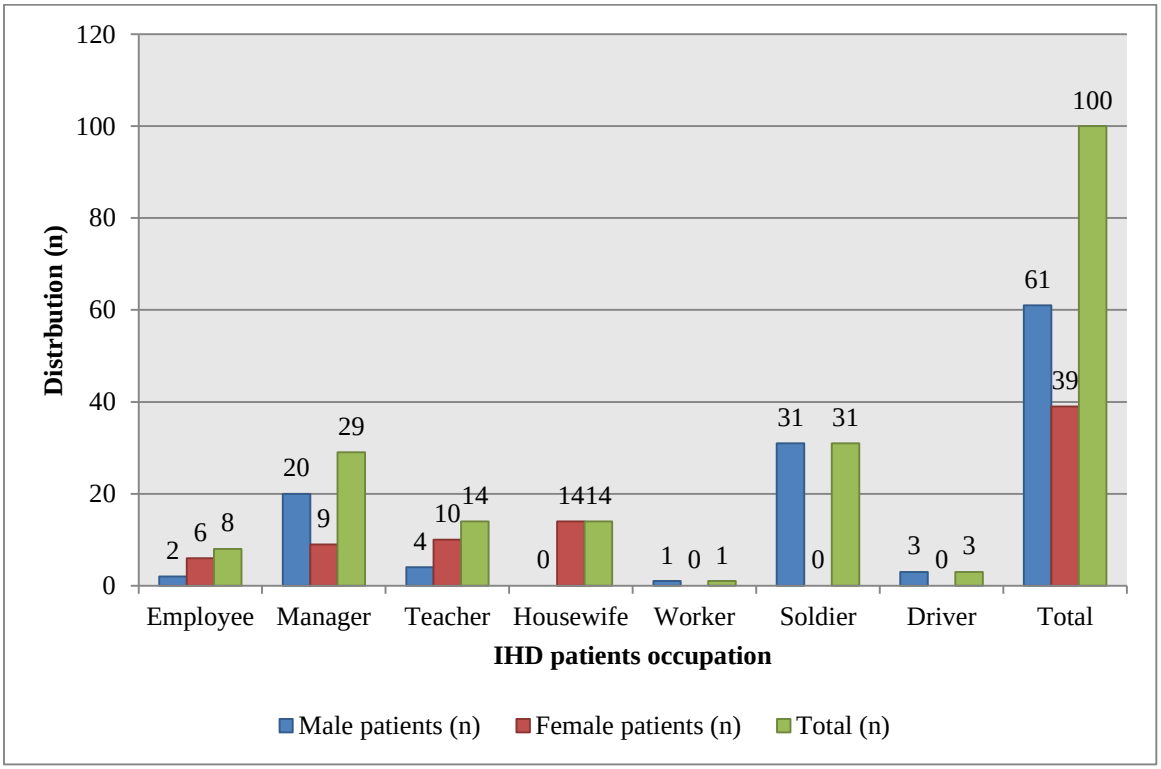

Figure 4.3: Distribution (n; %) of occupation among ischemic heart disease (IHD) patients.

The symptoms detected in IHD male and female patients include sweating (90.2%; 71.8%), weakness (85.3%; 97.4%), angina (80.3%; 71.8%), shortness of breath (72.1%; 79.5%), dizziness (63.9%; 82.1%) and nausea (60.7%; 51.3%), respectively (Table 4.4 and Figure 4.4).

Table 4.4: Symptoms presentation (n; %) in ischemic heart disease (IHD) patients

Patient symptoms	**Male patients (n; %)**	**Female patients (n; %)**
Angina (chest pain)	(49; 80.3%)	(28; 71.8%)
Shortness of breath	(44; 72.1%)	(31; 79.5%)
Sweating	(55; 90.2%)	(28; 71.8%)
Weakness	(52; 85.3%)	(38; 97.4%)
Dizziness	(39; 63.9%)	(32; 82.1%)
Nausea	(37; 60.7%)	(20; 51.3%)
Tachycardia	(22; 36.1%)	(17; 43.6%)
Palpations	(41; 67.2%)	(30; 76.9%)

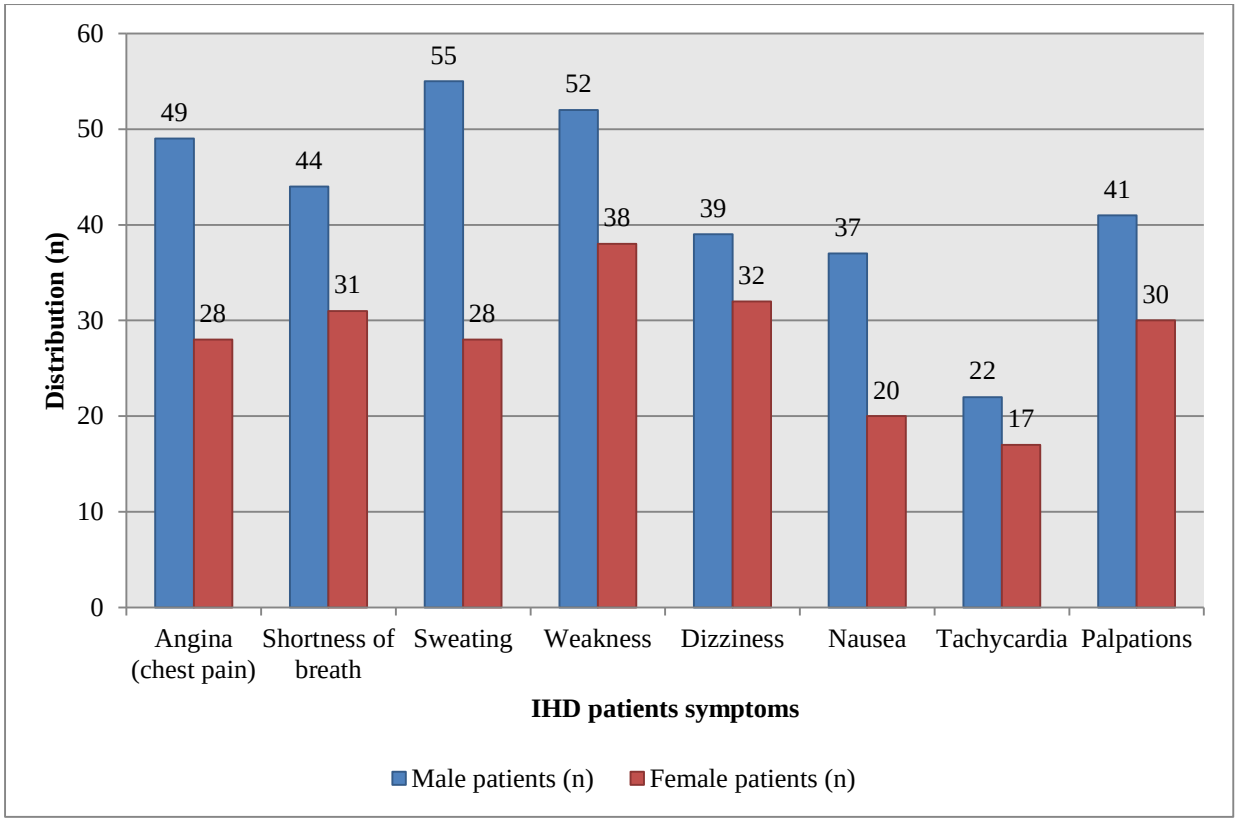

Figure 4.4: Symptoms presentation (n; %) in ischemic heart disease (IHD) patients.

Lifestyle risk factors of IHD patients in the current study were smoking (88.5%; 5.1%), absent physical activity (82%; 84.6%), high fat intake (55.7%; 61.5%), non-vegetarian diet intake (29.5%; 38.5%), obesity (24.6%; 43.6%) and alcohol intake (13.1%; 0%) in male and female patients, respectively (Table 4.5 and Figure 4.5).

Table 4.5: Lifestyle risk factors presented in ischemic heart disease (IHD) patients

Lifestyle risk factors of IHD	Male patients (n; %)	Female patients (n; %)
Smoking	(54; 88.5%)	(2; 5.1%)
Alcohol intake	(8; 13.1%)	(0; 0%;)
Non-vegetarian diet intake	(18; 29.5%)	(15; 38.5%)
High fat intake	(34; 55.7%)	(24; 61.5%)
Absent physical activity	(50; 82%)	(33; 84.6%)
Obesity	(15; 24.6%)	(17; 43.6%)

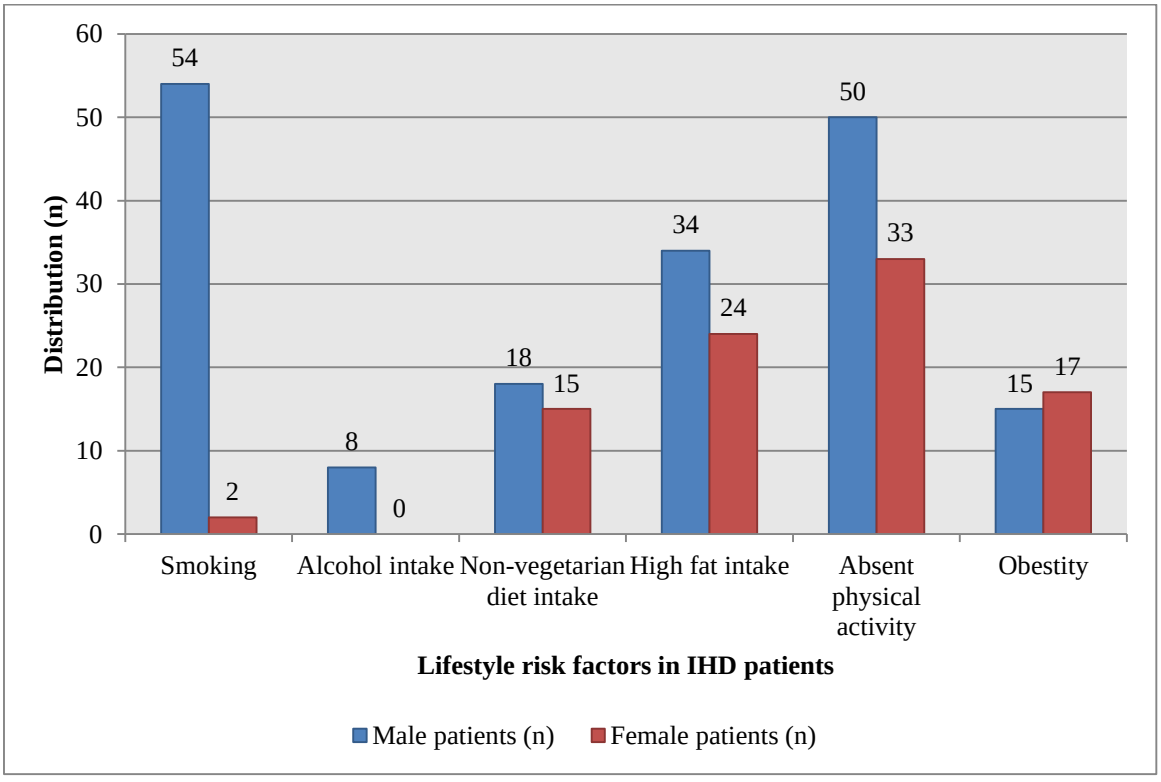

Figure 4.5: Lifestyle risk factors presented in ischemic heart disease (IHD) patients.

The LV volumes and systolic function by age decile in CAD male patients using CMRI were presented in Table 4.6 and Figure 4.6. The mean±SD was 28.9±3.5%, 53.3±11.2 ml, 100.6±7.1

bpm, 5.4±1.4 L/min, 189±14.3 ml and 136±3.1 ml for LVEF, SV, heart rate, cardiac output, EDV and ESV, respectively.

Table 4.6: Left ventricular (LV) volumes and systolic function by age decile in ischemic heart disease (IHD) male patients using cardiac magnetic resonance image (CMRI)

Males age ranges (years)	**13-23**	**24-34**	**35-45**	**46-56**	**57-67**	**68-78**	**79-89**	**90-100**	**Mean±SD**
LVEF (%)	34.1	30.5	30	29	27.4	25.6	31.4	22.8	28.9±3.5
SV (ml)	73	61	59	55	51	46	42	39	53.3±11.2
Heart rate (bpm)	104.1	114.8	101.7	92.7	98	93.5	97.6	102.6	100.6±7.1
Cardiac output (L/min)	7.6	7	6	5.1	5	4.3	4.1	4	5.4±1.4
EDV (ml)	214	200	197	190	186	180	175	171	189±14.3
ESV (ml)	141	139	138	135	135	134	133	132	136±3.1

LVEF, Left ventricle ejection fraction; SV, Stroke volume; EDV, End diastolic volume; ESV, End systolic volume

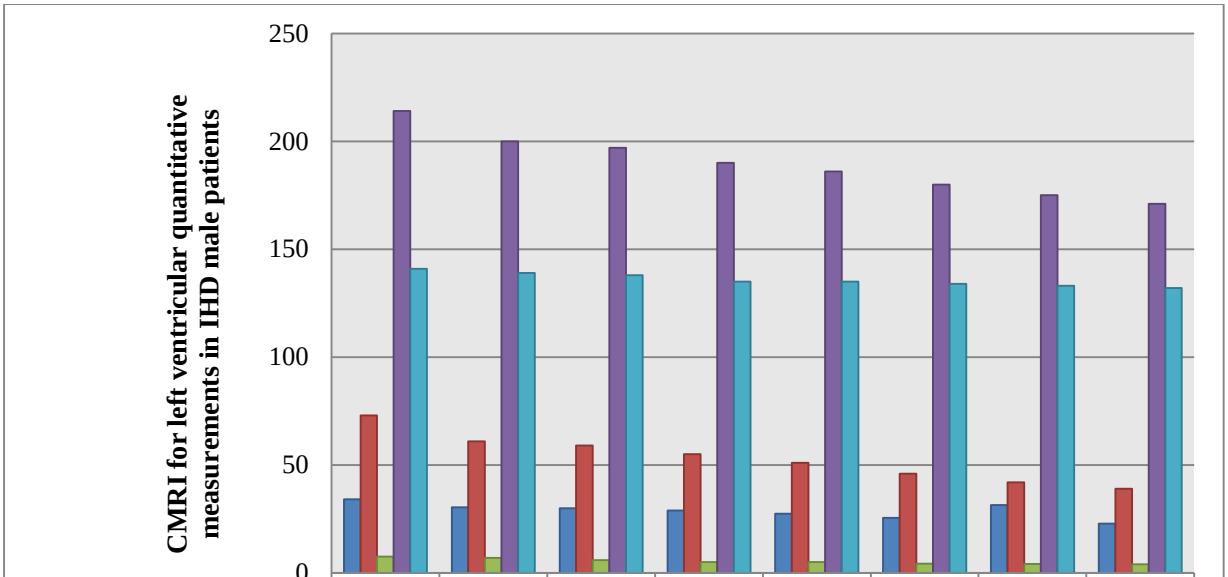

	13-23	24-34	35-45	46-56	57-67	68-78	79-89	90-100
LVEF (%)	34.1	30.5	30	29	27.4	25.6	31.4	22.8
SV (ml)	73	61	59	55	51	46	42	39
Cardiac output (L/min)	7.6	7	6	5.1	5	4.3	4.1	4
EDV (ml)	214	200	197	190	186	180	175	171
ESV (ml)	141	139	138	135	135	134	133	132

Figure 4.6: Left ventricular (LV) volumes and systolic function by age decile in ischemic heart disease (IHD) male patients using cardiac magnetic resonance image (CMRI).

In contrast, the LV volumes and systolic function by age decile in CAD, female patients using CMRI were presented in Table 4.7 and Figure 4.7. In addition, the mean±SD was 32±1.7%, 58±6.6 ml, 98.3±14.7 bpm, 5.8±1.5 L/min, 180±10.9 ml and 123±4.4 ml for LVEF, SV, heart rate, cardiac output, EDV and ESV, respectively.

Table 4.7: Left ventricular (LV) volumes and systolic function by age decile in ischemic heart disease (IHD) female patients using cardiac magnetic resonance image (CMRI)

Females age ranges (years)	**13-23**	**24-34**	**35-45**	**46-56**	**57-67**	**68-78**	**79-89**	**90-100**	**Mean±SD**
LVEF (%)	35	33.9	32.1	32.2	31.6	30.6	30	30.8	32±1.7
SV (ml)	70	65	59	58	56	53	51	52	58±6.6
Heart rate (bpm)	114.3	120	108.5	98.3	92.9	86.8	86.3	78.9	98.3±14.7
Cardiac output (L/min)	8	7.8	6.4	5.7	5.2	4.6	4.4	4.1	5.8±1.5
EDV (ml)	200	192	184	180	177	173	170	169	180±10.9
ESV (ml)	130	127	125	122	121	120	119	117	123±4.4
LVEF, Left ventricle ejection fraction; SV, Stroke volume; EDV, End diastolic volume; ESV, End systolic volume									

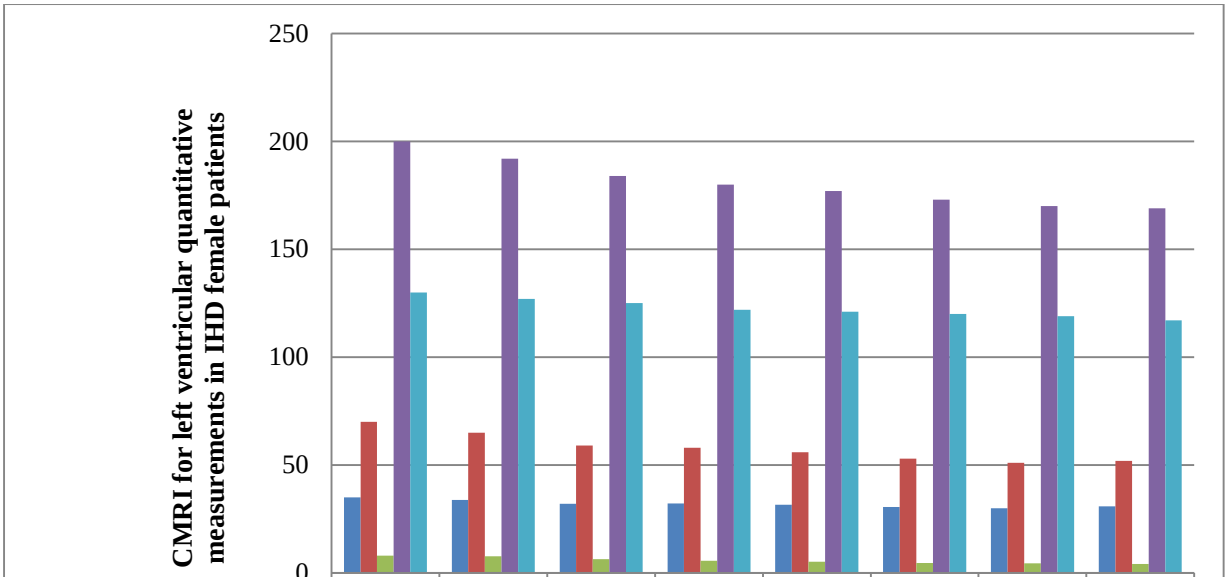

	13-23	24-34	35-45	46-56	57-67	68-78	79-89	90-100
LVEF (%)	35	33.9	32.1	32.2	31.6	30.6	30	30.8
SV (ml)	70	65	59	58	56	53	51	52
Cardiac output (L/min)	8	7.8	6.4	5.7	5.2	4.6	4.4	4.1
EDV (ml)	200	192	184	180	177	173	170	169
ESV (ml)	130	127	125	122	121	120	119	117

Figure 4.7: Left ventricular (LV) volumes and systolic function by age decile in ischemic heart disease (IHD) female patients using cardiac magnetic resonance image (CMRI).

Table 4.8: Two-dimensional echocardiography (2D echo) findings in ischemic heart disease (IHD) patients

Findings	**IHD male patients (n; %)**	**IHD female patients (n; %)**
Dilated left ventricle	(61; 100%)	(39; 100%)
Left ventricular global and regional systolic dysfunction	(61; 100%)	(39; 100%)
Hypokinesia in the anterior and septal wall	(61; 100%)	(39; 100%)
Normal right ventricle and systolic function	(61; 100%)	(39; 100%)
75% myocardial infarction involving mid anterior segment with low likelihood of viability	(57; 93.4%)	(32; 82.1%)
Mitral regurgitation	(13; 21.3%)	(4; 10.3%)
Dilated left atrium	(9; 14.8%)	(1; 2.6%)
Pericardial effusion	(2; 3.3%)	(0; 0%)
Intraventricular thrombus	(3; 4.9%)	(1; 2.6%)

In all IHD patients, the 2D echo findings were dilated left ventricle, left ventricular global and regional systolic dysfunction, hypokinesia in the anterior and septal wall and normal right ventricle and systolic function. Conditions as 75% myocardial infarction involving mid anterior segment with low likelihood of viability, mitral regurgitation, dilated left atrium, pericardial effusion and intraventricular thrombus present an incidence of 93.4%; 82.1%, 21.3%; 10.3%, 14.8%; 2.6%, 3.3%; 0% and 4.9%; 2.6% in IHD male and female patients, respectively (Table 4.8 and Figure 4.8).

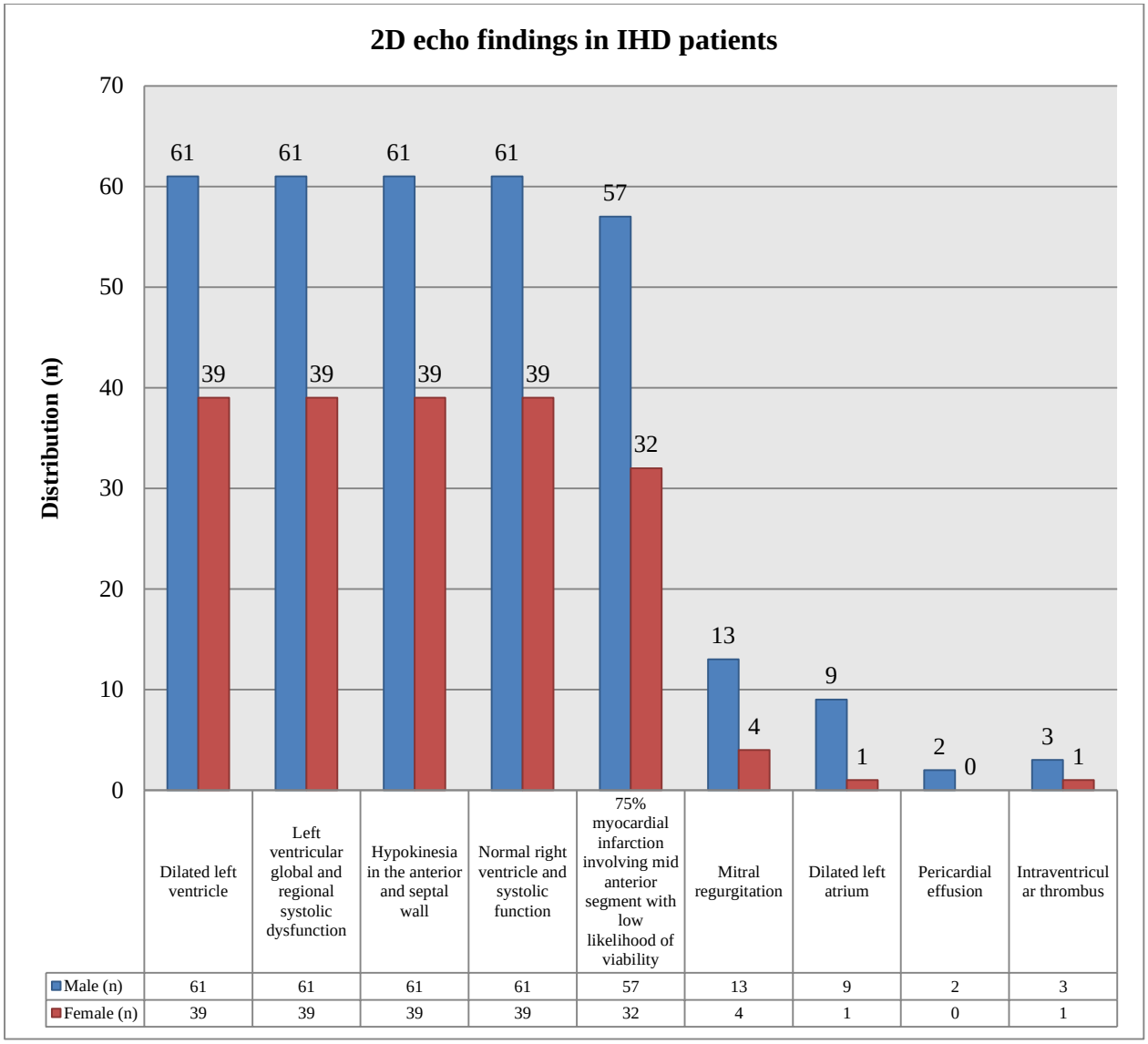

Figure 4.8: Two-dimensional echocardiography (2D echo) findings in ischemic heart disease (IHD) patients.

Diagnostic test characteristics revealed that CMRI in the diagnosis of IHD in Saudi patients presents a sensitivity, specificity and accuracy of 97.98%, 25% and 95.15%, respectively. While the sensitivity, specificity and accuracy of 2D echo in the diagnosis of IHD in Saudi patients were 97.87%, 11.11% and 90.29%, respectively. In addition, the positive and negative likelihood ratio for CMRI compared to 2D echo in the diagnosis of IHD were 1.31; 1.1 and 0.08; 0.19. Furthermore, the disease prevelance was determined to be 96.12% by using CMRI compared to a prevelance of 91.26% while using 2D echo. Positive and negative predictive value of CMRI and 2D echo in the diagnosis of IHD in Saudi patients were 97%; 92% and

33.33%; 33.33%, respectively (Table 4.9, Table 4.10 and Figure 4.9). Much more, the 95% confidence interval (CI), which is a type of estimate computed from the statistics of the observed data, was determine for the diagnostic test characteristics (Table 4.9, Table 4.10 and Figure 4.9).

Table 4.9: Diagnostic test characteristics of cardiac magnetic resonance image (CMRI) in the diagnosis of ischemic heart disease (IHD) in Saudi patients

True positive	97	
False Positive	3	
False negative	2	
True negative	1	
Statistics	**Value**	**95% confidence interval (CI)**
Sensitivity	97.98%	92.89% to 99.75
Specificity	25.00%	0.63% to 80.59%
Positive Likelihood Ratio	1.31	0.74 to 2.30
Negative Likelihood Ratio	0.08	0.01 to 0.72
Disease prevalence	96.12%	90.35% to 98.93%
Positive Predictive Value	97.00%	94.83% to 98.28%
Negative Predictive Value	33.33%	5.34% to 81.60%
Accuracy	95.15%	89.03% to 98.41%

Table 4.10: Diagnostic test characteristics of two-dimensional echocardiography (2D echo) in the diagnosis of ischemic heart disease (IHD) in Saudi patients

True positive	92	
False Positive	8	
False negative	2	
True negative	1	
Statistics	**Value**	**95% confidence interval (CI)**
Sensitivity	97.87%	92.52% to 99.74%
Specificity	11.11%	0.28% to 48.25%
Positive Likelihood Ratio	1.1	0.87 to 1.39
Negative Likelihood Ratio	0.19	0.02 to 1.91
Disease prevalence	91.26%	84.06% to 95.93%
Positive Predictive Value	92.00%	90.11% to 93.56%
Negative Predictive Value	33.33%	4.77% to 83.31%
Accuracy	90.29%	82.87% to 95.25%

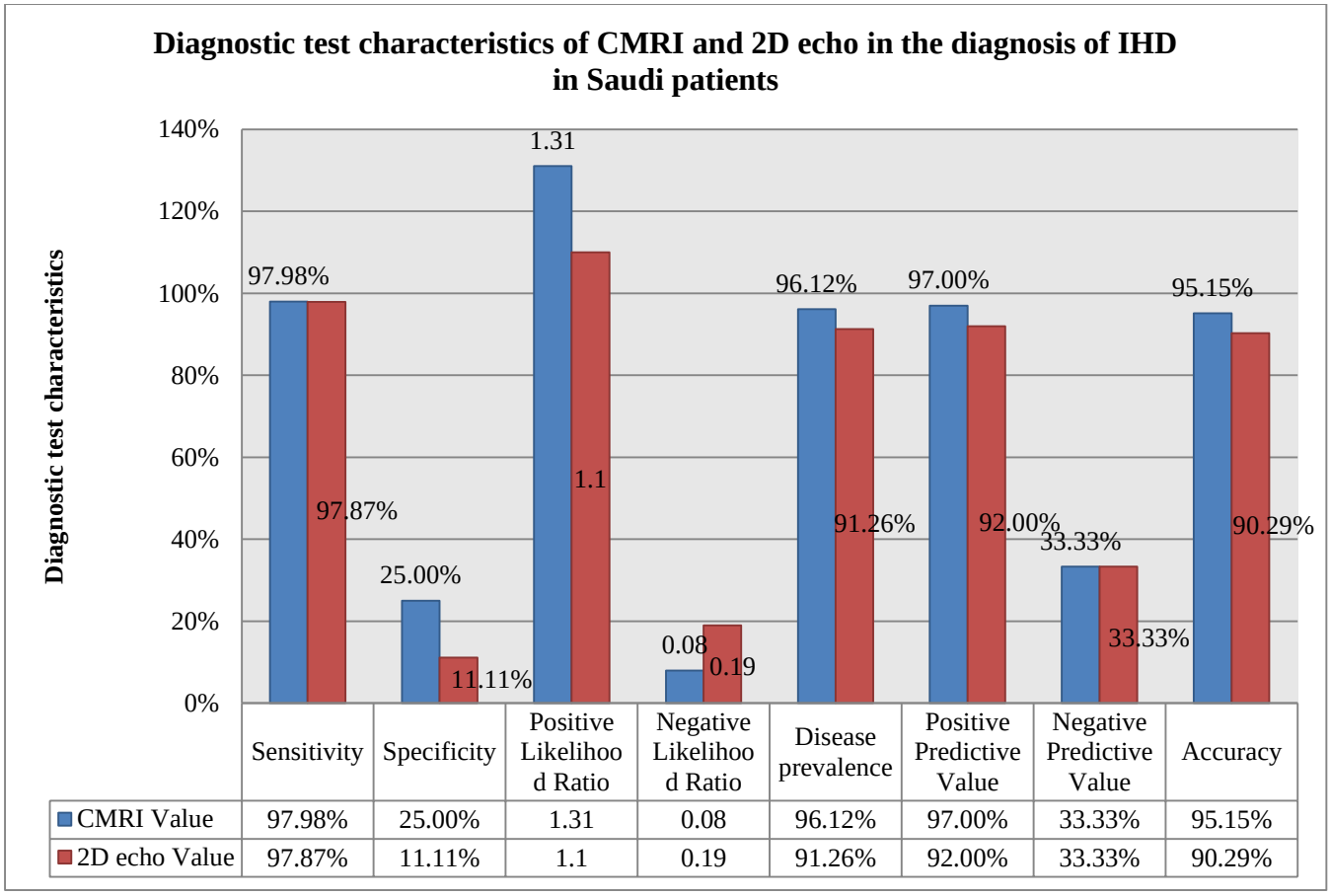

Figure 4.9: Diagnostic test characteristics of cardiac magnetic resonance image (CMRI) and two-dimensional echocardiography (2D echo) in the diagnosis of ischemic heart disease (IHD) in Saudi patients.

CHAPTER FIVE

DISCUSSION, CONCLUSION & RECOMMENDATIONS

Chapter Five

Discussion, conclusion and recommendations

5.1 Discussion

In developed countries, CAD continuos to be a major cause of death and disability. Since introduction of the CMRI as a non-invasive tool for depection of the CAD, the clinical value of myocardial MRI has been the subject for research work. Several comparative studies for evaluation of CMRI as a diagnostic tool for CAD using the conventional angiography as the gold standard have been published. The results of these researches concluded that CMRI is considered as accurate imaging tool in detection of myocardial viability (Abdelrahman et al., 2016). The CMRI has been applied for the measurements of LV volume, systolic function and mass for several years in the clinical arena, with standardized methods of short axis multi-slice acquisition (Bellenger & Pennell, 2002). The excellent accuracy and reproducibility of CMRI is well established, making it a gold standard technique which can be very cost effective (Grothues et al., 2002; Bellenger et al., 2000).

2D echo is well accepted for the evaluation of cardiac function (Cheitlin et al., 2003). It is the most employed cardiovascular imaging modality for assessment of cardiovascular disease and is often performed in patients without history of CAD. It is well established that several echocardiographic measurements provide powerful prognostic information for cardiovascular outcomes such as presence of LV hypertrophy, aortic sclerosis and LVEF (Cheitlin et al., 2003; Chaves et al., 2004). However, the association of these features with underlying CAD is less well established (Chang et al., 2009). More than half of the patients with major Q wave or a QS complex changes on the ECG from the Cardiovascular Health Study did not report a previous myocardial infarction (Chaves et al., 2004). 2D echo is often performed and abnormality found in patients withoud known CAD. Therefore it might offer a unique

apportunity to identify patients with unsuspected CAD who might have a worse outcome and warrant early medical or invasive intervention (Chang et al., 2009).

Findings of the CMRI and 2D echo in the current study were compared to those of the corresponding conventional coronary angiograms. Conventional invasive coronary angiography is the gold standard for the diagnosing the presence of significant stenosis, it is reserved for patients whose clinical risk is assessed as high or when stress testing indicates significant ischemic burden (Fihn et al., 2012). This study was directed with a sample of 100 Saudi patients that were clinically diagnosed to have IHD, recruited prospectively at the Radiology and Medical Imaging Department, King Fahad Medical City, Riyadh- Saudi Arabia (Table 4.1 and Figure 4.1) with an aim to study the value of usage 2D echo and CMRI as a diagnostic tool to diagnose IHD.

To the best of our knowledge, current study is the first study to correlate 2D echo findingis to CMRI results in IHD patients. Study results revealed that the majority of IHD male patients were from the Center of Saudi Arabia (44.3%) and the least location of IHD male patients was the East of Saudi Arabia (8.2%), while for IHD, female patients, the majority were located in the Center of Saudi Arabia (48.7%) and the least location was the West of Saudi Arabia (5.1%) as demonstrated in Table 4.2 and Figure 4.2. Regarding IHD male patients occupation (Table 4.3 and Figure 4.3), they were soldiers (50.8%), manager (32.8%), teacher (6.6%), driver (4.9%), employee (3.3%) and worker (1.6%). The distribution of percentage of IHD, female patients (Table 4.3 and Figure 4.3) were housewife (35.9%), teacher (25.6%), manager (23.1%) and employee (15.4%). Such findings could be compare with the findings of a study about normalized LV systolic and diastolic function by steady state free precession cardiovascular magnetic resonance (Maceira et al., 2006).

The symptoms detected in IHD male and female patients include sweating (90.2%; 71.8%), weakness (85.3%; 97.4%), angina (80.3%; 71.8%), shortness of breath (72.1%; 79.5%),

dizziness (63.9%; 82.1%) and nausea (60.7%; 51.3%), respectively (Table 4.4 and Figure 4.4). Lifestyle risk factors of IHD patients in the current study were smoking (88.5%; 5.1%), absent physical activity (82.%; 84.6%), high fat intake (55.7%; 61.5%), non-vegetarian diet intake (29.5%; 38.5%), obesity (24.6%; 43.6%) and alcohol intake (13.1%; 0%) in male and female patients, respectively (Table 4.5 and Figure 4.5). The current results could be compared with Chang et al. (2009) whom predicting clinically unrecognized CAD by using 2D echo in 238 patients without know CAD and their mean age was 62±13 years, 59% men, 29% diabetic and 45% had >2 risk factors for CAD.

Influence of gender on LV volume shows that LV volume is significantly larger in males ($p < 0.001$). On a multivariate analysis, gender had significant independent influence on normalized LV volume. While regarding influence of age on LV parameter, there was a significant decrease in absolute and normalized ESV with increasing age in females ($p = 0.013$). Normalized EDV also decreased with age in males and females ($p = 0.019$). LVEF did not show significant changes with age in either males or females. On multivariate analysis, age was independent predictor of all absolute and normalized ventricular volumes (EDV, ESV and SV). All absolute and normalized ventricular volumes decreased significantly with age (EDV both $p < 0.001$; ESV both $p = 0.001$; SV both $p < 0.01$) (Maceira et al., 2006). Such findings could be compared to our results on LV volumes and systolic function by age decile in ischemic heart disease (IHD) male and female patients using cardiac magnetic resonance image (CMRI) as demonstrated in (Table 4.6 and Figure 4.6) and (Table 4.6 and Figure 4.7).

In this reserach the 2D echo findings in IHD male and female patients were dilated left ventricle (100%; 100%), left ventricular global and regional systolic dysfunction (100%; 100%), hypokinesia in the anterior and septal wall and normal right ventricle and systolic function (100%; 100%), 75% myocardial infarction involving mid anterior segment with low likelihood of viability (93.4%; 82.1%), mitral regurgitation (21.3%; 10.3%), dilated left atrium (14.8%;

2.6%), pericardial effusion (3.3%; 0%) and intraventricular thrombus (4.9%; 2.6%) (Table 4.8 and Figure 4.8). Such findings could be compared to the findings of Chang et al. (2009) were myocardial perfusion abnormality was present in 200 patients (60%), coronary artery stenosis was present in 166 patients (51%), wall motion abnormality in 87 patients (26.5%). Thus, they stated that 2D echo findings offered incremental value over clinical information in prediction CAD by angiography (Chi square: 360 versus 320; $p = 0.02$).

One of the most important strengths of this study is that it used the diagnostic test to revealed the sensitivity, specificity and accuracy of CMRI in the diagnosis of IHD in Saudi patients in compare to 2D echo of the same disease and that was after the confirmation of the diagnosis of each case using the conventional angiography as the gold standard tool. Where it has been statistically proven that CMRI had a sensitivity, specificity and accuracy higer than that of 2D echo in the diagnosis of IHD (Table 4.9, Table 4.10 and Figure 4.9) which is an added value for the current study based on that this finding regarding sensitivity, specificity and accuracy is not available in comparable studies for comparison. Limitations of this study were there was a limited cohort sample size and the heterogeneity of the population due to the randomized selection process, which may affect the exactness of our outcomes and impair the strength of our conclusions, since it causes other age groups have a less factual validity if committed in future investigations. However, to the best of our knowledge, this is the first cohort study that compare between the usage of 2D echo and CMRI as a diagnostic tool in IHD patients which therefore represents the importance of this study.

5.2 Conclusion

In conclusion, CMRI gives a complete assessment of LV function, myocardial perfusion and viability and as well as the coronary anatomy. Although the availability of CMRI is limited at this time, but increase in training investigators and technologists, standardization of MRI protocols and awareness of the CMRI value would enhance the use of CMRI in clinical practice. 2D echo is central to the diagnosis, management and prognosis of the entire spectrum of IHD. Several features in 2D echo provide incremental value over clinical information in predicting the presence of physiological and anatomical IHD in patients without known IHD. The main drawback of 2D echo remains in the limited echogenicity of many patients and its undeniable operator dependence. One of the most important strengths of this study is that it revealed the sensitivity, specificity and accuracy of CMRI in the diagnosis of IHD in Saudi patients in compare to 2D echo of the same disease and that was after the confirmation of the diagnosis of each case using the conventional angiography as the gold standard tool.

5.3 Recommendations

- 2D echo is an accurate tool for the evaluation of patients with known or suspected IHD. Every patient should be evaluated clinically for pretest probability of IHD and risk of future cardiac events.
- Resting 2D echo is generally considered inadequate to rule out the presence of functionally significant IHD, especially in the absence of ongoing chest pain or ECG signs of ischemia.
- CMRI has emerged as a prime player in the clinical and preclinical detection of IHD as well in the prognosis assessment by offering a comprehensive approach for all spectrums of IHD patients.
- Currently available CMRI techniques as anatomic imaging with visualization of IHD and on the other hand, ischemia imaging with evaluation of the consequences of IHD to the heart, particularly myocardial perfusion and function and depiction of irreversible myocardial damage are able to fulfill the aims of imaging in IHD patients.
- CMRI is technically complicated and its use in clinical practice is relatively limited. With further improvements in education and training, as well as standardization of appropriate study protocols, CMRI will play a central role in managing patients with IHD.
- Conventional selective coronary angiography continues as a cornerstone in the evaluation of the coronary arteries and is indicated not only to diagnose IHD but also to assess its severity.

REFERENCES

References

A. O. Zurick III, M. Desai. CT and MR Cardiovascular Hemodynamics, In: Anwaruddin, S., Martin, J. M., Stephens, J. C., Askari, A. T., eds. Cardiovascular Hemodynamics: An Introductory Guide. 2nd ed. Humana Press, New York; 2013: 148.

Abdelrahman, S. F., Ali, M. T., Salem, M. A., Sabri, S. (2016). Utility of cardiac MRI in the assessment of myocardial viability: Evaluating its role using 3-T machine in correlation with SPECT. The Egyptian Journal of Radiology and Nuclear Medicine; 47: 73–81.

Aggarwal, N. R., Bond, R. M., & Mieres, J. H. (2018). The role of imaging in women with ischemic heart disease. Clinical Cardiology; 41: 194–202.

Ampanozi, G., Krinke, E., Laberke, P., Schweitzer, W., Thali, M. J., & Ebert, L. C. (2018). Comparing fist size to heart size is not a viable technique to assess cardiomegaly. Cardiovascular Pathology; 36: 1–5.

Andrew, B. Oh's Intensive Care Manual. 7th ed. London: Elsevier Health Sciences; 2013: 912–922.

Asanuma, T., Fukuta, Y., Masuda, K., Hioki, A., Iwasaki, M., & Nakatani, S. (2012). Assessment of myocardial ischemic memory using speckle tracking echocardiography. JACC Cardiovascular Imaging; 5: 1–11.

ASCI CCT and CMR Guideline Working Group. Chan CW, Choi BW, Jinzaki M, Kitagawa K, Tsai IC, Yong HS, et al. ASCI 2010 standardized practice protocol for cardiac magnetic

resonance imaging: a report of the Asian Society of Cardiovascular Imaging cardiac computed tomography and cardiac magnetic resonance imaging guideline working group. Int J Cardiovasc Imaging; 2010; 26: 187–202.

Atkinson, D. J., & Edelman, R. R. (1991). Cineangiography of the heart in a single breath hold with a segmented turbo FLASH sequence. Radiology; 178: 357–360.

Badiwala, M. V., Verma, S., & Rao, V. (2009). Surgical management of ischemic mitral regurgitation. Circulation; 120: 1287–1293.

Baumgartner, H., Bonhoeffer, P., De Groot, N. M., de Haan, F., Deanfield, J. E., Galie, N., & et al. (2010). ESC Guidelines for the management of grown-up congenital heart disease (new version 2010). European Heart Journal; 31: 2915–2957.

Bellenger, N. G. and Pennell, D. J. Ventricular function. In W. J. Manning, D. J. Pennell (Ed.). Cardiovasuclar magnetic resonance. New York, NY Churchill Livingstone; 2002: 99–111.

Berry, W., & McKenzie, C. (2010). Use of inotropes in critical care. Clinical Pharmacist; 2: 395.

Betts, J. G. Anatomy & physiology. 1st ed. OpenStax; 2013.

Bogaert, J., & Rademakers, F. E. (2001). Regional nonuniformity of normal adult human left ventricle. Am J Physiol Heart Circ Physiol; 280: H610–620.

Bruder, O., Wagner, A., Lombardi, M., Schwitter, J., & van Rossum, A. e t al., 2013. European cardiovascular magnetic resonance (EuroCMR) registry-multi national results from 57 centers in 15 countries. J. Cardiovasc Magn Reson; 15: 1.

Bruder, O., Wagner, A., Lombardi, M., Schwitter, J., van Rossum, A., Pilz, G., & et al. 2013). European Cardiovascular Magnetic Resonance (EuroCMR) registry--multi national results from 57 centers in 15 countries. J Cardiovasc Magn Reson; 15: 9.

Buckert, D., Witzel, S., Steinacker, J. M., Rottbauer, W., & Bernhardt, P. (2018). Comparing Cardiac Magnetic Resonance–Guided Versus Angiography-Guided Treatment of Patients With Stable Coronary Artery Disease. J Am Coll Cardiol Img; 11: 987-996.

Capotosto, L., Massoni, F., De Sio, S., Ricci, S. & Vitarelli, A. (2018). Early Diagnosis of Cardiovascular Diseases in Workers: Role of Standard and Advanced Echocardiography. BioMed Research International; 2018: 15.

Carlsson, M., Ubachs, J. F., Hedström, E., Heiberg, E., Jovinge, S., & Arheden, H. (2009). Myocardium at risk after acute infarction in humans on cardiac magnetic resonance: quantitative assessment during follow-up and validation with single-photon emission computed tomography. JACC Cardiovasc Imaging; 2: 569–576.

Chang, S. A., & Kim, R. J. (2016). The Use of Cardiac Magnetic Resonance in Patients with Suspected Coronary Artery Disease: A Clinical Practice Perspective. Journal of cardiovascular ultrasound; 24: 96–103.

Chang, S. M., Hakeem, A., Nagueh, S. F. (2009). Predicting clinically unrecognized coronary artery disease: use of two- dimensional echocardiography. Cardiovasc Ultrasound; 7: 10.

Charison, F. J., Moran, A. E., Freedman, G., Norman R. E., & Stapelberg, N., et al., 2013. The contribution of major depression to the global burden of ischemic heart disease: A comparative risk assessment. BMC Med; 11: 1.

Chatzizisis, Y. S., Murthy, V. L., & Solomon, S. D. (2013). Echocardiographic evaluation of coronary artery disease. Coron Artery Dis., 24: 613–23.

Chaves, P. H., Kuller, L. H., O'Leary, D. H., Manolio, T. A., & Newman, A. B. (2004). Subclinical cardiovascular disease in older adults: Insights from the cardiovascular health study. The American Journal of Geriatric Cardiology; 13: 137–151.

Cheitlin, M. D., Armstrong, W. F., Aurigemma, G. P., Beller, G. A., Bierman, F. Z., Davis, J. L., & et al. (2003). ACC/AHA/ASE 2003 guideline update for the clinical application of echocardiography: Summary article: A report of the American College of Cardiology/American Heart Association task force on practice guidelines (ACC/AHA/ASE committee to update the 1997 guidelines for the clinical application of echocardiography). Circulation; 108: 1146–1162.

Colledge, N. R., Walker, B. R., & Ralston, S. H. Davidson's principles and practice of medicine. 21st ed. Edinburgh: Churchill Livingstone/Elsevier; 2010.

Dall'Armellina, E., Karamitsos, T. D., Neubauer, S., & Choudhury, R. P. (2010). CMR for characterization of the myocardium in acute coronary syndromes. Nat Rev Cardiol; 7: 624–36.

Daly, C., & Kwong, R. Y. (2013). Cardiac MRI for myocardial ischemia. Methodist DeBakey cardiovascular journal; 9: 123–131.

Davis, J. P., & Tikunova, S. B. (2008). Ca2+ exchange with troponin C and cardiac muscle dynamics. Cardiovascular Research, 77: 619–626.

De Carvalho, F. S., Mukai, K., Clayton, J., & Ordovas, K. (2017). Cardiac MRI: A preferred method for assessing myocardial ischemia and infarct burden. Appl Radiol; 46: 21–29.

de Roos A., Nikolaou K. CT and MRI in Suspected Ischemic Heart Disease. In: Hodler J., Kubik-Huch R., von Schulthess G., eds. Diseases of the Chest, Breast, Heart and Vessels 2019-2022. 1st ed. IDKD Springer Series. Springer, Cham; 2019.

De, P. R., Ho, S. Y., Salerno-Uriarte, J. A., Tritto, M., Spadacini, G. (2002). Electroanatomic analysis of sinus impulse propagation in normal human atria. J Cardiovasc Electrophysiol, 13: 1–10.

Dorland's. Dorland's Illustrated Medical Dictionary. 32nd ed. Elsevier; 2012: 1461.

Elamin, A., Abukonna, A., Elmalik, B. A., Ali, M., & Yousef, M. et al. (2016). Accuracy of dynamic contrast enhanced magnetic resonance imaging (DCE-MRI) in detecting breast tumors. Br. J. Med. Med. Res; 18: 1–10.

Esmaeilzadeh, M., Parsaee, M., & Maleki, M. (2013). The role of echocardiography in coronary artery disease and acute myocardial infarction. The Journal of Tehran University Heart Center; 8: 1–13.

Fauci, A. S., Braunwald, E., Kasper, D. L., Hauser, S. L., Longo, D. L., Jameson, J. L., Loscalzo, J. Harrison's Principles of Internal Medicine. 18th ed. McGraw-Hill Professional; 2011: 1811.

Figueras, J., Barrabés, J. A., Serra, V., Cortadellas, J., Lidón, R. M., Carrizo, A., & et al. (2010). Hospital outcome of moderate to severe pericardial effusion complicating ST-elevation acute myocardial infarction. Circulation; 122: 1902–1909.

Fihn, S. D., Gardin, J. M., Abrams, J., Berra, K., Blankenship, J. C., Dallas, A. P., et al. (2012). ACCF/AHA/ACP/AATS/PCNA/SCAI/STS Guideline for the diagnosis and management of patients with stable ischemic heart disease: a report of the American College of Cardiology Foundation/American Heart Association Task Force on Practice Guidelines, and the American College of Physicians, American Association for Thoracic Surgery, Preventive Cardiovascular Nurses Association, Society for Cardiovascular Angiography and Interventions, and Society of Thoracic Surgeons. J Am Coll Cardiol; 60: e44–164.

Florian, A., Jurcut, R., Ginghina, C., & Bogaert, J. (2011). Cardiac magnetic resonance imaging in ischemic heart disease: a clinical review. Journal of medicine and life; 4: 330–345.

Foley, J. R., Plein, S., & Greenwood, J. P. (2017). Assessment of stable coronary artery disease by cardiovascular magnetic resonance imaging: Current and emerging techniques. World journal of cardiology; 9: 92–108.

Francone, M., Carbone, I., Agati, L., Bucciarelli Ducci, C., Mangia, M., Iacucci, I., & et al. (2011). Utility of T2-weighted short-tau inversion recovery (STIR) sequences in cardiac MRI: an overview of clinical applications in ischaemic and non-ischaemic heart disease. Radiol Med; 116: 32–46.

Ganame, J., Messalli, G., Masci, P. G., Dymarkowski, S., Abbasi, K., Van de Werf, F., & et al. (2011). Time course of infarct healing and left ventricular remodelling in patients with reperfused ST segment elevation myocardial infarction using comprehensive magnetic resonance imaging. Eur Radiol; 21: 693–701.

Gerber, I. L., & Foster, E. Echocardiography in the coronary care unit: Management of acute MI, detection of complication, and prognostic implications. In: Otto, M. C., eds. The practice of clinical echocardiography. 5th ed. Philadelphia: Elsevier; 2007: 305–315.

Gillebert, T. C., De Pauw, M., & Timmermans, F. (2013). Echo-Doppler assessment of diastole: Flow, function and haemodynamics. Heart; 99: 55–64.

Goldstein, J. A. (2002). Pathophysiology and management of right heart ischemia. Journal of the American College of Cardiology; 40: 841–853.

Greaves, S. C. (2002). Role of echocardiography in acute coronary syndromes. Heart; 88: 419–425.

Grigioni, F., Detaint, D., Avierinos, J. F., Scott, C., Tajik, J., & Enriquez-Sarano, M. (2005). Contribution of ischemic mitral regurgitation to congestive heart failure after myocardial infarction. Journal of the American College of Cardiology; 45: 260–267.

Grothunes, F., Smith, G. C., Moon, J. C. C., Bellenger, N. G., Collins, P., Klein, H. U., et al. (2002). Comparison of interstudy reproducibility of cardiovascular magnetic resonance with two-dimensional echocardiography in normal subjects and in patients with heart failure or left ventricular hypertrophy. Am J Cardiol; 90: 29–34.

Guaricci, A. I., Galderisi, M., Aquaro, G., Carrabba, N., & Gianluca, P. (2018). Ischemic Heart Disease: New Insights from Imaging Diagnostic Techniques. BioMed research international; 2018: 5723502.

Hall, J. Guyton and Hall textbook of medical physiology. 12th ed. Philadelphia: Saunders/Elsevier; 2011.

Hoit, B. D. (2011). Strain and strain rate echocardiography and coronary artery disease. Circulation: Cardiovascular Imaging; 4: 179–190.

Imazio, M., Negro, A., Belli, R., Beqaraj, F., Forno, D., Giammaria, M., & et al. (2009). Frequency and prognostic significance of pericarditis following acute myocardial infarction

treated by primary percutaneous coronary intervention. American Journal of Cardiology; 103: 1525–1529.

Jamal, F., Kukulski, T., Sutherland, G. R., Weidemann, F., D'Hooge, J., Bijnens, B., & et al. (2002). Can changes in systolic longitudinal deformation quantify regional myocardial function after an acute infarction? An ultrasonic strain rate and strain study. Journal of the American Society of Echocardiography; 15: 723–730.

Jo, Y., Kim, J., Park, C. H., Lee, J. W., Hur, J. H., Yang, D. H., & et al. (2019). Guideline for Cardiovascular Magnetic Resonance Imaging from the Korean Society of Cardiovascular Imaging-Part 1: Standardized Protocol. Korean journal of radiology; 20: 1313–1333.

Jung, J. H., & Yoon, Y. E. (2017). Advanced Noninvasive Cardiac Imaging using Cardiac Magnetic Resonance Imaging in the Diagnosis and Evaluation of Coronary Artery Disease. Annals of Nuclear Cardiology; 3: 143–149.

Kirchhof, P., Benussi, S., Kotecha, D., Ahlsson, A., Atar, D., Casadei, B., & et al. (2016). 2016 ESC Guidelines for the management of atrial fibrillation developed in collaboration with EACTS. Europace; 18: 1609 –1678.

Kühl, H. P., Beek, A. M., van der Weerdt, A. P., Hofman, M. B., Visser, C. A., Lammertsma, A. A., & et al. (2003). Myocardial viability in chronic ischemic heart disease: comparison of contrast-enhanced magnetic resonance imaging with (18) F-fluorodeoxyglucose positron emission tomography. J Am Coll Cardiol; 41: 1341–1348.

La, M. A., Sutaria, N., & Prasad, S. K. (2007). MRI in Ischemic heart disease: From coronaries to myocardium. Indian J Radiol Imaging; 17: 98–108.

Lancellotti, P., Moura, L., Pierard, L. A., Agricola, E., Popescu, B. A., Tribouilloy, C., & et al. (2010). European association of echocardiography recommendations for the assessment of valvular regurgitation. Part 2: Mitral and tricuspid regurgitation (native valve disease). European Journal of Echocardiography; 11: 307–332.

Lang, R. M., Badano, L. P., Mor-Avi, V., Afilalo, J., Armstrong, A., Ernande, L., & et al. (2015). Recommendations for cardiac chamber quantification by echocardiography in adults: An update from the American Society of echocardiography and the european association of cardiovascular imaging. Journal of the American Society of Echocardiography; 28: 1–39.

Lang, R. M., Bierig, M., Devereux, R. B., Flachskampf, F. A., Foster, E., Pellikka, P. A., & et al. (2005). Recommendations for chamber quantification: A report from the American society of echocardiography‘s guidelines and standards committee and the chamber quantification writing group, developed in conjunction with the European association of echocardiography, a branch of the European society of cardiology. Journal of the American Society of Echocardiography; 18: 1440–1463.

Larose, E. (2006). Below radar: contributions of cardiac magnetic resonance to the understanding of myonecrosis after percutaneous coronary intervention. Circulation; 114: 620–622.

Leischik, R., Dworrak, B., Sanchis-Gomar, F., Lucia, A., Buck, T., & Erbel, R. (2016). Echocardiographic assessment of myocardial ischemia. Ann Transl Med; 4: 259.

Levine, R. A., & Schwammenthal, E. (2005). Ischemic mitral regurgitation on the threshold of a solution: From paradoxes to unifying concepts. Circulation; 112: 745–758.

Longo, D., Fauci, A., Kasper, D., Hauser, S., Jameson, J., & Loscalzo, J. Harrison's Principles of Internal Medicine. 18th ed. McGraw-Hill Professional; 2011: 1811.

Maceira, A. M., Prasad, S. K., Khan, M., & Pennell, D. J. (2006). Normalized left ventricular systolic and diastolic function by steady state free precession cardiovascular magnetic resonance. J Cardiovasc Magn Reson; 8: 417–26.

Mahmoud, M. Z. (2017). Echocardiography in the evaluation of chest pain in the emergency department. Pol. J. Radiol; 82: 798–805.

Mahmoud, M. Z., Fagiri, M. A., Al-Motrfi, A. F. & Sulieman, A. (2013). Magnetic resonance imaging findings in knee joint pain at King Saud medical city, Saudi Arabia. Int. J. Sci. Res; 2: 4–7.

Marwick, T. H. (2009). The future of echocardiography. European Journal of Echocardiography; 10: 594–601.

McCrohon, J. A., Moon, J. C., Prasad, S. K., McKenna, W. J., Lorenz, C. H., Coats, A. J., & et al. (2003). Differentiation of heart failure related to dilated cardiomyopathy and coronary

artery disease using gadolinium-enhanced cardiovascular magnetic resonance. Circulation; 108: 54–59.

McMurray, J. J., Adamopoulos, S., Anker, S. D., Auricchio, A., Böhm, M., Dickstein, K., & et al. (2012). ESC guidelines for the diagnosis and treatment of acute and chronic heart failure 2012: the task force for the diagnosis and treatment of acute and chronic heart failure 2012 of the European society of cardiology. Developed in collaboration with the Heart Failure Association (HFA) of the ESC. European Heart Journal; 33: 1787–1847.

Medical Advisory Secretariat. (2010). Cardiac magnetic resonance imaging for the diagnosis of coronary artery disease: an evidence-based analysis. Ontario health technology assessment series; 10: 1–38.

Mitchell, C., Rahko, P. S., Blauwet, L. A., Canaday, B., Finstuen, J. A., Foster, M. C., & et al. (2019). Guidelines for Performing a Comprehensive Transthoracic Echocardiographic Examination in Adults: Recommendations from the American Society of Echocardiography. J Am Soc Echocardiogr; 32: 1–64.

Mohieldin, A. E., Mohamed, D. A., Mahmoud, M. Z., Fagiri, M. A. & Abukonna, A. (2016). Effect of age and gender variation in normal pituitary gland height using magnetic resonance imaging. Br. J. Med. Med. Res; 18: 1–8.

Montalescot, G., Sechtem, U., Achenbach, S., Andreotti, F., Arden, C., Budaj, A., & et al. (2013). 2013 ESC guidelines on the management of stable coronary artery disease: the Task

Force on the management of stable coronary artery disease of the European Society of Cardiology. Eur Heart J; 34: 2949–3003.

Moore, K. L., Dalley, A. F., & Agur, A. M. R. Clinically Oriented Anatomy. 7th ed. Wolters Kluwer Health/Lippincott Williams & Wilkins; 2009.

Morton, G., Plein, S., & Nagel, E. (2010). Noninvasive coronary angiography using computed tomography versus magnetic resonance imaging. Ann Intern Med; 152: 827–828.

Nandalur, K. R., Dwamena, B. A., Choudhri, A. F., Nandalur, M. R., & Carlos, R. C. (2007). Diagnostic performance of stress cardiac magnetic resonance imaging in the detection of coronary artery disease: a meta-analysis. J Am Coll Cardiol; 50: 1343–1353.

Nikolaou, K., Alkadhi, H., Bamberg, F., Leschka, S., & Wintersperger, B. J. (2011). MRI and CT in the diagnosis of coronary artery disease: indications and applications. Insights Imaging; 2: 9–24.

Otsuji, Y., Handschumacher, M. D., Liel-Cohen, N., Tanabe, H., Jiang, L., Schwammenthal, & et al., (2001). Mechanism of ischemic mitral regurgitation with segmental left ventricular dysfunction: Three-dimensional echocardiographic studies in models of acute and chronic progressive regurgitation. Journal of the American College of Cardiology; 37: 641–648.

Piérard, L. A., & Carabello, B. A. (2010). Ischaemic mitral regurgitation: Pathophysiology, outcomes and the conundrum of treatment. European Heart Journal; 31: 2996–3005.

Pocock, G., Christopher D. Richards, C. D., & Richards, D. A. Human Physiology. 5th ed. London: Oxford University Press; 2006.

Ponikowski, P., Voors, A. A., Anker, S. D., Bueno, H., Cleland, J. G., Coats, A. J., & et al. (2016). 2016 ESC Guidelines for the diagnosis and treatment of acute and chronic heart failure: The Task Force for the diagnosis and treatment of acute and chronic heart failure of the European Society of Cardiology (ESC). Developed with the special contribution of the Heart Failure Association (HFA) of the ESC. Eur J Heart Fail; 18: 891–975.

Reed, C. Roebuck, B., Lee, W., Lee, R. CSET: California Subject Examinations for Teachers. 3rd ed. New York: Kaplan Pub; 2008: 154.

Reeder, S. B., Du, Y. P., Lima, J. A. C., & Bluemke, D. A. (2001). Advanced Cardiac MR Imaging of Ischemic Heart Disease. RadioGraphics; 21: 1047–1074.

Rieber, J., Huber, A., Erhard, I., Mueller, S., Schweyer, M., Koenig, A., & et al. (2006). Cardiac magnetic resonance perfusion imaging for the functional assessment of coronary artery disease: a comparison with coronary angiography and fractional flow reserve. Eur Heart J; 27: 1465–1471.

Sawlani, R. N., & Collins, J. D. (2016). Cardiac MRI and Ischemic Heart Disease: Role in Diagnosis and Risk Stratification. Curr Atheroscler Rep; 18: 23.

Sechtem, U., Tanner, F. C., Gaemperli, O. (2014). The Year in Cardiology 2013: imaging in ischaemic heart disease, European Heart Journal; 35: 344–348.

Shah, A. M., & Solomon, S. D. (2012). Myocardial deformation imaging: Current status and future directions. Circulation; 125: e244–248.

Sicari, R., & Cortigiani, L. (2017). The clinical use of stress echocardiography in ischemic heart disease. Cardiovasc Ultrasound; 15: 7.

Smith, P. K., Puskas, J. D., Ascheim, D. D., Voisine, P., Gelijns, A. C., Moskowitz, A. J., et al. (2014). Surgical treatment of moderate ischemic mitral regurgitation. New England Journal of Medicine; 371: 2178–2188.

Śpiewak, M. (2015). Imaging in coronary artery disease. Cardiac magnetic resonance. Cor et Vasa; 57: e453–e461.

Starr, C., & Evers, C. Biology: Today and Tomorrow with Physiology. 5th ed. Cengage Learning; 2009: 422.

Strach, K., Meyer, C., Schild, H., & Sommer, T. (2006). Cardiac stress MR imaging with dobutamine. Eur Radiol; 16: 2728–2738.

Stuber, M., Botnar, R. M., Fischer, S. E., Lamerichs, R., Smink, J., Harvey, P., & et al. (2002). Preliminary report on in vivo coronary MRA at 3 Tesla in humans. Magn Reson Med; 48: 425–429.

Susan, S. Gray's anatomy: the anatomical basis of clinical practice. 40th ed. London: Churchill Livingstone; 2008.

Sutton, S. J., & Scott, M. (2002). A prediction rule for left ventricular dilatation post-MI? European Heart Journal; 23: 509–511.

Thielmann, M., Hunold, P., Böhm, C., Massoudy, P., & Jakob, H. (2007). Magnetic resonance imaging in coronary artery bypass surgery – improvement of global and segmental function in patients with severely compromized left ventricular function. Vasc Health Risk Manag; 3: 763–768.

Thompson, A. C. M., Maredia, N. (2017). Cardiovascular magnetic resonance imaging for the assessment of ischemic heart disease. Continuing Cardiology Education; 3: 56–63.

Tops, L. F., Roest, A. A., Lamb, H. J., Vliegen, H. W., Helbing, W. A., van der Wall, E. E., & et al. (2005). Intraatrial repair of transposition of the great arteries: use of MR imaging after exercise to evaluate regional systemic right ventricular function. Radiology; 237: 861–867.

Tortora, G. J., Derrickson, B. H. Principles of human anatomy. 11th ed. Hoboken, NJ: J. Wiley; 2009.

Tsang, T. S., Abhayaratna, W. P., Barnes, M. E., Miyasaka, Y., Gersh, B. J., Bailey, K. R., & et al. (2006). Prediction of cardiovascular outcomes with left atrial size: Is volume superior to area or diameter? Journal of the American College of Cardiology; 47: 1018–1023.

Uhlén, M., Fagerberg, L., Hallström, B. M., Lindskog, C., Oksvold, P., Mardinoglu, A. & et al. (2015). Tissue-based map of the human proteome. Science; 347: 1260419.

Vahanian, A., Alfieri, O., Andreotti, F., Antunes, M. J., Barón-Esquivias, G., Baumgartner, H, & et al. (2012). Guidelines on the management of valvular heart disease (version 2012): the Joint Task Force on the Management of Valvular Heart Disease of the European Society of Cardiology (ESC) and the European Association for Cardio-Thoracic Surgery (EACTS). Eur J Cardiothorac Surg; 42: S1–44.

Votavová, R., Linhartová, A., Kořínek, J., Marek, J., & Linhart, A. (2015). Echocardiography in coronary artery disease. Cor Et Vasa; 57: e408–e418.

Wieben, O., Francois, C., & Reeder, S. B. (2008). Cardiac MRI of ischemic heart disease at 3 T: potential and challenges. Eur J Radiol; 65: 15–28.

Windecker, S., Kolh, P., Alfonso, F., Collet, J. P., Cremer, J., Falk, V., & et al. (2014). ESC/EACTS Guidelines on myocardial revascularization: The Task Force on Myocardial Revascularization of the European Society of Cardiology (ESC) and the European Association for Cardio-Thoracic Surgery (EACTS) Developed with the special contribution of the European Association of Percutaneous Cardiovascular Interventions (EAPCI). Eur Heart J; 35: 2541–2619.

Wong, N. D. (2014). Epidemiological studies of CHD and the evolution of preventive cardiology. Nat. Rev. Cardiol; 11: 276–289.

Yelgec, N. S., Dymarkowski, S., Ganame, J., & Bogaert, J. (2007). Value of MRI in patients with a clinical suspicion of acute myocarditis. Eur Radiol; 17: 2211–2217.

Zidan, M. M. A., Hassan, I. A., Elnour, A. M., Ali, W. M., Mahmoud, M. Z., Alonazi, B., & et al. (2018). Incidental extraspinal findings in the lumbar spine during magnetic resonance imaging of intervertebral discs. Heliyon; 4: e00803.

APPENDIX

Sudan University of Science and Technology
College of Graduate Studies

Data collection sheet

Cardiac Magnetic Resonance Imaging (CMRI) and Two-dimensional Echocardiography (2D echo) in the Diagnosis of Ischemic Heart Disease (IHD)

A. Patient data:

- Patient ID: ……
- Patient address: ……
- Patient age: ……
- Patient gender: Male ☐ Female ☐
- Patient occupation: ……

B. Patient complain:

Patient complain					
Complain	**Yes**	**No**	**Complain**	**Yes**	**No**
Angina (chest pain)			Dizziness		
Shortness of breath			Nausea		
Sweating			Tachycardia		
Weakness			Palpations		
Others: ……					

C. Patient lifestyle risk factors for IHD:

Patient lifestyle risk factors for IHD					
Patient lifestyle risk factors for IHD	**Yes**	**No**	**Patient lifestyle risk factors for IHD**	**Yes**	**No**
Smoking			High fat intake		
Alcohol intake			Absent physical activity		
Non-vegetarian diet intake			Obesity		

D. CMRI of LV volumes and systolic function values in IHD patients:

CMRI LV volumes and systolic function values in IHD patients	**Value**
LVEF	..... (%)
SV	..... (ml)
Heart rate	..... (bpm)
Cardiac output	..... (L/min)
EDV	..... (ml)
ESV	..... (ml)

E. 2D echo findings in IHD patients:

2D echo findings in IHD patients					
2D echo findings in IHD patients	**Yes**	**No**	**2D echo findings in IHD patients**	**Yes**	**No**
Dilated left ventricle			Mitral regurgitation		
Left ventricular global and regional systolic dysfunction			Dilated left atrium		
Hypokinesia in the anterior and septal wall			Pericardial effusion		
Normal right ventricle and systolic function			Intraventricular thrombus		
75% myocardial infarction involving mid anterior segment with low likelihood of viability			Others …….		